Mapping the interactions between ATP and the sarcoplasmic reticulum Ca^{2+}-ATPase with ATP and ATP analogs studied by Fourier transform infrared spectroscopy

Dissertation

zur Erlangung des Doktorgrades
der Naturwissenschaften

vorgelegt beim Fachbereich Physik
der Johann Wolfgang Goethe-Universität
in Frankfurt am Main

von

Man Liu

aus Heilongjiang, China

Frankfurt 2003

(DF1)

vom Fachbereich Physik

der Johann Wolfgang Goethe-Universität als Dissertation angenommen.

Dekan: Prof. Dr. H. Schmidt-Böcking

Gutachter: Prof. Dr. W. Mäntele

PD Dr. A. Barth

Datum der Disputation: Nov 19, 2003

1. Introduction

1.1 Aims of my work

Ligand binding to proteins controls vast numbers of cellular processes and has attracted great scientific and economic interest. The flexibility of protein and ligand is an important determinant of the interaction and often leads to ligand binding modes that cannot be anticipated from structures obtained with other ligands. This work uses different ligands to bind to the same enzyme in order to map the interactions between the enzyme and ligand, and investigate the binding modes with infrared spectroscopy. Approaches like this are welcome in the field of ligand-protein recognition because the most informative techniques, NMR and X-ray crystallography, are laborious and problematic for some systems. Methods like fluorescence and luminescence that require less expenditure also provide less molecular information. This technology gap can be bridged by IR spectroscopy.

Infrared spectroscopy, one of the methods of vibrational spectroscopy, has several advantages for the elucidation of the molecular mechanism of proteins, such as high time resolution, universal applicability from small soluble proteins to large membrane proteins under near-physiological conditions and high molecular information content combined with a sensitivity high enough to detect a change in the environment around a single atom of a large protein (Barth et al., 2002). Work summarized in recent reviews (Carey et al., 1995; Deng et al., 1999; Barth et al., 2000; Wharton, 2000) has shown that the vibrational spectrum changes characteristically when a ligand binds to a protein. This provides a direct observation of ligand binding — no marker compound has to be introduced to report the binding process, as with many other methods. Previous work has mostly focused on individual interactions between a ligand and a protein by monitoring the influence of the protein environment on the vibrational frequency of a particular group of the ligand, identified with the help of isotopic labeling (Belasco et al., 1980; Baenziger et al., 1993; Cepus et al., 1998).

This project employs a different approach to probe the role of individual functional groups of a ligand in the interaction with a protein: using infrared spectroscopy what is monitored is the protein conformational change induced by binding of analogs of the native ligand, which are modified at specific functional groups of the ligand. This identifies those functional groups that are important in the interaction with the protein. Structure-interaction relationships are obtained that are similar to structure-activity relationships in drug development that relate the chemical structure of compounds to their pharmacological activity.

Time-resolved Fourier transform infrared (FTIR) spectroscopy was used in this work. Detection of small IR absorbance changes in the vibrational spectrum generally associated with protein reactions requires the high sensitivity of FTIR spectroscopy and the reactions have to be triggered directly in the IR cuvette, for which the photolytical release of nucleotides from photolabile derivatives, i.e. P^3-1-(2-nitrophenyl)ethyl nucleotides (caged nucleotides) was used (Kaplan et al., 1978).

This work studies adenosine triphosphate (ATP) binding to the sarcoplasmic reticulum (SR) Ca^{2+}-ATPase of the muscle cells (Hasselbach et al., 1961; Hasselbach, 1974; Andersen, 1989; Lee et al., 2001), the following enzyme phosphorylation and phosphoenzyme conversion reactions. The sarcoplasmic reticulum regulates the muscle activity by release and reuptake of calcium ions (Hasselbach, 1979). The release of Ca^{2+} from this organelle induces contraction of muscle, and the reuptake of Ca^{2+} from the cytosol switches off contraction, consequently causing the muscle relaxation. Ca^{2+} reuptake is done by the SR Ca^{2+}-ATPase (see chapter 1.2) that catalyses Ca^{2+} transport against a concentration gradient from the cytoplasm of muscle cells into SR for inhibiting contraction and relaxing the muscle. The energy required for this active transport process is provided by hydrolysis of the substrate ATP. The substrate specificity of the SR Ca^{2+}-ATPase is not high and not only ATP, but also some other nucleotides and non-nucleotide substrates enable Ca^{2+} uptake (Hasselbach, 1979, 1981; Inesi et al., 1985; Lacapere et al., 1990; Wakabayashi et al., 1990; McIntosh, 1998). Here, ATP and several ATP analogs are used (see chapter 1.2.3).

The aims of this work are to identify the functional groups in a model study that demonstrates the pharmaceutical potential of infrared spectroscopy, to investigate the impact of the functional groups of ATP on the conformational changes from one enzyme state to another enzyme state, to study and compare the kinetics of the reaction steps of nucleotide binding, enzyme phosphorylation, and phosphoenzyme conversion with ATP and ATP analogs.

1.2 The sarcoplasmic reticulum Ca^{2+}-ATPase and nucleotides

1.2.1 The sarcoplasmic reticulum

Muscle cells have a specialized "smooth-endoplasmic-reticulum-like" organelle called the *sarcoplasmic reticulum*, which sequesters lumen from the cytosol. The sarcoplasmic reticulum (SR) was first identified as the major mobilizable intracellular storage compartment of Ca^{2+} in skeletal muscles through the work of W. Hasselbach, S. Ebashi, and A. Weber, reviewed in (Ebashi, 1991). The SR is arranged as an elaborated system of tubules and cisternae and forms a lacelike network in the cytoplasm of muscle cells (Alberts et al., 1989), as shown in Fig. 1.2-1. The release of Ca^{2+} from this organelle to the cytosol and its subsequent reuptake from the cytosol to the organelle, which mediate the rapid contraction and relaxation of muscles during each round of muscle contraction (Hasselbach, 1979) are performed by the enzyme in the membrane of the SR vesicles. The channel responsible for Ca^{2+} release from the sarcoplasmic reticulum is the ryanodine receptor, whereas Ca^{2+} ions are reuptaken by the *Ca^{2+}-ATPase* (Stokes et al., 2000b).

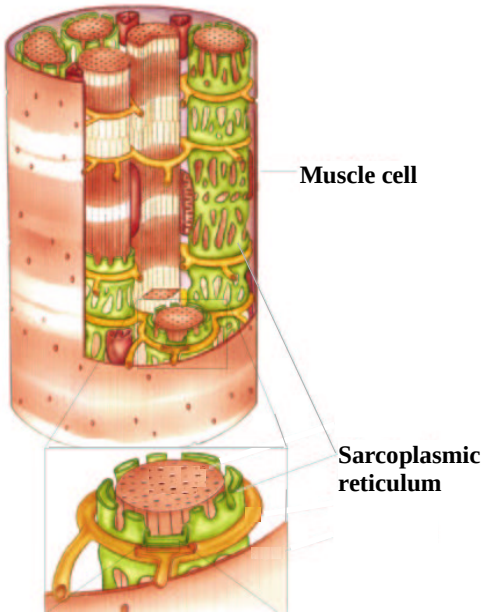

Fig. 1.2-1 The scheme of the sarcoplasmic reticulum in a muscle cell, from 2001 *Lippincott Williams & Wilkins*.

In 1948 Kielley and Meyerhof (Kielley et al., 1948) first described an ATP hydrolyzing enzyme present in aqueous muscle extracts. This enzyme was described as a Ca^{2+} pump first by Hasselbach and Makinose (Hasselbach et al., 1961). They found two ATP hydrolyzing enzymes were present in the SR membrane: the calcium-independent and the calcium-dependent ATPase (Hasselbach, 1974). In the absence of calcium ions ATP is hydrolyzed very slowly by an enzyme called the *basic ATPase* that is moderately activated by magnesium ions and has a very low

nucleotide specificity (Makinose et al., 1965). Its affinity for ATP is relatively low so that at ATP concentration below 0.1 mM its activity becomes negligible. The other ATPase is the Ca^{2+}-ATPase, which is the major membrane protein (about 80% of protein mass) in the SR (Alberts et al., 1989; Darnell et al., 1990). The Ca^{2+}-ATPase lowers the cytosolic Ca^{2+} concentration by pumping Ca^{2+} from the cytosol into the SR, thus inhibiting contraction and relaxing the muscle (Darnell et al., 1990).

1.2.2 The sarcoplasmic reticulum Ca^{2+}-ATPase

Classification of ion motive ATPases

Every cell type throughout the biological world contains an ATP synthesis/hydrolysis cycle. This cycle is of critical importance to individual cell function and to the function of intact prokaryotic or eukaryotic organisms. Consequently, the ATP synthesis/hydrolysis cycle must be able to respond on demand to energy needs and to operate in a "tightly coupled" manner. This remarkable feat is accomplished by a diverse variety of ATPases. At least three classes of ATPases are ion motive ATPases. They can be grouped as the P-, V-, and F-type (Pedersen et al., 1987).

The P-type ATPases are a large family of membrane proteins that are responsible for the active transport of cations across biological membranes in order to keep the cationic cellular milieu in the correct balance (against the prevailing concentration gradient). They share a conserved five-residues sequence around the phosphorylated aspartyl residue, other conserved sequences, and a similar membrane topography. The functional core of these pumps appears to be a single polypeptide that couples ion transport in the transmembrane region with ATP hydrolysis in a cytoplasmic region (Andersen, 1995). They generally transport different cations in two directions and can be electrogenic. The transport of the first cation is activated by ATP hydrolysis, and the other, in the second part of the cycle, is associated with dephosphorylation of phosphoenzyme (McIntosh, 1998). The family can be divided into three major subgroups: type I, those ATPases that transport heavy metals such as Cu^{2+}, Cd^{2+} and Hg^{2+}; type IIA, the Na^+, K^+-ATPase, the H^+, K^+-ATPase and the sarcoplasmic/endoplasmic reticulum Ca^{2+}-ATPases, which is studied here; and type IIB, the plasma membrane Ca^{2+}-ATPase and the H^+-ATPase in plants and yeasts (Fagan et al., 1994; Moller et al., 1996). Type I is characterized by an N-terminus with assumed binding sites for heavy metals and with small molecular masses (70-85 kDa). Type II ATPases have higher molecular masses (100-135 kDa). They are important for driving secondary cotransport systems and for other cellular functions in eukaryotic cells. Type IIB differs from type IIA in

particular by the presence of an extended C-terminal hydrophilic tail that regulates ATPase activity by interaction with calmodulin in plasma membrane Ca^{2+}-ATPase and by other effectors in proton ATPases. A fundamental property of the P-type ATPases is their ability to bind the substrate ATP with high affinity and to catalyze the phosphorylation (hence the name P-type ATPase) of a conserved aspartic acid residue in the presence of activating ions (Clausen et al., 2001). The formation as well as the further processing of the aspartyl phosphorylated intermediate is associated with protein conformational changes that couple the events in the catalytic site with changes in the ion binding sites leading to ion translocation across the membrane. The energy required to move cations against their electrochemical potential gradients comes from the hydrolysis of the terminal phosphate bond of ATP, to give ADP and P_i.

The V-type ATPases are defined as those associated with membrane bound organelles other than the mitochondria and the endoplasmic or sarcoplasmic reticulum. The F-type ATPases are defined as those of the F_0F_1 type in bacteria, chloroplasts and mitochondria (Amzel, 1983; Senior et al., 1983; Hatefi, 1985).

General introduction of the SR Ca^{2+}-ATPase

The SR Ca^{2+}-ATPase (Fig. 1.2-2) belongs to the type IIA group of the P-type ATPases family. The Ca^{2+}-ATPase is a single, large, multipass transmembrane polypeptide chain containing 997 amino acid residues with sequence similarity to the α subunit of Na^+, K^+-ATPase (Skriver et al., 1981; Hebert et al., 1988) and has about 110 kDa molecular mass.

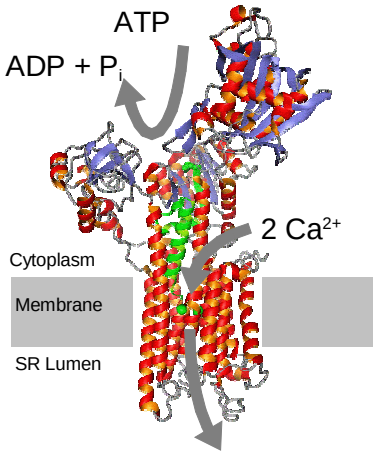

Fig. 1.2-2 The sarcoplasmic reticulum Ca^{2+}-ATPase (PDB ID: 1EUL), by courtesy of A. Barth.

The Ca^{2+}-ATPase pumps Ca^{2+} ions against a concentration gradient (1 : 10^4~10^5) from the cytoplasm of muscle cells into the SR lumen (Hasselbach et al., 1961; Hasselbach, 1974). This causes muscle cells to relax after cytosolic calcium increases during excitation. Hydrolysis of one ATP molecule supplies the energy for two Ca^{2+} ions transport. The high affinity of the enzyme

cytosolic surface for the Ca^{2+} ions (K_M=10^{-7} M, K_M, the Michaelis constant, is the substrate concentration at which the reaction velocity is half-maximal) allows it to transport Ca^{2+} very efficiently from the cytosol ([Ca^{2+}]=10^{-7}–10^{-6} M) to the SR lumen, where total Ca^{2+} ion concentration can be as high as 10^{-2} M. The activity of Ca^{2+}-ATPase is also regulated so that if the cytosolic Ca^{2+} ion concentration becomes too high, the rate of calcium pumping increases until the concentration is reduced to less than 1 μM.

Phospholipid structure was found to have direct effects on the activity of the Ca^{2+}-ATPase, reviewed in (Lee et al., 1995). Changes in the thickness of the lipid bilayer can lead to changes in the Ca^{2+} binding region. Phosphorylation and dephosphorylation of the ATPase are more sensitive to changes in lipid structure than Ca^{2+} binding.

Mechanism of Ca^{2+} transport by the SR Ca^{2+}-ATPase

The mechanism of the SR Ca^{2+}-ATPase action is usually discussed in terms of the E1-E2 model, as shown in Fig. 1.2-3, developed from the Post-Albers scheme for the Na^+, K^+-ATPase (De Meis, 1981). The model proposes that the Ca^{2+}-ATPase exists in two distinct forms, E1 and E2. For Ca^{2+} transport, the ATPase undergoes conformational changes and forms several intermediates upon a series of substrate binding and dissociation, and couples the conformational changes of the catalytic sites in the cytoplasmic region with the Ca^{2+} translocation in the transmembrane region (Darnell et al., 1990; Kendrew et al., 1994; Kanazawa et al., 1995; McIntosh, 2000).

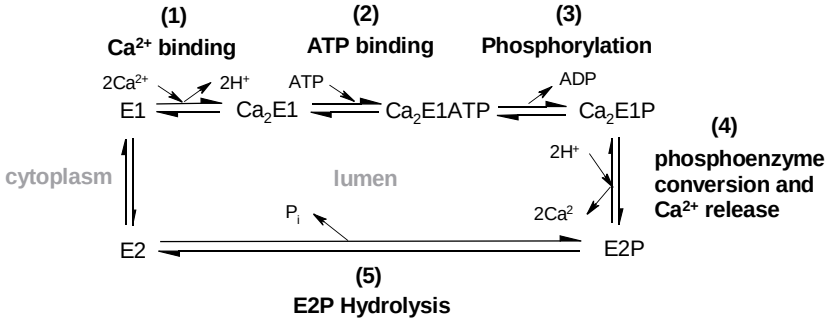

Fig. 1.2-3 The E1-E2 model of the reaction cycle of the SR Ca^{2+}-ATPase.

When the protein is in the conformational state E1, two Ca^{2+} bind to the sites in the transmembrane region and Ca_2E1 forms. ATP then binds to the nucleotide binding site in the cytoplasmic region (see "Crystal structures of the SR Ca^{2+}-ATPase" and Fig. 1.2-4) and Ca_2E1ATP forms. The bound ATP is then hydrolyzed to ADP while the liberated phosphate P_i is transferred to the aspartic acid residue 351 (Asp-351) forming a high energy acyl phosphate bond in the ADP-sensitive intermediate Ca_2E1P (this intermediate is able to synthesize ATP in

the presence of ADP). The protein then changes the conformation to the ADP-insensitive intermediate E2P (this intermediate is unable to synthesize ATP in the presence of ADP), decreasing the affinity of the binding sites to Ca^{2+}. The free energy of hydrolysis of the aspartyl-phosphate bond is simultaneously reduced in the magnitude when the protein changes its conformation from Ca_2E1P to E2P. The Ca^{2+} ions then dissociate from the binding sites, and the aspartyl-phosphate bond is hydrolyzed. Then E2 forms. After E2 converts to E1, the ATPase can bind Ca^{2+} ions with high affinity again (Andersen, 1989) (for recent reviews see Moller et al., 1996, and MacLennan et al., 1997). It is generally accepted that each reaction cycle involves two calcium ions bound with a cooperative mechanism and slow kinetics to interacting domains of the enzyme (Inesi et al., 1980; Dupont, 1982). The kinetics of ATP binding and dissociation (Pickart et al., 1984) present to be slow (37 s^{-1} at 25°C), whereas the phosphorylation is very fast (>116 s^{-1} at 25°C). This unbranched reaction cycle calls for strict stoichiometry of two calcium ions pumped per ATP hydrolyzed. However, under some experimental conditions other stoichiometries have been observed, one way to account for those observations is to allow some branches in reaction mechanism (Gafni et al., 1985).

The reaction cycle of the Ca^{2+}-ATPase is reversible. This ensures the efficient use of chemical energy stored in ATP and leads to ATP synthesis and Ca^{2+} release to the cytoplasm, provided that intact vesicles previously loaded with calcium are given Mg^{2+}, ADP and P_i in the absence of external Ca^{2+}. The coupling between ATP synthesis and Ca^{2+} release is lost when ADP and P_i are omitted from the assay medium. As a result, Ca^{2+} is released through the ATPase without concomitant ATP synthesis (reviewed in Wolosker et al., 1995, and De Meis et al., 1996).

There are some other similar or even more complicated models of the reaction cycle (De Meis et al., 1979; Inesi et al., 1985; Stahl et al., 1987; Teruel et al., 1987; Danko et al., 2001a, b; Lee et al., 2001). The model shown in Fig. 1.2-3 is the one most authors agree on and it is also suitable for the results of this work.

Mg^{2+} is the physiological co-substrate for both ATP and P_i phosphorylation reactions. However, MgATP is not the only possible substrate for phosphorylation in the forward direction. CaATP, MnATP, CoATP, ZnATP and LaATP have also been shown to induce ATPase activity with higher or lower turnover rates, as compared with the MgATP-induced turnover (Yamada et al., 1980; Shigekawa et al., 1983; Henao et al., 1989; Mintz et al., 1997). In the reverse direction, phosphorylation by P_i has also been shown to occur in the absence of Mg^{2+}, using Co^{2+}, Mn^{2+}, Cd^{2+}, Ni^{2+} or Ca^{2+}. With Ca^{2+}, phosphorylation by P_i can only be transient as Ca^{2+} binding to the high-affinity transport sites dephosphorylates E2P.

Several chemicals, for example thapsigarin (TG) and fluorescein isothiocyanate (FITC), have been used very often to investigate the mechanism and structure-function relationship of the SR Ca^{2+}-ATPase. TG can inhibit the activity of the Ca^{2+}-ATPase in the absence of Ca^{2+} by fixing the enzyme in a form analogous to the E2 state (Sagara et al., 1991). FITC is a lysine reactive fluorophore and has intense fluorescence that has facilitated its use as a probe of nucleotide binding sites for not only the Ca^{2+}-ATPase but also other ATPases (Pick et al., 1981; Clore et al., 1982; White et al., 1987; Abu-Abed et al., 2002). The trinitrophenylate derivatives of AMP, ADP and ATP (TNP-AMP, -ADP and -ATP) are also fluorescent probes of the Ca^{2+}-ATPase nucleotide binding site (Moczydlowski et al., 1981a). These three nucleotide analogs exhibit a dramatic enhancement of fluorescence upon binding to the phosphorylated Ca^{2+}-ATPase (Dupont et al., 1982; Watanabe et al., 1982; Berman, 1986).

Crystal structures of the SR Ca^{2+}-ATPase

The Ca^{2+}-ATPase was first visualized in early electron micrographs of SR as granules or knobs on the outer surface of isolated vesicles. Advances were made with the discovery that vanadate could induce two dimensional crystalline arrays of the Ca^{2+}-ATPase (Dux et al., 1983). Further studies of these crystals produced an 8 Å resolution structure (Aravind et al., 1998; Zhang et al., 1998; Stokes et al., 2000a). In 2000, Toyoshima *et al.* (Toyoshima et al., 2000) presented the 2.6 Å resolution structure of the Ca^{2+}-ATPase in the presence of Ca^{2+}, abbr. as Ca_2E1, obtained by X-ray diffraction of three-dimensional crystals, which provides the first high resolution view of this important family of molecules. In 2002, Toyoshima and Nomura (Toyoshima et al., 2002) described the 3.1 Å resolution structure of the Ca^{2+}-ATPase in the absence of Ca^{2+} and in the presence of thapsigargin, abbr. as E2TG. The determination of these two crystal structures gives the opportunity for an analysis of conformational changes on the Ca^{2+}-ATPase.

The Ca^{2+}-ATPase crystal structures of the Ca^{2+}-loaded state Ca_2E1 (Toyoshima et al., 2000) (Fig. 1.2-4, left) and of TG-loaded state E2TG (Toyoshima et al., 2002) (Fig. 1.2-4, right) show two regions, the cytoplasmic region and the transmembrane region. In the transmembrane region are ten transmembrane α-helices. Two Ca^{2+} ions are bound in this region between helices M4, M5, M6 and M8 (Toyoshima et al., 2000). Recent reviews of Lee (Lee, 2002a, b) analyzed the conformational changes on the Ca^{2+}-ATPase in the E1 and E2 states, helix-helix and helix-lipid interactions in the transmembrane region, and discussed the characteristics of Ca^{2+} binding sites. In the cytoplasmic region there are three clear globular domains (Toyoshima et al., 2000), the nucleotide binding domain (N domain), the phosphorylation domain (P domain) and the actuator domain (A domain), as shown in Fig. 1.2-4.

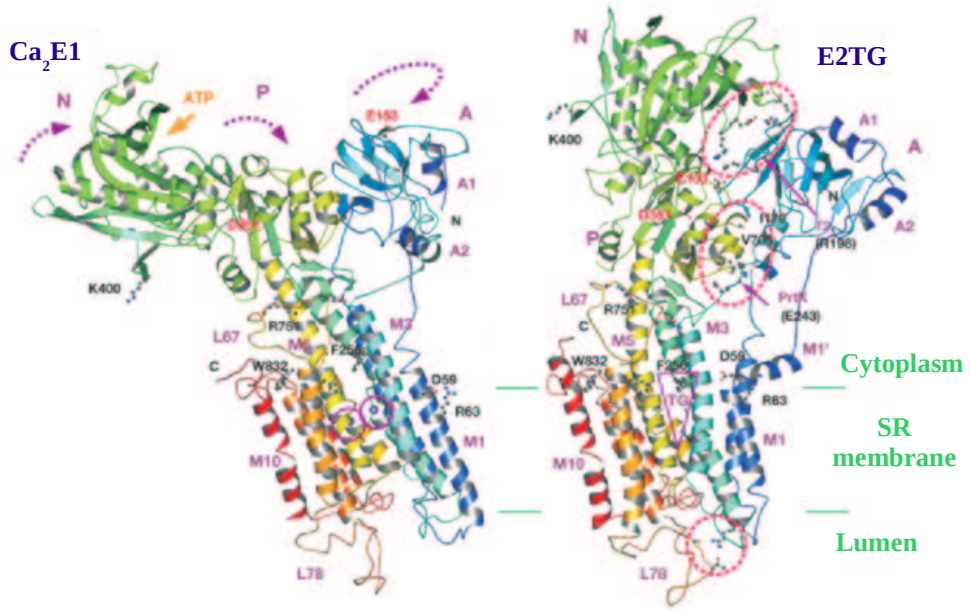

Fig. 1.2-4 Ribbon representation of the sarcoplasmic reticulum Ca^{2+}-ATPase in the Ca^{2+}-bound form Ca_2E1 and E2TG form in the absence of Ca^{2+} but in the presence of thapsigargin (TG) from Toyoshima *et al.* 2002. Colors change gradually from the amino terminus (blue) to the carboxyl terminus (red). Three cytoplasmic domains are labeled (N, P and A). Transmembrane helices (M1-M10) are numbered. L67 and L78 are the loops between M6-M7 and M7-M8. Two purple spheres (circled) in Ca_2E1 represent bound Ca^{2+}. Red circles in E2TG indicate extra hydrogen bonds. Large arrows in Ca_2E1 indicate the direction of movement of the cytoplasmic domains during the change from Ca_2E1 to E2TG. ATP, binding pocket for the adenosine moiety of ATP. Several residues are marked: E183 (A domain), F256 (thapsigargin-binding site), D351 (P domain, phosphorylation site), and K400 (N domain, phospholamban-binding site). E, Glu; F, Phe; D, Asp; K, Lys.

At the center of the cytoplasmic headpiece is the P domain, which contains the residue of phosphorylation Asp-351. The P domain contains a seven-stranded parallel β-sheet with eight short associated α-helices. The residue of phosphorylation Asp-351 is situated in the C-terminal end of the central β-strand, as it is usually the case for nucleotide-binding proteins with a Rossman fold. Around Asp-351, the residues critical for ATP hydrolysis are clustered and form a highly negatively charged surface that is accessible to solvent. The structure of the P domain is analogous to that of the haloacid dehalogenases (Aravind et al., 1998; Stokes et al., 2000a).

The N domain is the largest of the three cytoplasmic domains and is inserted into the sequence of the P domain (like the subdomain inserted into the catalytic domain of the haloacid dehalogenases). It has a seven-stranded antiparallel β-sheet sandwiched by two bundles of α-helices linked to the P domain by two loops (Toyoshima et al., 2000). This presumably gives the N domain considerable flexibility with respect to the rest of the structure, and explains the fact that several proteases release a stable fragment to the corresponding N domain of the Ca^{2+}-ATPase, which retains the ability to bind nucleotides (Champeil et al., 1998). Identified from chemical labeling experiments and mutations, residues involved in ATP binding such as Thr-441,

Lys-492, Lys-515, Phe-487, Arg-560 *et al.* (Maruyama et al., 1989; Yeagle, 1993; McIntosh et al., 1996; Moller et al., 1996) are localized in the N domain (Toyoshima et al., 2000) and form a positively charged binding pocket, in marked contrast to the region around the phosphorylation site at Asp-351 that is negatively charged.

The 145 residues between stalks M2 and M3, together with the 50 residues in the N-terminal region, form the A domain (Toyoshima et al., 2000; Lee et al., 2001). This domain is almost isolated from the rest of the structure, being connected to the transmembrane region by three long loops. The A domain is supposed to undergo a large amount of rotation and its strong association with the N and P domain occur most likely during the conversion from Ca_2E1P to E2P (Danko et al., 2001a, b). The rearrangement of the A domain is likely a key event in the whole reaction cycle.

FTIR spectra of sarcoplasmic reticulum in the Ca_2E1 and E2V (bound with vadanate) state did not show visible differences by direct inspection, but subtle differences appeared after data processing by Fourier deconvolution or derivation (Arrondo et al., 1987). Including this study, research with FTIR difference spectroscopy (Barth et al., 1994, 1996, 1998; Georg et al., 1994; Von Germar et al., 2000) show that the conformational changes in the reactions of nucleotide binding and phosphoenzyme formation are small and the net change of secondary structure involves only about 10-residues.

1.2.3 Substrate and substrate analogs used in this work

In addition to ATP, the Ca^{2+}-ATPase catalyzes the hydrolysis of ITP, GTP, CTP, UTP, and 2'-deoxyATP (De Meis et al., 1973; Pick et al., 1981; Highsmith, 1984; Coan et al., 1993). The lack of specificity spreads to non-nucleotide energy-rich compounds such as acetyl phosphate, *p*-nitrophenylphosphate (Inesi, 1971; Nakamura et al., 1978; Rossi et al., 1979; Inesi et al., 1980). The affinity of the enzyme for ATP is one or more orders of magnitude higher than for the other substrates. All these nucleotides and non-nucleotides phosphorylate the ATPase and sustain Ca^{2+} transport (but only ATP increases the rate of turnover at high concentration). The stoichiometry of calcium ions transported per substrate molecule is different with some non-nucleotide substrates like *p*-nitrophenylphosphate, methyl-umbelliferylphosphate or furylacyloylphosphate (Rossi et al., 1979), being one to one only. ATP regulates nearly all the steps in the reaction cycle of Ca^{2+} transport. Non-hydrolyzable ATP analogs such as ADP, AMPPNP and AMPPCP accelerate Ca^{2+} binding (Mintz et al., 1995).

In this work ATP and several ATP analogs were used. Their structures are shown in Fig. 1.2-5.

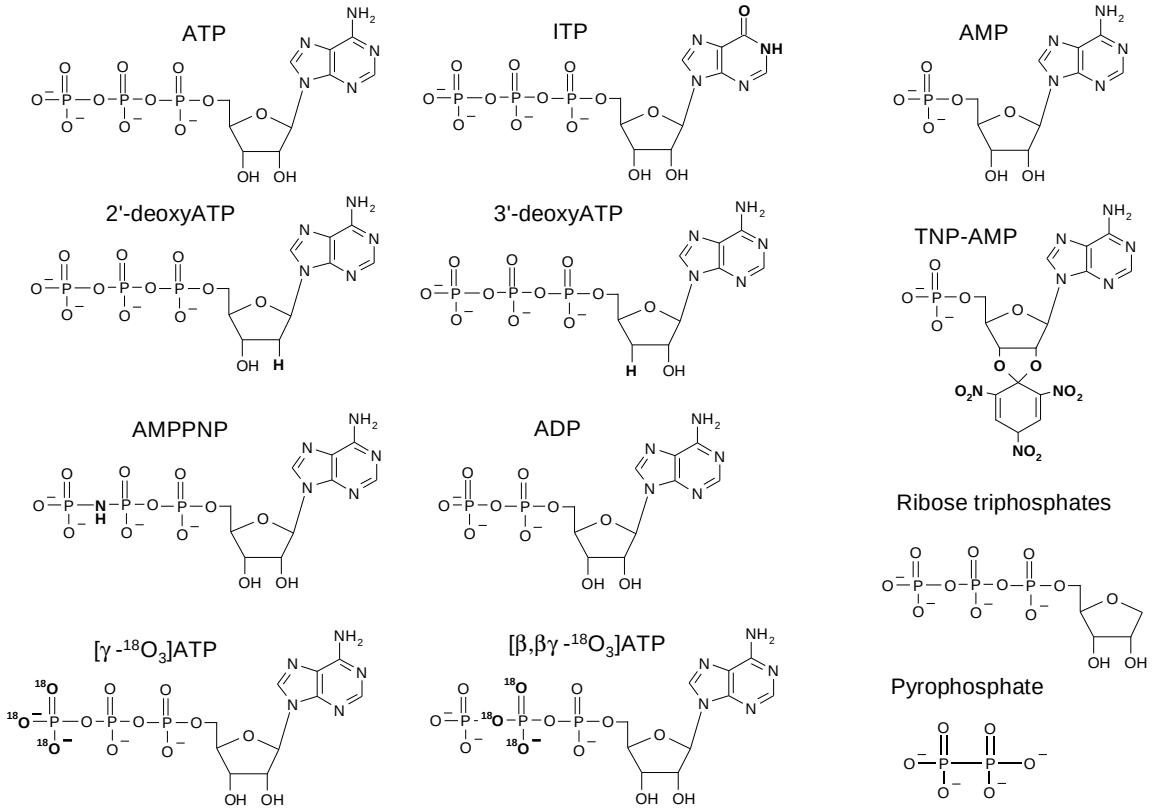

Fig. 1.2-5 Structures of ATP and ATP analogs used in this work.

The functional groups of these ATP analogs differ from that of ATP and this gives the chance to investigate the impact of these functional groups on ATP binding to the SR Ca^{2+}-ATPase and subsequent reactions, and to obtain more information on protein-ligand recognition. The effect of the adenine ring can be addressed by comparing ATP with ITP and ribose triphosphate. The impact of the β- and γ-phosphate can be demonstrated by comparing ATP with AMP, ADP, AMPPNP, [β,βγ-$^{18}O_3$]ATP and [γ-$^{18}O_3$]ATP.

The conformational change of TNP-AMP binding to the Ca^{2+}-ATPase in solution was investigated by infrared spectroscopy here, because nucleotide binding to the ATPase has been studied intensively by using TNP adenosine phosphates, which are fluorescent ATP analogues (Moczydlowski et al., 1981a), reviewed in (McIntosh, 1998). TNP-nucleotides have been used not only because of their high fluorescence yield and photolabeling properties, but also on account of their high binding affinity. TNP-ATP, -ADP, and -AMP bind with high affinity for the catalytic sites of the Na^+, K^+-ATPase (Moczydlowski et al., 1981a, b), gastric H^+, K^+-ATPase (Faller, 1989, 1990) and the SR Ca^{2+}-ATPase (Dupont et al., 1982, 1983; Watanabe et al., 1982; Berman, 1986; McIntosh et al., 1996). TNP-AMP was used as ATP analogue in the crystal structure of the Ca_2E1 state of the SR Ca^{2+}-ATPase (Toyoshima et al., 2000). It binds to the catalytic nucleotide binding site of the Ca^{2+}-ATPase (Nakamoto et al., 1984; Suzuki et al.,

1990). However there is evidence that the structure with ATP is different from that with TNP-AMP, because (i) TNP-AMP binding to the ATPase cannot provide strong resistance against proteinase K and V8 whereas ATP and adenosine 5'-(β,γ-methylene)triphosphate (AMPPCP) can (Danko et al., 2001a, b); (ii) ATP binding destroys the Ca_2E1 crystals in contrast to TNP-AMP (Toyoshima et al., 2000).

The influence of the ribose ring can be studied by comparing ATP with 2'-deoxyATP and 3'-deoxyATP. The five-membered furanose ring systems in ribo- and deoxyribonucleotides are never planar. Instead they pucker in either envelope or twist forms for reducing its energy. The two principle and preferred puckering modes of the sugar conformations are $C_{2'}$-*endo* and $C_{3'}$-*endo*, because nonbonding interactions between furanose ring substituents are at a minimum (Saenger, 1984). The puckering mode of ATP and deoxyATPs are different because of the different OH groups in different positions.

1.3 Fourier transform infrared spectroscopy

1.3.1 General principles of infrared spectroscopy

The potential energy of a molecule comprises translational energy, rotational energy, vibrational energy and electronic energy. Among them, Molecular vibrations give rise to absorption bands throughout most of the infrared (IR) region of the spectrum (2.5–25 μm) (Colthup et al., 1990). The change in molecular vibrational energy after infrared absorption is given by the Bohr equation,

$$\Delta E = E_2 - E_1 = h c \tilde{\nu} \quad (1\text{-}1),$$

where E_1 is the initial energy, E_2 is the final energy, h is Planck's constant, and $\tilde{\nu}$ is the wavenumber (cm^{-1}) reciprocal of the wavelength. When the photon energy $E_p = h c \tilde{\nu}$ is equal to ΔE, the photon can be absorbed by a molecule and activate the molecule vibration from the ground state to generally the first excited state (Arrondo et al., 1993). According to the selection rule, only a molecular vibration that causes a change in the dipole moment of the molecule absorbs the infrared light. While the absorption frequency depends on the molecular vibrational frequency, the absorption intensity depends on how effectively the infrared photon energy can be transferred to the molecule, and this depends on the change in the dipole moment that occurs as a result of molecular vibration.

IR spectroscopy is used as one of the classic tools to determine molecular structures and interactions since the middle of last century. When molecules exhibit an intrinsic order of repeating units such as the protein backbone that can be visualized as a row of peptide bonds, the overlap in IR spectra is simpler, and detailed band analysis can provide some of the desired information on structure and interactions between the ligand and protein or among the subunits (Siebert, 1995). The band assignments to protein secondary structure of the amide I and amide II mode in the IR spectral region is listed in Table 1-1.

Table 1-1. Band assignments in amide I and amide II region of infrared spectroscopy (Cantor et al., 1980; Arrondo et al., 1993; Goormaghtigh et al., 1994a, b).

Secondary structure	α–helix	Antiparallel β–sheets	Parallel β–sheets	Turns	Random coil
Amide I	1653	1632, 1685	1630, 1645	1662, 1686, 1694	1656
Amide II	1516, 1546	1530	1530, 1550	1568, 1548	1535

Another application of infrared spectroscopy is the use of difference spectra, which is related to functional aspects of proteins. To understand the molecular mechanisms of enzymes, information on the interaction of participating molecules is needed. The infrared difference spectra formed between different enzyme states contain bands of only those groups that undergo changes during the transition from one state to the other, whereas the large background absorbance of the enzyme can be subtracted.

1.3.2 Fourier transform infrared spectroscopy

Fourier transform infrared (FTIR) spectrometer, involving a special mathematical treatment of spectral data as the name implies, produces an interferometric pattern that, after passing through the sample, reaches the detector. The Michelson interferometer is most commonly used in instruments in protein studies (for detailed theory of the Michelson interferometer see Griffiths et al., 1986). The output of the interferometer is measured as signal intensity *I* as a function of the optical path difference *d*. It is called the interferogram *I(d)*,

$$I(d) = \int_{-\infty}^{\infty} B(\tilde{\nu}) \cos(2\pi \tilde{\nu} d)\, d\tilde{\nu} \qquad (1\text{-}2),$$

The interferogram is a plot of intensity vs. optical path difference or time dependent mirror position. The interferometric data are then Fourier transformed into the frequency domain and the detected IR intensity *I* as a function of $\tilde{\nu}$, $I(\tilde{\nu})$, is obtained.

The advantages of FTIR spectroscopy are summarized as *Felgett Advantage* (all frequencies are observed simultaneously in short time that results in a large signal-to-noise ratio), *Jacquinot Advantage* (more energy flows through the system allowing greater sensitivity) and *Connes Advantage* (an internal laser reference to facilitate digitization of data and for frequency calibration). Additional advantages of FTIR spectroscopy include less sample heat-up (samples far away from the light source), no sample emission contributions, easiness in spectral mathematical treatments, etc. (Arrondo et al., 1993). With these advantages FTIR spectroscopy has become a powerful tool for the characterization of protein structure lying between that of the purely predictive and the molecular coordinate approaches. Information concerning protein secondary structure ranging from global aspects of protein conformation to very subtle rearrangements associated with ligand binding or point mutations can be obtained (reviewed in Braiman et al., 1988; Jackson et al., 1995).

1.3.3 Studying protein-ligand interaction with time-resolved FTIR spectroscopy

FTIR spectroscopy has been used to study the dynamics of proteins and protein-ligand interactions. Two approaches have been applied: (i) analyzing the change of the secondary structure population in conformational substates with changing the temperature and/or pressure; (ii) following the ligand binding process or conformational changes using time-resolved FTIR. The latter is studied here.

Rapid scan FTIR spectroscopy allows one to collect the spectral data within milliseconds. This makes it possible to follow in real time the formation and decay of intermediates in the enzyme reaction cycle (Griffiths et al., 1986; Braiman et al., 1988; Barth et al., 1996). With rapid scanning it is possible to obtain a complete record of an event lasting up to ~30 min with millisecond time resolution at 2-8 cm^{-1} spectral resolution. In the study of membrane proteins, their large background absorbance compared with the amplitude of the transient absorbance changes requires a number of successive interferograms to be averaged so that the resulting difference spectra will have adequate signal-to-noise ratios.

In this work time-resolved changes are studied in the infrared difference spectra of the Ca^{2+}-ATPase that occur after nucleotide binding. Infrared absorbance changes were monitored at time intervals of 65 ms and were evaluated in order to observe the different protein states or intermediates and to analyze the kinetics of reaction steps with different nucleotide binding to the ATPase.

2. Materials and Methods

2.1 Materials

SR vesicles from rabbit hind leg and back muscle, prepared according to the method of Hasselbach and Makinose as described in (De Meis et al., 1971), were a grateful gift from Prof. Dr. W. Hasselbach (Max Plank Institut für Medizinische Forschung, Heidelberg, Germany). Vesicles were stored at -20°C in 300 mM sucrose, 100 mM KCl and 1 mM $CaCl_2$. The Ca^{2+}-ATPase constitutes approximate 70% of the total protein content in this preparation (Hasselbach, 1974). The final Ca^{2+}-ATPase concentration of 16 mg/ml was determined according to the Coomassie blue test by Dr. D. Thönges as described (Bio-Rad Laboratories, 1977).

Caged nucleotides were synthesized by Dr. J. E. T. Corrie, Dr. A. Barth and Dr. F. von Germar at the National Institute for Medical Research, London, as described (Walker et al., 1988; Barth et al., 1995, 1996, 1997a, b).

Chemicals are from the following companies: Sigma-Aldrich, Fluka, Roth, Merck, Serva, Biomol, and Molecular Probes (for details see chapter 5.2).

Four kinds of dialysis buffer, as shown in Table 2-1, were used to find the optimal buffer for nucleotide binding.

Table 2-1 Dialysis buffers

Buffer name	**Buffer component**
Buffer I	10 mM imidazole (pK_a 7.0) / HCl, 20 µM $CaCl_2$, 10 mM KCl
Buffer MeI	10 mM 4-methylimidazole (pK_a 7.5) / HCl, 20 µM $CaCl_2$, 10 mM KCl
Buffer M	10 mM MOPS (pK_a 7.2) / KOH, 20 µM $CaCl_2$, 10 mM KCl
Buffer P	10 mM KH_2PO_4 / K_2HPO_4 (pK_a 7.21), 20 µM $CaCl_2$

2.2 Preparation of samples

2.2.1 Infrared samples for the nucleotide-ATPase interaction experiments

After 90-min dialysis of the SR vesicles in the buffer at 4°C, infrared samples were prepared by vacuum drying 15 µl of SR suspension and additions of other compounds on a CaF_2 window with a trough of 5 µm depth and 8 mm diameter, and then immediately rehydrating the sample with 0.8 µl H_2O. The sample was sealed with a second flat CaF_2 window.

The composition of samples was designed to accumulate the Ca_2E1P state in samples termed *type I samples*, also used for buffer optimization (see chapter 3.1.1) and titration of signals (see chapter 3.1.2), and the E2P state in samples termed *type II samples* (see chapter 3.6). The sample composition based on 1 µl sample volume is given in Table 2-2.

Table 2-2 Composition of samples used in FTIR measurements. A23187, Ca^{2+} ionophore; DMSO, dimethyl sulfoxide; DTT, dithiothreitol.

Sample name	ATPase	Buffer	pH	Ca^{2+}	K^+	Mg^{2+}	caged nucleotide	A23187	DMSO	DTT	Temperature
	mM	mM		mM	mM	mM	mM	mg/ml	%	mM	°C
Type I samples	1.2	150	7.5	10	150	0	10	0.5	0	10	1
Type II samples	1.2	150	7.5	0.3	0	5	10	0.5	20	10	25

The buffer is 4-methylimidazole in all experiments with exception of the buffer optimization experiments, in which pH values changes from pH 6.5 to pH 7.8 (see chapter 3.1.1).

In the samples with caged derivatives of ATP, 2'-deoxyATP, [β,βγ-$^{18}O_3$]ATP and [γ-$^{18}O_3$]ATP, 1 mg/ml adenylate kinase were added for reproducing ATP or deoxyATP from ADP or deoxyADP, respectively. Adenylate kinase was found to work for both ADP and 2'-deoxyADP to form ATP/AMP and 2'-deoxyATP/2'-deoxyAMP (Resnick et al., 2000). Adenylate kinase catalyzes the reaction of producing ATP/AMP or deoxyATP/deoxyAMP from two ADP or deoxyADP molecules, and therefore decreases ADP of deoxyADP concentration. The samples with adenylate kinase will be first flashed and then kept in room temperature for ~1 hour to equilibrate. The new-formed ATP are hydrolyzed and consumed by the ATPase during the equilibration and the ATPase will be in the Ca_2E1 state again. Then these samples can be flashed another several times without the interference of ADP. Thus, the samples with adenylate kinase can be used at least 6 times (Barth et al., 1996) and the deviation caused by the different samples can be reduced. Spectra obtained from the average of several flashes show nearly no difference from spectra obtained from the first flash. In this work, samples with adenylate kinase were

applied at most 3 flashes.

2.2.2 Control samples

Five kinds of control samples were prepared for different purposes. Control I and II samples were for detecting the photolysis signals. Control III samples were for verifying whether the signals obtained are from nucleotide binding to the *Ca^{2+}-ATPase* or to other proteins in the membrane of the SR vesicles. Control IV samples can display whether caged ATP and caged AMPPNP bind to the Ca^{2+}-ATPase. Control V samples were used to detect whether the weak bands (0.1 mOD) observed are real signals induced by interactions between the ATPase and the substrates.

Control I samples: the control I samples composition was the same as the type I samples but in the absence of the SR vesicles. Instead, 15 µl buffer was added to retain the same pH value and ion concentrations. Control I samples were prepared with ATP, [β,βγ-$^{18}O_3$]ATP and [γ-$^{18}O_3$]ATP.

Control II samples: in the control II samples the nucleotide binding site was already saturated with AMPPNP at the beginning of the experiment. The composition of these samples is the same as that of type I samples with 10 mM caged AMPPNP except for the presence of 5 mM AMPPNP. Photolysis of caged AMPPNP in these samples did not lead to further nucleotide binding, they only revealed the effects of caged compound photolysis in the presence of the ATPase.

Control III samples: control III samples were for the confirmation of the signals, i.e. whether the IR signals obtained were from the Ca^{2+}-ATPase or other proteins in SR vesicles. For this purpose, thapsigargin (TG) (Kijima et al., 1991; Sagara et al., 1991, 1992) was used to selectively inhibit the Ca^{2+}-ATPase in control III samples. Control III samples were made as described in the following: after 60-min dialysis of SR vesicles in 4-methylimidazole buffer (4°C, pH 7.5), 15 µl of SR suspension were incubated first with 0.6 mM EGTA for 5 min and then with 1 µl of 1.2 mM TG for 5 min at 20°C. After the incubation, the samples were prepared as described in chapter 2.2.1. The composition in control III samples was the same like type I samples with the exception of the following: 0.3 mM $CaCl_2$, 5 mM $MgCl_2$, 0.6 mM EGTA and 1.2 mM TG.

Control IV samples: these samples were prepared in the same way like type I samples as described in chapter 2.2.1 but with different amount of caged ATP (2.5–50 mM) or caged AMPPNP (3.3–50 mM), for detecting whether *caged ATP* or *caged AMPPNP* binds to the Ca^{2+}-

ATPase.

Control V samples: these samples were prepared in the same way like type I samples as described in chapter 2.2.1 but with 0.3 mM ATPase and 1 mM caged AMPPNP, for detecting whether smaller IR signals were real bands from interactions between the ATPase and nucleotides.

2.2.3 Samples for competition experiments

There were three sets of competition experiments, one with TNP-AMP and caged AMPPNP both at different concentrations, one with ribose triphosphate at different concentrations and 10 mM caged AMPPNP, and another with 10 mM pyrophosphate and 10 mM caged ATP. After 60-min dialysis of SR vesicles in 10 mM 4-methylimidazole/HCl (pH 7.5), 0.2 mM $CaCl_2$, 10 mM KCl, samples were prepared as type I samples in Table 2-2. DTT was added at the same concentration as caged AMPPNP or caged ATP.

2.2.4 Samples for absorption spectra of sugar puckering modes

500 mM ATP, 2'-deoxyATP or 3'-deoxyATP dissolved in H_2O were used to record absorption spectra for studying the puckering mode of ATP and deoxyATPs. Samples were prepared by vacuum drying 2 µl of 250 mM nucleotides and addition of different concentrations of KOH on a BaF_2 window with a trough of 5 µm depth and 8 mm diameter, and then immediately rehydrating the sample with 1 µl H_2O. The sample was sealed with a second flat BaF_2 window. 1000 mM, 1500 mM or 2000 mM KOH were in the samples to obtain different protonation states of nucleotides.

2.2.5 E2TG samples with ATP and EGTA

Samples with 0.6 mM EGTA, 4.8 mM thapsigargin (TG), 0.3 mM free Ca^{2+}, 5 mM Mg^{2+} and 3 mM released ATP were prepared to study the inhibition of TG. The ATPase was first incubated with EGTA for 5 min. 0.6 mM EGTA are enough to chelate free Ca^{2+} ions in the samples but not enough to chelate completely the bound Ca^{2+} ions from the ATPase, and therefore the ATPase was in Ca_2E1 state. Then the ATPase was incubated with TG for 130 min at room temperature. The other addition of components is the same as type I samples. After that the samples were prepared the same like type I samples as described in chapter 2.2.1 and measured as described in chapter 2.3.1 at 1°C.

2.3 Fourier transform infrared spectroscopic measurements

2.3.1 Time-resolved FTIR measurements

Time-resolved FTIR measurements were performed with a modified Bruker IFS 66 spectrometer equipped with a HgCdTe detector of selected sensitivity. Data were acquired with double sided interferograms in a forward-backward mode at a spectral resolution of 4 cm^{-1} with the Blackman-Harris 4-term apodization function. The time needed for one interferometer cycle was 65 ms. As shown in Fig. 2.3-1, the measurement started with recording of the reference spectrum coadded from 300 scans (I_R) characterizing the unperturbed sample in the Ca_2E1 state. Photolytic release of nucleotides from their respective caged derivatives was triggered by flash series with a Xenon flash tube (N-185C, Xenon Corporation, Woburn MA, USA) or a XeCl excimer laser. The number of photolysis flashes needed for saturating signals was determined as described in chapter 2.3.3 and 3.1.2. The time was then set to zero. Subsequently 10 spectra with 1 scan (I_1), 10 spectra with 4 scans (I_2), 10 spectra with 40 scans (I_3) and 10 spectra with 300 scans (I_4) each were recorded. A kinetic baseline measurement was done in the same way without the photolysis flash before the real measurement as shown in Fig. 2.3-1.

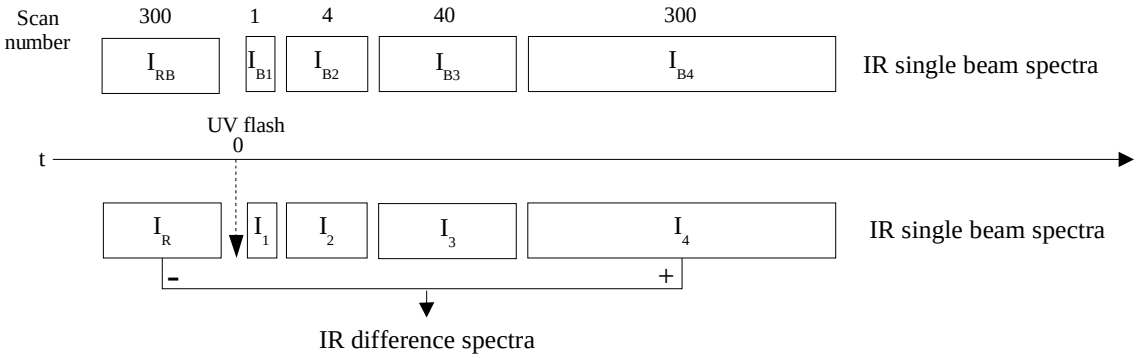

Fig. 2.3-1 The scheme of data acquisition in time-resolved FTIR measurements.

Time-resolved FTIR measurements of the Ca^{2+}-ATPase reaction were performed at 1°C for measurements of nucleotide binding and phosphorylation, and at 25°C for those of E2P formation and E2P hydrolysis. Difference spectra were obtained by subtracting the reference spectrum recorded before the flash from the spectra obtained after photolytic release of nucleotide (Fig. 2.3-1). They reflect nucleotide binding, phosphorylation and phosphoenzyme hydrolysis, respectively, as well as the photolysis reaction. For better observation and understanding of the bands induced by nucleotide-ATPase interactions, a photolysis spectrum was then subtracted to eliminate the photolysis bands that overlay with the protein bands (see chapter 2.4.4). The resulting spectra are named *nucleotide binding spectra, Ca_2E1P formation spectra*. *E2P formation spectra* were shown without subtraction of photolysis signals.

2.3.2 Photolysis of caged nucleotides

Photolysis of caged nucleotides was triggered by a Xenon flash tube or a XeCl excimer laser. The voltage of the flash tube was set to make the flash tube produce a flash energy of ~150 mJ in the spectral range from 305 nm to 424 nm at the area of the samples. With one flash, a photolysis yield of up to ~30% was obtained. The excimer laser was set to produce similar photolysis efficiency at 308 nm as the flash tube. With the excimer laser several flashes can be applied in a short time (50 ms delay between two flashes) and a large proportion of caged nucleotides can be photolyzed. A Schott UG11 filter was used to block the flash light of the Xenon tube in the infrared region. The reaction of caged ATP photolysis is shown in Fig. 2.3-2 as a representative. The byproduct absorbs at ~1690 cm^{-1}. The reaction between DTT and the byproduct can eliminate this band and induces another small band at ~1640 cm^{-1}.

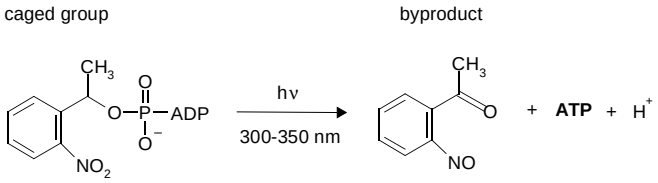

Fig. 2.3-2 The reaction of photolysis of caged ATP.

2.3.3 Titration of signals

In order to obtain saturating signals, the amplitude of bands at 1641/1628 cm^{-1} was titrated by repeating an experiment on the same sample up to eight times. In this experiment a reference spectrum coadded from 300 scans was first recorded; then a photolysis flash was applied; at last a spectrum coadded from 300 scans was recorded in a time interval of 0–19.5 s when the ADP-sensitive phosphoenzyme Ca_2E1P had formed (see chapter 3.3.2). The number of flashes needed for saturating signals was used in subsequent experiments to ensure that the amount of released nucleotides was sufficient for saturating binding-induced signals.

2.3.4 Absorbance measurements of sugar puckering modes

Absorbance spectra of 500 mM ATP, 2'- or 3'-deoxyATP dissolved in KOH solution at different pH values were measured using two BaF_2 windows (5 µm pathlength) with a Bruker Vector 22 spectrometer equipped with a deuterated triglycine sulfate (DTGS) detector at 20°C. Data were acquired with double sided interferograms in a forward-backward mode at a spectral resolution of 4 cm^{-1} with the Blackman-Harris 4-term apodization function. The experiments started with recording a background spectrum coadded from 10 scans without samples and then a sample absorption spectrum coadded from 10 scans with samples.

2.4 Data processing

2.4.1 Normalization of ATPase concentrations

Up to 23 experiments were averaged to obtain one final spectrum. To prevent the possible predominance of individual samples with high protein content in the averaged difference spectra and for a better comparison of samples, the difference spectra were normalized to a standard protein concentration before averaging spectra from different samples. For this, difference spectra were multiplied by a factor that was needed to normalize the respective absorption spectra measured in H_2O before the photolysis flash to an amide II absorbance of 0.26 (absorbance difference between 1546 and 1492 cm^{-1}) as described (Barth et al., 1998). The amide II band was chosen for the normalization because it is less sensitive to errors in water subtraction that eliminates a strong water band in the amide I region. The absorbance in the amide II region does not depend on the presence of ATP and ATP analogs because they do not absorb in this region.

2.4.2 Evaluation of kinetic data

For fitting of selected marker bands of reaction steps to a kinetic model, integration of band intensities, between point 1 and 2 as shown in Fig. 2.4-1, was performed with respect to a base line that was drawn between two data points (averages of point 3-4 and point 5-6) of the spectrum at each side of the chosen band (integration method “E” of OPUS 3.1). The integral intensity was used here to improve the signal-to-noise ratio. Moreover, the integral intensity shows much less sensitivity to the instrumental resolution and has much greater theoretical significance because it is proportional to the square of the change in the dipole moment with respect to the normal coordinate (Colthup et al., 1990).

The time constants of nucleotide binding and ATPase phosphorylation with type I samples and

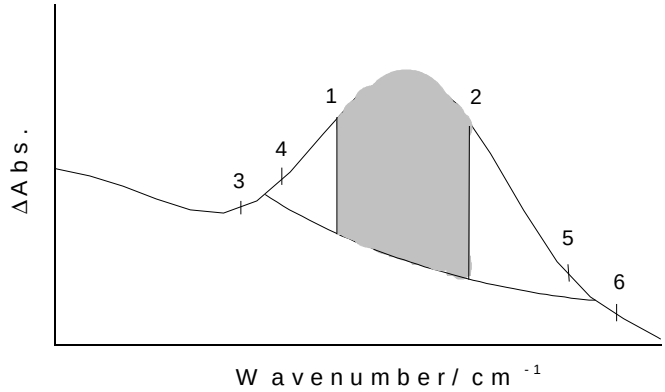

Fig. 2.4-1 Illustration of band intensity integration.

of E2P formation and E2P hydrolysis with type II samples were obtained by fitting the integral intensities of marker bands at 1628, 1641 cm^{-1} for nucleotide binding, at 1721, 1549 cm^{-1} for phosphorylation (Barth et al., 1996), and at 1711, 1689, 1653, 1571, and 1193 cm^{-1} for E2P formation (Barth et al., 1996) and E2P hydrolysis. The time constants of photolytic release of nucleotides was calculated using the marker bands at 1465, 1381 and 1330 cm^{-1} (Barth et al., 1995). The time constants of phosphorylation were obtained first by fitting the integral band intensities of 1721 and 1549 cm^{-1} with a first order exponential equation (Origin 5.0). Then the time constants of nucleotide binding were determined by fitting the integral intensities of 1628 and 1641 cm^{-1} with a second order exponential equation with one time constant fixed by the corresponding time constant of phosphorylation. With type II samples, the E2P state was accumulated. Because of different experimental conditions (different sample components and higher temperature), nucleotide binding and phosphorylation are too fast to be observed. E2P formation and E2P hydrolysis were observed. Therefore, the time constants of E2P formation and E2P hydrolysis were obtained by fitting the intensities of the five marker bands with a second order exponential equation.

The time constants for a given reaction obtained from the different selections of infrared bands were averaged to get the final time constant for the reaction. The standard errors were calculated with all the individual experiments and bands.

2.4.3 Calculation of difference spectra

The difference spectra were calculated as indicated in Fig. 2.4-2. Reference and sample spectra are labeled "-" and "+", respectively. The difference spectra show the changes of the absorbance of the ATPase states (Ca_2E1N, Ca_2E1P, E2P) after photolytic release of nucleotide minus the absorbance of the Ca_2E1 state. At the appropriate time after photolysis of nucleotides, difference spectra represent the absorbance changes associated with nucleotide binding ($Ca_2E1 \rightarrow Ca_2E1N$), Ca_2E1P formation ($Ca_2E1 \rightarrow Ca_2E1P$) and E2P formation ($Ca_2E1 \rightarrow$ E2P). From these difference spectra, the absorbance changes associated with phosphorylation ($Ca_2E1N \rightarrow$

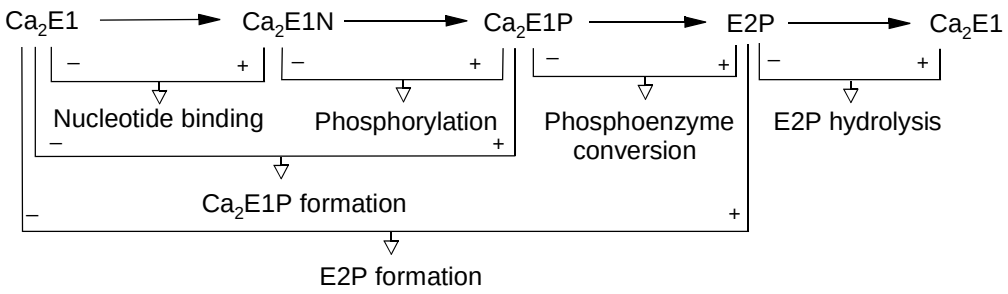

Fig. 2.4-2 Reaction steps investigated here and the calculation of difference spectra.

Ca_2E1P), phosphoenzyme conversion ($Ca_2E1P \rightarrow E2P$) and E2P hydrolysis ($E2P \rightarrow Ca_2E1$) can be calculated. The photolysis signals existing in the spectra of each state except for the Ca_2E1 state were subtracted as described in chapter 2.4.4.

The ATP release spectrum and the photolysis spectrum

The spectra obtained with control I samples show signals induced by the photolysis of caged ATP in the absence of the ATPase. It is named the *ATP release spectrum*. The same time interval as used for the ATP binding spectrum was chosen to coadd the spectra and obtain the ATP release spectrum. Ten experiments were averaged for the ATP release spectrum. It was used to compare the vibrational modes of phosphate groups of bound ATP in the presence of the ATPase and free ATP in the absence of the ATPase (see chapter 3.2.1 and 3.4.1).

The spectrum obtained with control II samples, in which the nucleotide binding sites had been already saturated with AMPPNP at the beginning of the experiment, shows only signals caused by the photolysis of caged AMPPNP in the presence of the ATPase. It is named the *photolysis spectrum*. The conditions of recording the photolysis spectrum are as close as possible to the conditions used in the binding, phosphorylation and competition experiments. 10 experiments were averaged for the photolysis spectrum. The photolysis spectrum was interactively subtracted from the raw difference spectra to obtain the *nucleotide binding spectra*, *Ca_2E1P formation spectra* and the *competition spectra*. The criterion of the correct multiplication factor for the photolysis spectrum in the subtraction was described in chapter 2.4.4. However, because of the different phosphate groups between AMPPNP, ATP and other ATP analogs, the spectra obtained after subtraction of the photolysis spectrum was discussed outside the phosphate absorption region, i.e. above 1300 cm^{-1}.

Control III spectrum, control IV spectra and control V spectra

With the purposes of preparing control III, IV and V samples as described in chapter 2.2.2, control III, control IV and control V spectra were measured and processed in the same way as nucleotide binding spectra as described below. The photolysis spectrum was subtracted.

Nucleotide binding spectra

For obtaining the nucleotide binding spectra ($Ca_2E1 \rightarrow Ca_2E1N$, Fig. 2.4-2), time intervals after the photolysis flash were defined in which the nucleotide-ATPase complex Ca_2E1N accumulates according to the kinetic evaluation of the marker bands (see chapter 2.4.2 and 3.3.1). The time intervals of nucleotide binding (Δt_{nb}), the numbers of experiments from different samples, the

numbers of applied photolysis flashes and the amount of released nucleotides are shown in Table 2-3. For ADP, after recording the ADP binding spectrum with 2 flashes, another 4 flashes were given to determine the full amplitude of the ADP binding bands (8.75 mM released ADP in total). The full amplitude of the ADP binding marker bands at 1628 and 1641 cm^{-1} obtained after the sixth flash (see chapter 3.1.2) was used to normalize the spectrum obtained after two flashes to the full signal amplitude. This procedure gives saturating binding signals while minimizing the photolysis signals. The typical amplitude of the marker bands after the first two flashes was 88% of the full amplitude.

Photolysis spectra averaged in the same time intervals as the respective nucleotide binding spectra were interactively subtracted as described in chapter 2.4.4.

Table 2-3. Experimental data for obtaining spectra. Δt_{nb}, the time interval of nucleotide binding; Δt_{E1P}, the time interval of Ca_2E1P formation.

Nucleotide	nucleotide binding (Δt_{nb}) / s	Ca_2E1P formation (Δt_{E1P}) / s	No. of experiments / No. of samples	Concentrations of nucleotide / No. of flash
ATP	0.46 - 0.90	5.84 – 68.1	23 / 12	3 mM / 1 flash
[β,βγ-$^{18}O_3$]ATP	0.46 - 0.90	5.84 – 68.1	17 / 6	3 mM / 1 flash
[γ-$^{18}O_3$]ATP	0.46 - 0.90	5.84 – 68.1	13 / 8	3 mM / 1 flash
AMPPNP	0.46 - 3.24	–	4 / 4	3 mM / 1 flash
ADP	0.46 - 3.24	–	5 / 5	8.75 mM / 6 flashes
2'-deoxyATP	0.46 - 3.24	21.4 – 68.1	8 / 4	3 mM / 1 flash
3'-deoxyATP	0.46 - 3.24	165.4 – 224	3 / 3	3 mM / 1 flash
ITP	0.72 - 3.32	26.7 -68.1	4 / 4	6.6 mM / 3 flashes

<u>Ca_2E1P formation spectra</u>

Ca_2E1P formation spectra ($Ca_2E1 \rightarrow Ca_2E1P$, Fig. 2.4-2) were obtained by subtracting the reference spectrum (Ca_2E1) from the spectrum of the protein in the Ca_2E1P state obtained in the time intervals shown in Table 2-3 determined by the kinetic evaluation of the marker bands (chapter 2.4.2). The photolysis spectra averaged in the same time interval were subtracted using the same subtraction factors as for the respective nucleotide binding spectra (chapter 2.4.4).

<u>Phosphorylation spectra</u>

By subtracting the nucleotide binding spectrum from the Ca_2E1P formation spectrum, the phosphorylation spectrum ($Ca_2E1N \rightarrow Ca_2E1P$, Fig. 2.4-2) was obtained. In this subtraction, photolysis signals were subtracted at the same time.

E2P formation spectra

For obtaining E2P formation spectra ($Ca_2E1 \rightarrow E2P$, Fig. 2.4-2) time intervals after the photolysis flash(es) were evaluated in which the ADP-insensitive phosphoenzyme E2P accumulates according to the kinetic evaluation (see chapter 2.4.2 and 3.3.3). They are from 0.32–2.54 s for ATP (3 mM), and from 1.51–16.3 s for ITP (6.6 mM). Six and five experiments from different samples were averaged for E2P formation spectra with ATP and ITP, respectively. Photolysis signals were not subtracted.

Competition spectra with TNP-AMP and AMPPNP

TNP-AMP titration of the TNP-AMP → AMPPNP competition spectra: at the beginning of an competition experiment, TNP-AMP was bound to the ATPase. After the photolysis flash, ~3 mM AMPPNP were released from 10 mM caged AMPPNP, competed with TNP-AMP and partially replaced TNP-AMP from the binding sites. The resulting difference spectra are named *TNP-AMP → AMPPNP competition spectra* or shorter *competition spectra*. Different concentrations of TNP-AMP were used to determine the TNP-AMP concentration that saturates the binding sites (see chapter 3.4.4). Two to three experiments from different samples were averaged for each competition spectrum.

AMPPNP titration of the TNP-AMP → AMPPNP competition spectra: in order to identify the AMPPNP concentration that can nearly completely replace 5 mM TNP-AMP from the binding sites, an AMPPNP titration of competition spectra was performed in eight consecutive kinetic FTIR experiments on one sample with one flash for each experiment (see chapter 3.4.4). In these experiments, 5 mM TNP-AMP and 30 mM caged AMPPNP were present. In the first experiment, ~3.7 mM AMPPNP was released (here the power supply of the flash tube was adjusted to give a photolysis yield of 12%); in the second a total of ~7 mM AMPPNP was present; and so on. Signals from two samples were averaged for the AMPPNP titration of competition spectra.

These competition spectra were obtained by averaging the spectra in the time interval of 0.46–3.24 s as the AMPPNP binding spectrum.

TNP-AMP binding spectrum

TNP-AMP → AMPPNP competition spectra described above show the difference in absorbance between the Ca_2E1AMPPNP state and the Ca_2E1TNP-AMP state, *i.e.* absorbance of Ca_2E1AMPPNP minus absorbance of Ca_2E1TNP-AMP. The AMPPNP binding spectrum (see

"Nucleotide binding spectra"), measured under the same conditions but without TNP-AMP added, shows the difference in absorbance between the Ca_2E1AMPPNP state and the Ca_2E1 state, *i.e.* absorbance of Ca_2E1AMPPNP minus absorbance of Ca_2E1. By subtracting the competition spectrum from the AMPPNP binding spectrum, the difference in absorbance between the Ca_2E1TNP-AMP state and the Ca_2E1 state was obtained as shown in Fig. 2.4-3. This spectrum is the *TNP-AMP binding spectrum*.

	the AMPPNP binding spectrum:	**$A(Ca_2E1AMPPNP) - A(Ca_2E1)$**
minus	the TNP-AMP → AMPPNP competition spectrum:	**$A(Ca_2E1AMPPNP) - A(Ca_2E1TNP\text{-}AMP)$**
	the TNP-AMP binding spectrum:	**$A(Ca_2E1TNP\text{-}AMP) - A(Ca_2E1)$**

Fig. 2.4-3 Calculation of the TNP-AMP binding spectrum. A(ATPase state) is the infrared absorbance of that state.

Competition spectra with ribose triphosphate and AMPPNP or with pyrophosphate and ATP

Competition spectra with ribose triphosphate and AMPPNP or with pyrophosphate and ATP were obtained in the same way as nucleotide binding spectra, as described above.

Confidence level spectra

As described above, the TNP-AMP binding spectrum was obtained by subtracting two normalized difference spectra. In order to assess the confidence level of a double difference spectrum like this, AMPPNP binding spectra of 4 samples were divided into two groups with 2 spectra in each group. The spectra in each group were averaged. The confidence level spectra were obtained by subtracting the averaged spectra. Since three possibilities exist to group the spectra, three confidence level spectra were obtained. These spectra show the reproducibility of the experiments (Fig. 3.4-9B).

2.4.4 Subtraction of the photolysis spectrum

The photolysis spectrum obtained with control II samples shows only signals caused by the photolysis of caged AMPPNP in the presence of the ATPase and was used to subtract the photolysis bands from the raw difference spectra, which results in the “pure” nucleotide binding spectra and Ca_2E1P formation spectra showing predominantly bands arising from the interaction between nucleotide and the ATPase and, ideally, no photolysis signals. The subtraction factor was interactively judged to be correct when the 1525 cm^{-1} region of the processed spectrum corresponded to that region in the spectrum obtained with [^{15}N]caged ATP (Von Germar et al., 2000). With this compound, because of labeling at the nitro position of the (2-nitrophenyl)ethyl-ester group (caged group in Fig. 2.3-2), the photolysis band at 1525 cm^{-1} shifts to 1499 cm^{-1},

which allows the identification of protein bands in the 1525 cm^{-1} region. Because the released ATP from [^{15}N]caged ATP is identical to that released by unlabeled [^{14}N]caged ATP, the same interactions between the protein and the nucleotide are expected. Thus the spectrum obtained with [^{15}N]caged ATP can be used as a reference for a complete compensation for the 1525 cm^{-1} band of the photolysis reaction.

The same time interval was used to coadd spectra for both the raw difference spectrum and the photolysis spectrum. The photolysis spectrum is identical to that of other caged nucleotides above 1300 cm^{-1}, *i.e.* outside the region of phosphate absorption. The subtraction factors are shown in Table 2-4.

Table 2-4 Subtraction factors of photolysis signals for nucleotide binding and Ca_2E1P formation spectra.

Nucleotide	ATP	AMPPNP	ADP	2'-deoxyATP	3'-deoxyATP	ITP
Subtraction Factor	0.2	0.37	1.4	0.67	0.55	0.77

2.4.5 Calculation of the change of backbone structure and interaction index

In order to quantify and compare the structural changes of the polypeptide backbone induced by binding of ATP and ATP analogs, a change of backbone structure and interaction (COBSI) index was introduced (Barth et al., 1996). The calculation of COBSI index for the nucleotide binding spectra was carried out in the amide I region (1700–1610 cm^{-1}). It relates the integral intensity of difference spectra that is redistributed upon nucleotide binding to the integral total protein absorbance. The calculation formula is shown in Fig. 2.4-4. Half of the sum of the integral positive and negative difference bands is divided by the integral total protein absorbance. The integral total protein absorbance is the averaged value from all the samples.

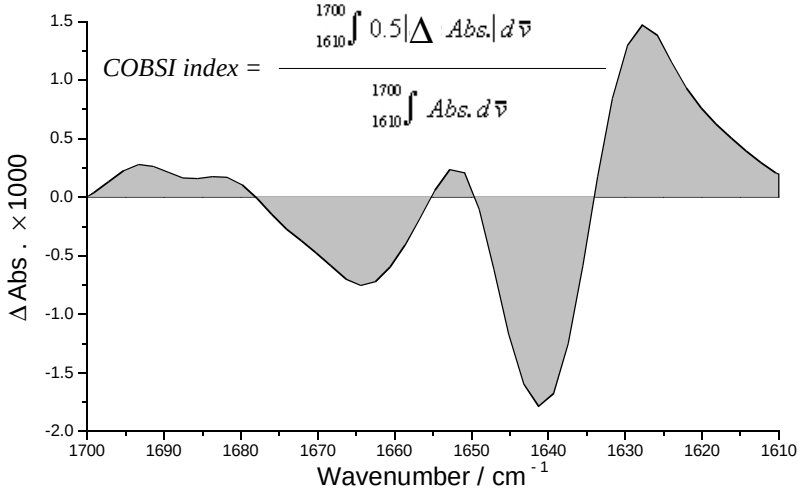

Fig. 2.4-4 Calculation of the change of backbone structure and interaction (COBSI) index with the ATP binding spectrum.

2.4.6 Estimation of [Ca_2E1AMPPNP] from the infrared spectra

In studying of TNP-AMP binding, the amplitude difference between 1644 and 1627 cm^{-1} in the competition spectra was used to estimate the concentration of the AMPPNP-ATPase complex Ca_2E1AMPPNP, [EA]. At the selected wavenumbers, the spectrum was hardly affected by TNP-AMP binding or dissociation (see circled positions in the TNP-AMP binding spectrum in Fig. 3.4-9 that are zero at these wavenumbers) and therefore reflected the concentration of Ca_2E1AMPPNP. The AMPPNP-induced amplitude difference at a given TNP-AMP concentration divided by the maximum amplitude difference at zero TNP-AMP concentration gives the ratio between [EA] and the total ATPase concentration [E_t]. This ratio represents the fraction of ATPase that binds AMPPNP, while the remaining fraction binds TNP-AMP. The fit to the data in Fig. 3.4-7C was calculated with the equation below.

$$EA = \frac{\{k(T-1)+1+A-\sqrt{(k(T-1)+1+A)^2-4A(1-k)}\}}{(2-2k)}$$

in the equation, EA = [EA] / [E_t], T = [T_t] / [E_t], A = [A_t] / [E_t], k = k_{AMPPNP} / $k_{TNP\text{-}AMP}$.

k_{AMPPNP} and $k_{TNP\text{-}AMP}$ are the dissociation constants of AMPPNP and TNP-AMP, respectively. [T_t] is the total concentration of TNP-AMP; [A_t], the total concentration of AMPPNP is 3 mM; and [E_t] is 1.2 mM. The derivation of this formula assumed that the concentration of free enzyme is zero justified by the high concentration of nucleotides used (mM). Various k values were tested in a manual fitting procedure. The best fitting result was that with the smallest sum of the squares of deviations between the fit data and the measured data.

2.4.7 Absorption spectra of nucleotide puckering modes in 900-800 cm^{-1}

Absorption spectra of 500 mM ATP, 2'- or 3'-deoxyATP dissolved in 1500 mM KOH were measured from 900 – 800 cm^{-1}. By using the program "Fit Multi-peaks: Gaussian" of Origin 5.0, the absorbance spectra were fitted with bands at 889, 828 and 815 cm^{-1} for ATP, at 896, 834 and 814 cm^{-1} for 2'-deoxyATP, and at 900, 845, 828 and 814 cm^{-1} for 3'-deoxyATP. The population of the $C_{2'}$-*endo* and $C_{3'}$-*endo* puckering modes of 500 mM ATP, 2'- or 3'-deoxyATP in 1500 mM KOH was obtained by calculating the ratio of the areas of bands fitted to the spectrum near 830 cm^{-1} for $C_{2'}$-*endo* puckering and near 814 cm^{-1} for $C_{3'}$-*endo* puckering (Wartell et al., 1986; Taillandier et al., 1987; Ouali et al., 1993). The areas of these two bands were calculated by integration of these bands with Origin 5.0 fitting program.

3. Results and Discussion

3.1. Determination of experiment conditions

3.1.1 pH and buffer conditions

To optimize buffer conditions for studies of nucleotide-ATPase interactions, ATP and ITP were chosen because ATP is the native substrate of the Ca^{2+}-ATPase and the amplitude of ITP binding spectra was previously found to be buffer-dependent (F. von Germar and A. Barth, unpublished). Four buffers (Table 2-1) at different pH values were used to optimize sample conditions.

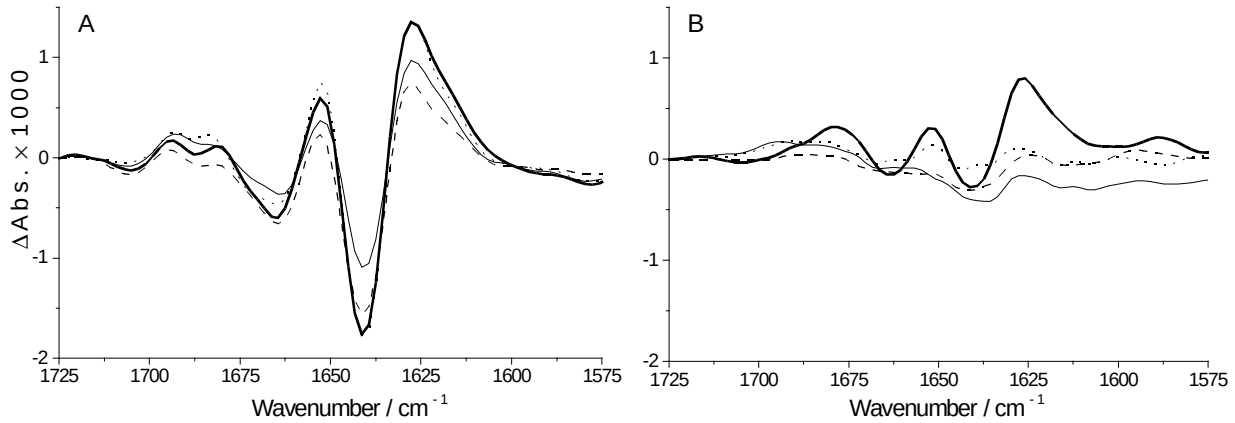

Fig. 3.1-1 Infrared difference spectra of (**A**) ATP and (**B**) ITP binding in different buffers (1°C, pH 7.5, 3 mM nucleotide, see Table 2-1 and 3-1). Buffer I, imidazole: *dashed* line; buffer MeI, methylimidazole: *solid-bold* line; buffer M, MOPS: *solid-thin* line; buffer P, phosphate buffer: *dotted* line.

Different rates of the binding-induced conformational changes and different amplitudes of the nucleotide binding bands were observed, depending on buffer and pH value. Fig. 3.1-1 shows spectra at pH 7.5 for the four buffers. The spectra in Fig. 3.1-1 show mainly the region of the amide I vibration (1700–1610 cm^{-1}) of the protein backbone, which monitors the conformational change of secondary structures. There are only minor contributions of the photolysis reaction in this region. As shown in Fig. 3.1-1A, similar spectra with medium to large binding bands (Table 3-1) were observed in all four buffers for ATP. ATP binding bands are largest in 4-methylimidazole and phosphate buffer. The pH value for obtaining the largest nucleotide binding bands depends on the buffer, the optimum range for 4-methylimidazole being pH 7.0 to 7.5. Fig. 3.1-1B shows that ITP binding bands were always smaller and evolved more slowly. The largest ITP binding signals were obtained with 4-methylimidazole. The results are summarized in Table 3-1.

The buffer effects can be attributed to a sensitivity of ATPase conformation to the composition

of the solvent (Hasselbach et al., 1975). A buffer effect has been observed previously for other partial reactions of the Ca^{2+}-ATPase: whereas the phosphoenzyme E2P accumulates in imidazole/HCl at pH 7.0, 1ºC and in the presence of 1 mM $CaCl_2$, it is not this case when imidazole is replaced by MOPS/LiOH, in which a mixture of the phosphoenzymes Ca_2E1P and E2P is present under steady state conditions (A. Barth, unpublished). According to the results above, 4-methylimidazole at pH 7.5 was used as the standard buffer for further studies in order to get fast nucleotide binding and large signals.

Table 3-1. Dependence of binding-induced infrared signals on buffer and pH values.

	BINDING RATE / ***marker band amplitude***				
	Buffer	**pH 6.5**	**pH 7.0**	**pH 7.5**	**pH 7.8**
Caged ATP	I		F / ***ml***	F / ***ml***	F / ***m***
	MeI		F / ***l***	F / ***l***	F / ***m***
	M	F / ***l***	F / ***l***	F / ***m***	
	P			F / ***l***	F / ***l***
Caged ITP	I		S / ***s***	M / ***s***	M / ***m***
	MeI		S / ***s***	M / ***m***	M / ***m***
	M	M / ***s***	M / ***s***	M / ***s***	
	P			S / ***s***	M / ***s***

Buffer: I, imidazole; MeI, 4-methylimidazole; M, MOPS; P, phosphate buffer.

marker band amplitude: difference of the amplitude of two nucleotide binding bands at 1628 and 1641 cm^{-1}. ***l***, large (more than 0.003); ***ml***, medium large (between 0.003 and 0.002); ***m***, medium (between 0.002 and 0.001); ***s***, small (less than 0.001).

BINDING RATE: judged from the time to obtain half of the *marker band amplitude*, F, fast (0.1 - 0.6 s); M, medium (1–3 s); S, slow (longer than 3 s).

3.1.2 Titration of nucleotide binding

After buffer conditions were optimized, nucleotide concentrations necessary to obtain saturating IR signals were determined. For this purpose the difference in amplitude of the band pair at 1628 and 1641 cm^{-1} in the amide I region that is sensitive to conformational changes was used. This difference is termed *maximum signal amplitude* (MSA, see chapter 2.3.3). Fig. 3.1-2 shows the result of titration with ATP and ATP analogs by applying a total of 8 flashes with which ~9.4 mM nucleotide were released from caged derivatives. As shown in Fig. 3.1-2, the binding-induced MSA reaches saturating values with one flash for ATP, AMPPNP, 2'- and 3'-deoxyATP, with six flashes for ADP and with three flashes for ITP. From the photolysis efficiency of 30%, the saturating nucleotide concentration was then calculated on the basic of 1 µl of sample volume: 3 mM (1 flash) for ATP, AMPPNP, 2'- and 3'-deoxyATP, 8.75 mM (6

flashes) for ADP and 6.6 mM (3 flashes) for ITP. Non-saturating signals are unexpected at the high concentrations of nucleotides used here because of the relatively high affinity of the ATPase to nucleotides measured in diluted samples. However, they were observed and this effect may be explained by a different affinity of the ATPase to nucleotides when it is present at the high concentration needed for infrared samples. Lower affinity of the ATPase for ADP, ITP and deoxyATPs with respect to ATP was observed before (Pickart et al., 1984; Mukohata et al., 1986; Coan et al., 1993). Here lower affinity of the ATPase only for ADP and ITP was observed. The difference may be due to the different sample conditions between the references and this work. From a methodological point of view, the results demonstrate that infrared spectroscopy can detect the affinity difference between ATP and ATP analogs.

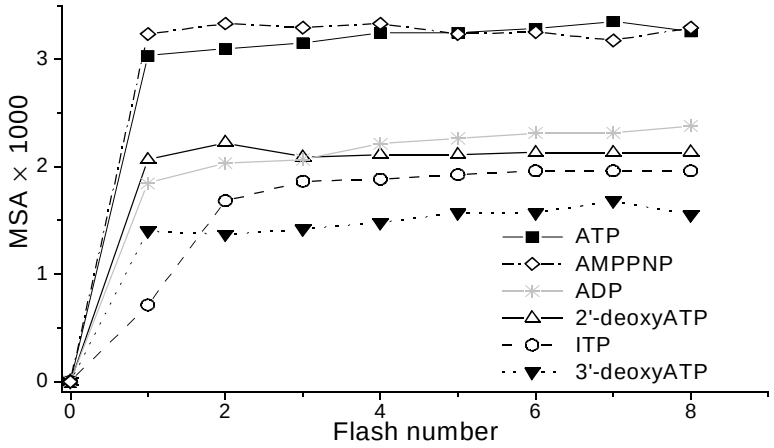

Fig. 3.1-2 Titration of IR signals of Ca_2E1P formation (1°C, pH 7.5). MSA is the difference between the absorbance change of the band pair at 1628 and 1641 cm^{-1}. Data points are connected by lines to guide the reader's eyes.

For the titration experiments, spectra were evaluated in a time slot (0–19.5 s) when the ADP-sensitive phosphoenzyme Ca_2E1P accumulated (see chapter 3.3). Strictly speaking, the titration experiments have therefore determined the nucleotide concentration necessary for a saturating concentration of Ca_2E1P, but not for a saturating concentration of the nucleotide-ATPase complex Ca_2E1N. However, the reactions of nucleotide binding and phosphorylation were well separated in time which ensured that Ca_2E1N also saturated in the time slot evaluated for the nucleotide binding spectra, as discussed in chapter 3.1.3.

3.1.3 Time intervals for the observation of three ATPase intermediates

In order to determine the time intervals for the calculation of nucleotide binding spectra, Ca_2E1P formation spectra and E2P formation spectra, a kinetic evaluation of the three reaction steps was performed, as discussed in more detail in chapter 3.3. Here the time intervals used for obtaining corresponding spectra of the three reaction steps are discussed. As listed in Table 3-2, the time

intervals for each nucleotide binding spectrum were chosen starting from 3 times of the binding reaction time constants (except for 2'-deoxyATP) and ending at about half of the phosphorylation time constants to get nearly pure binding spectra as shown in the plots of chapter 3.4. For obtaining the Ca_2E1P formation spectra, the time intervals were chosen starting from 3 times of the time constants of phosphorylation for ATP, ITP, 2'--deoxyATP. The end time for Ca_2E1P formation spectra was identical in order to pursue good signal-to-noise ratio and the fact that the decay of Ca_2E1P was inhibited in these samples. Phosphorylation with 3'-deoxyATP cannot be observed for sure in the measuring time window of 0–224 s (see chapter 3.5). However, the accumulation of Ca_2E1P with 3'-deoxyATP seems to be nearly 40% of that with ATP before the end of the measurement, according to the integral band intensity of 1721 cm^{-1} (see chapter 3.3.2). For comparing enzyme phosphorylation with ATP and other ATP analogs, the time interval of 165.4–224 s was used for 3'-deoxyATP.

Table 3-2. Time constants of nucleotide binding (t_n) and phosphorylation (t_p), and the time intervals for obtaining nucleotide binding spectra (Δt_{nb}) and Ca_2E1P formation spectra (Δt_{E1P}).

Nucleotide	ATP	[β,βγ-$^{18}O_3$]ATP	[γ-$^{18}O_3$]ATP	AMPPNP	ADP	2'-deoxyATP	3'-deoxyATP	ITP
t_n / s	0.11	0.12	0.13	0.1	0.13	0.25	0.1	0.23
t_p / s	2	1.6	2.1	-	-	6.67	54.5	8.66
Δt_{nb} / s	0.46–0.90	0.46–0.90	0.46–0.90	0.46–3.24	0.46–3.24	0.46–3.24	0.46–3.24	0.72–3.32
Δt_{E1P} / s	5.84–68.1	5.84–68.1	5.84–68.1	-	-	21.4–68.1	165.4–224	26.7-68.1

For 2'-deoxyATP the starting time of 0.46 s used for nucleotide binding spectra averaging is close to the time constant for 2'-deoxyATP binding (see chapter 3.3.1). However, increasing the starting time to 0.8 s for 2'-deoxyATP does not change the MSA value by more than 3%. Therefore the time slot was kept for averaging consistent with that for ATP and as large as possible for an optimum signal to noise ratio.

For obtaining the E2P formation spectra with ATP and ITP, the time intervals were chosen starting from 3 times of the time constants of E2P formation for ATP (0.10 s) and ITP (0.51 s) (see chapter 3.3.3), and ending before significant hydrolysis of E2P. Therefore, the E2P formation spectra were averaged from 0.32–2.54 s for ATP, and from 1.51–16.3 s for ITP.

3.2 Control experiments

3.2.1 Control I – the ATPase-free control experiments

With the ATPase-free control I samples the ATP release spectrum was obtained (*black-bold* line) as shown in Fig. 3.2-1. The signals were caused by the photolytic release of ATP in the absence of the ATPase, i.e. absorbance of free ATP minus absorbance of caged ATP. The small positive band at 1636 cm^{-1} in the ATP release spectrum is due to a reaction of the photolysis byproduct with DTT (Barth et al., 1997a, b); the bands at 1526 and 1348 cm^{-1} were assigned to antisymmetric (ν_{as}) and symmetric (ν_s) stretching vibrations of the nitro group of caged ATP (Barth et al., 1990, 1995); the bands below 1300 cm^{-1} show the absorbance changes of phosphate groups of caged ATP and free ATP (Takeuchi et al., 1988; Barth et al., 1990, 1995, 1997a, b). The experimental conditions for control I samples in the absence of the ATPase were different from those of nucleotide binding and Ca_2E1P formation experiments that were in the presence of the ATPase. Therefore, the ATP release spectrum was not used for subtraction of photolysis signals. However, the ATP release spectrum is useful to study the interactions of the bound phosphate groups. By subtracting the ATP release spectrum from the raw ATP binding spectrum with a suitable weighting factor, the signals of caged ATP photolysis can be subtracted and the double difference spectrum generated shows the absorbance difference of bound ATP minus free ATP, as well as the absorbance change of the ATPase upon ATP binding. This will be discussed in detail in chapter 3.4.1.

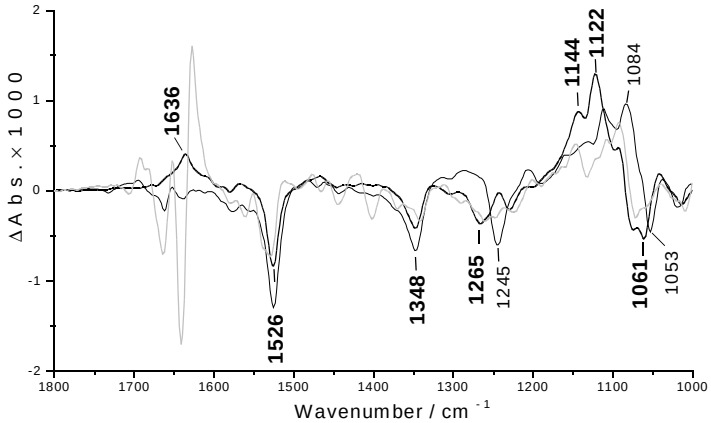

Fig. 3.2-1 Comparison of the ATP photolysis release spectrum (*black-bold* line), the photolysis spectrum (*black-thin* line), and the raw ATP binding spectrum (*grey* line) without subtraction of photolyis signals (1 °C and pH 7.5).

3.2.2 Control II – the AMPPNP-ATPase control experiments

Control II samples only revealed the effects of caged compound photolysis in the presence of the ATPase. As shown in Fig. 3.2-1, the photolysis spectrum obtained with control II samples above

1300 cm^{-1} shows only the photolysis signals at 1526 and 1348 cm^{-1} and no nucleotide binding signals. The bands below 1300 cm^{-1} are in different positions compared with the ATP release spectrum. The reason is that AMPPNP was released in control II experiments, but ATP was released in control I experiments. The -NH group between the β- and γ-phosphate of AMPPNP (Fig. 1.2-5) results in different absorption in the phosphate region below 1300 cm^{-1}, as compared to ATP which has an oxygen atom between the β- and γ-phosphate. Above 1300 cm^{-1} the photolysis signals of control I and II samples are identical with the exception of the byproduct band at 1636 cm^{-1}. This may indicate that the reaction of the byproduct with DTT proceeds via a different route or is slower in the presence of the ATPase. Because the conditions of control II samples are closer to the conditions used in the binding experiments, Ca_2E1P formation experiments and competition experiments than those of control I samples, the control II photolysis spectrum was used to subtract the photolysis signals above 1300 cm^{-1} for all caged nucleotides used here to obtain the "pure" nucleotide binding spectra and Ca_2E1P formation spectra (see chapter 2.4.4).

3.2.3 Control III – origin of absorbance changes with TG-ATPase samples

Fig. 3.2-2 shows the AMPPNP binding spectrum and control III spectrum after subtraction of photolysis signals. In control III samples the Ca^{2+}-ATPase was selectively inhibited by thapsigargin (TG) in the presence of 0.6 mM EGTA (Kijima et al., 1991; Sagara et al., 1991, 1992; Fortea et al., 2001). The control III spectrum (*black-bold* line) does not show binding signals because TG locks the ATPase in the E2TG state and inhibits nucleotide binding. The spectrum obtained without TG but with 0.6 mM EGTA (*grey* line) shows the AMPPNP binding spectrum with the amplitude reduced to approximately 50%. Since TG selectively inhibits the

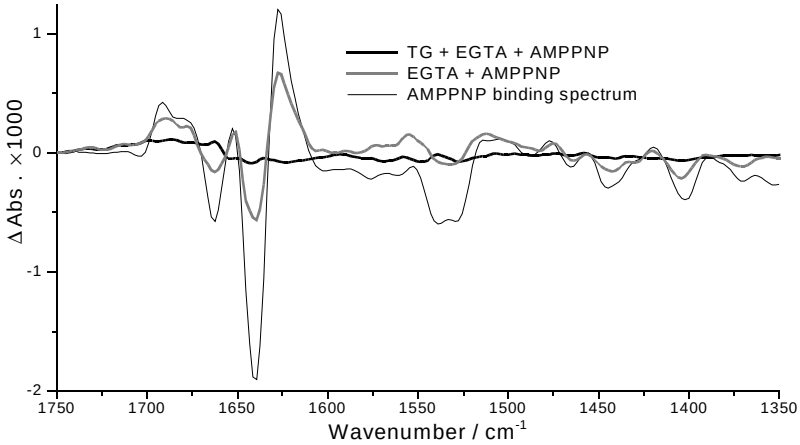

Fig. 3.2-2 The difference spectra with and without TG in the samples after subtraction of the photolysis spectrum: with 3 mM AMPPNP (*black-thin* line), with 1.2 mM TG, 0.6 mM EGTA and 3 mM AMPPNP (*black-bold* line), and with 0.6 mM EGTA and 3 mM AMPPNP (*grey* line).

Ca^{2+}-ATPase, the signals obtained after release of AMPPNP in the absence of TG can be concluded to be induced by AMPPNP binding to the *Ca^{2+}-ATPase.*

In a previous study (Barth et al., 1991), fluorescein isothiocyanate (FITC) was used to determine the origin of binding signals. FITC labels Lys-515 of the Ca^{2+}-ATPase and blocks the nucleotide binding site. FITC labeled samples did not show binding signals either, which indicates that infrared signals are induced by *nucleotide binding* to the Ca^{2+}-ATPase. Moreover, samples in the presence of 20 mM EGTA alone, in which the ATPase was in a Ca^{2+}-free state, did not show significant ATP induced infrared absorbance changes. The absence of Ca^{2+} is known to inhibit the ATPase.

From these control experiments, it can be inferred that the infrared signals observed in this work were caused by nucleotide binding to the Ca^{2+}-ATPase.

3.2.4 Control IV – interactions between caged nucleotide and the Ca^{2+}-ATPase

Control IV samples were prepared with different amount of caged ATP to detect whether caged ATP binds to the ATPase. Binding spectra are shown in Fig. 3.2-3. With up to 15 mM ATP released (50 mM caged ATP), binding signals can be observed. This shows that caged ATP at 50 mM does not bind to the Ca^{2+}-ATPase. Otherwise, the binding signals would be smaller than that in the binding spectrum of 3 mM ATP, which is the saturating concentration of ATP binding to the Ca^{2+}-ATPase as detected in chapter 3.1.2.

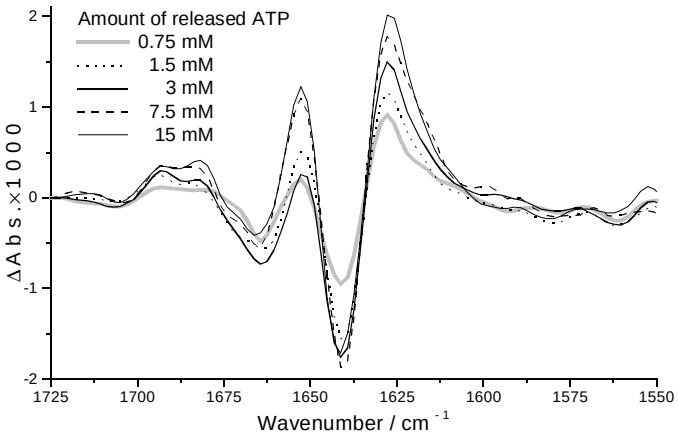

Fig. 3.2-3 ATP binding spectra with different amount of released ATP. The photolysis spectrum has been subtracted.

With 0.75 and 1.5 mM released ATP, the binding spectra show smaller amplitude. This reveals that the amount of ATP is not enough to saturate the binding sites. With 7.5 and 15 mM ATP, larger amplitudes compared to that obtained with 3 mM ATP are in the limits of reproducibility.

It was also investigated whether caged AMPPNP binds to the ATPase as shown in Fig. 3.2-4. In

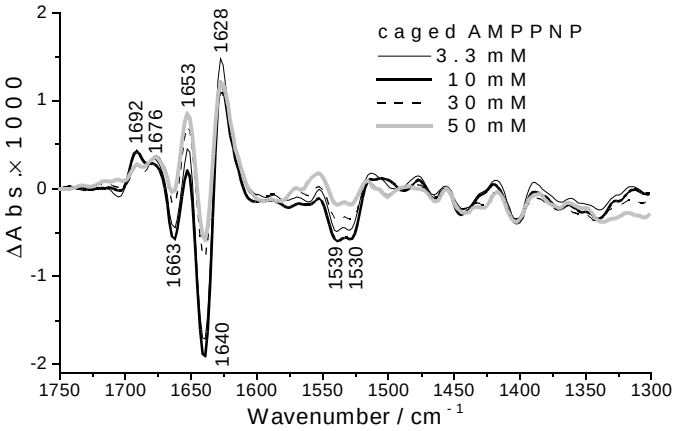

Fig. 3.2-4 AMPPNP binding spectra with different concentrations of caged AMPPNP in the samples (1°C, pH 7.5, 1.2 mM ATPase). The photolysis signals have been subtracted.

the range of 1–10 mM caged AMPPNP the binding-induced infrared spectra were identical within the experimental errors. However, the amplitude decreases to 2/3 when 30 or 50 mM caged AMPPNP were used. This shows that the conformational change upon AMPPNP binding is unaffected by the concentration of caged AMPPNP up to a concentration of 10 mM. Caged AMPPNP binds to the ATPase only when its concentration is higher than 10mM.

3.2.5 Control V – reliability of IR spectroscopy

Control V samples with 0.3 mM ATPase and 0.3 mM AMPPNP were prepared to analyze the reliability of IR spectroscopy on detecting small signals. Fig. 3.2-5 shows the spectra obtained with different amount of AMPPNP binding to different amount of the ATPase. The spectrum

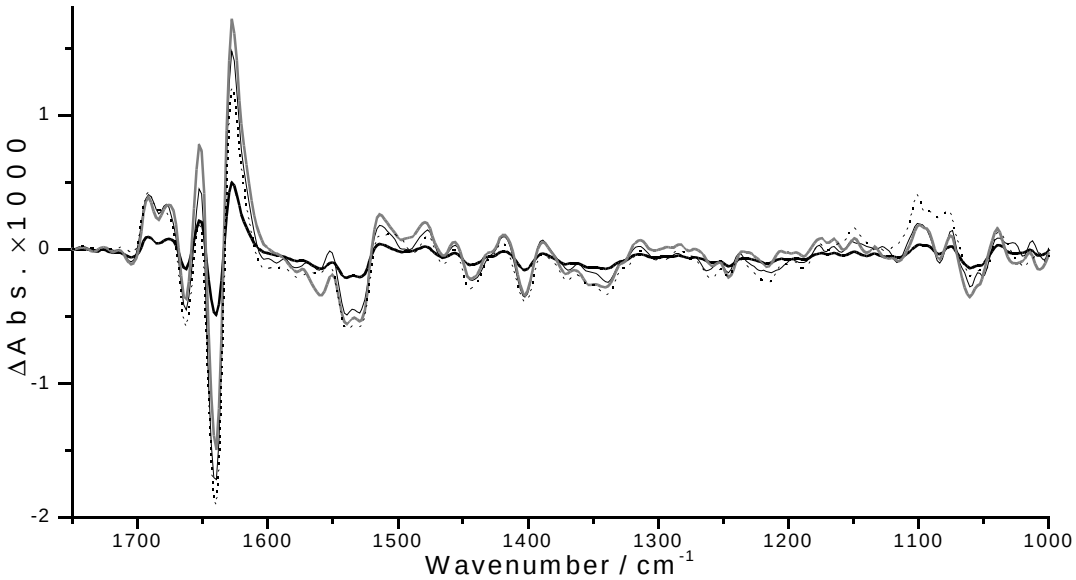

Fig. 3.2-5 Comparison of spectra obtained with 0.3 mM AMPPNP binding to 0.3 mM ATPase (*black-bold* line), with 1 mM AMPPNP binding to 1.2 mM ATPase (*black-thin* line), with 3 mM AMPPNP binding to 1.2 mM ATPase (*dotted* line), and the spectrum obtained with 0.3 mM AMPPNP binding to 0.3 mM ATPase normalized to the ATPase concentration of 1.2 mM (*grey* line).

obtained with only 0.3 mM ATPase and 0.3 mM AMPPNP shows small amplitude of binding signals. However, after normalizing this spectrum to the ATPase concentration of 1.2 mM used for all the other experiments (the concentration of AMPPNP was normalized to 1.2 mM at the same time), the normalized spectrum shows same band positions and similar amplitudes in nearly all spectral regions shown here. This shows that all the small signals obtained with less ATPase and less AMPPNP are real binding bands. Same band amplitudes were observed in the normalized spectrum and the spectrum obtained with 1 mM ATPase and 1 mM AMPPNP. This is due to the same ratio of the amount of the ATPase and AMPPNP in these two experiments. These results show the high reliability of IR spectroscopy to detect small IR absorbance changes.

3.3 Kinetics of three reaction steps in the reaction cycle of Ca^{2+} transport

As described in chapter 2.4.2, the time constants of nucleotide binding, phosphorylation, E2P formation and E2P hydrolysis were obtained by fitting the integral intensities of corresponding marker bands with exponential equations. These results supply the criterion to select the time frame for observing certain protein states and to obtain the corresponding nucleotide binding spectra, Ca_2E1P formation spectra and E2P formation spectra as discussed in chapter 3.1.3.

3.3.1 Kinetics of nucleotide binding to the Ca^{2+}-ATPase

With type I samples, nucleotide binding was observed first. The reaction of nucleotide binding is highlighted in Fig. 3.3-1 as part of the Ca^{2+} transport reaction cycle. As described in chapter 2.4.2, the bands at 1628 and 1641 cm^{-1} were used as marker bands for the nucleotide binding reaction. The kinetic traces and the fitting results are shown in Fig. 3.3-2 with the integral absorbance change of the band at 1628 cm^{-1} as a representative.

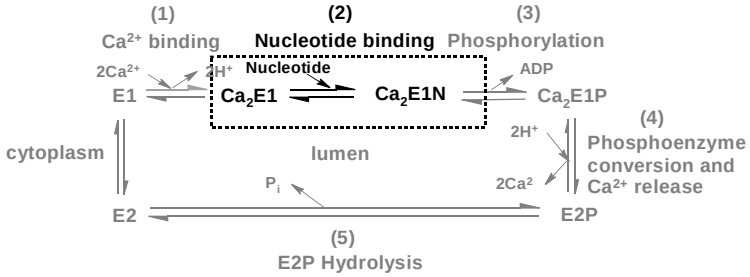

Fig. 3.3-1 The nucleotide binding reaction in the Ca^{2+} transport reaction cycle.

The time constant of nucleotide binding observed with ATP, [β,βγ-$^{18}O_3$]ATP, [γ-$^{18}O_3$]ATP, AMPPNP, ADP and 3'-deoxyATP is ~0.1 s, with ITP and 2'-deoxyATP ~0.25 s. The kinetics of photolytic release was also calculated using the marker bands at 1465, 1381 and 1330 cm^{-1} (Barth et al., 1995). The time constant of photolytic release is ~0.25 s, which is comparable to the calculated time constants of nucleotide binding. This indicates that the photolytic release of nucleotides is the rate-limiting step compared with nucleotide binding. The slowly released nucleotide binds to the ATPase fast and the time constants observed for nucleotide binding actually reflect the photolytic release of nucleotide.

3.3.2 Kinetics of ATPase phosphorylation with different nucleotides

After nucleotide binding, the enzyme was phosphorylated with type I samples. The reaction is shown in Fig. 3.3-3. The time constants of ATPase phosphorylation were measured using the marker bands at 1721 and 1549 cm^{-1} as described in chapter 2.4.2. The kinetics of these two

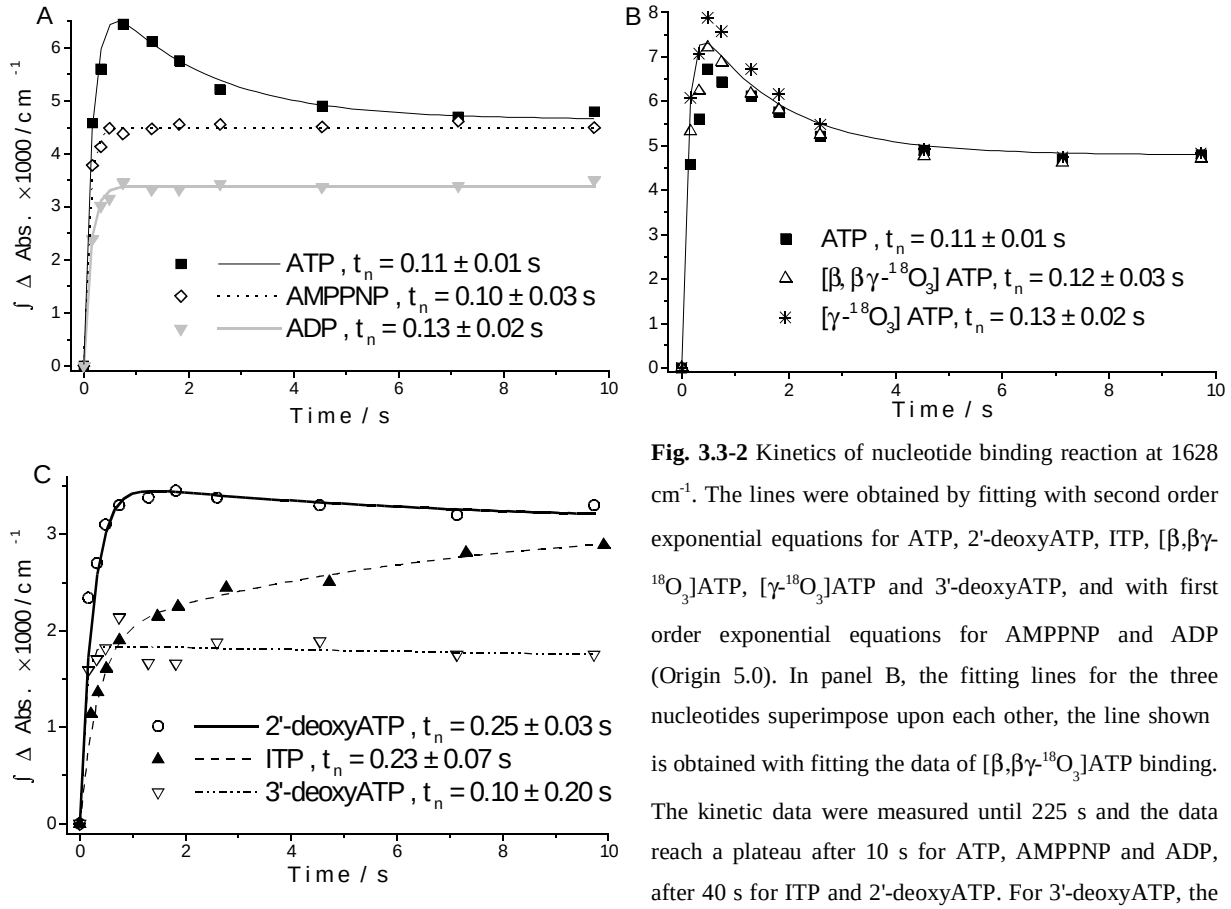

Fig. 3.3-2 Kinetics of nucleotide binding reaction at 1628 cm^{-1}. The lines were obtained by fitting with second order exponential equations for ATP, 2'-deoxyATP, ITP, [β,βγ-$^{18}O_3$]ATP, [γ-$^{18}O_3$]ATP and 3'-deoxyATP, and with first order exponential equations for AMPPNP and ADP (Origin 5.0). In panel B, the fitting lines for the three nucleotides superimpose upon each other, the line shown is obtained with fitting the data of [β,βγ-$^{18}O_3$]ATP binding. The kinetic data were measured until 225 s and the data reach a plateau after 10 s for ATP, AMPPNP and ADP, after 40 s for ITP and 2'-deoxyATP. For 3'-deoxyATP, the data decreased during the measurements.

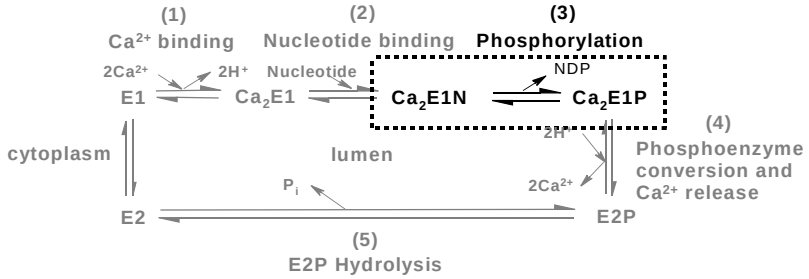

Fig. 3.3-3 Phosphorylation and Ca_2E1P formation in the Ca^{2+} transport reaction cycle.

bands is shown in Fig. 3.3-4 and 3.3-5. The time constants of phosphorylation (t_p) for ATP and ATP analogs except for 3'-deoxyATP were obtained by averaging the kinetic fitting results of both bands at 1721 and 1549 cm^{-1}. With 3'-deoxyATP, t_p was determined by the fitting result of the band at 1721 cm^{-1} for the reasons discussed below (Fig. 3.3-5).

ATPase phosphorylation is fast with ATP (t_p = 2.0 ± 0.37 s), [β,βγ-$^{18}O_3$]ATP (t_p = 1.6 ± 0.23 s) and [γ-$^{18}O_3$]ATP (t_p = 2.1 ± 0.26 s), and is slow with ITP (t_p = 8.66 ± 0.78 s) and 2'-deoxyATP (t_p = 6.67 ± 0.73 s). The isotopic labels at the oxygen atoms of the β- and γ-phosphate do not affect the velocity of enzyme phosphorylation. Slow phosphorylation of the ATPase with ITP

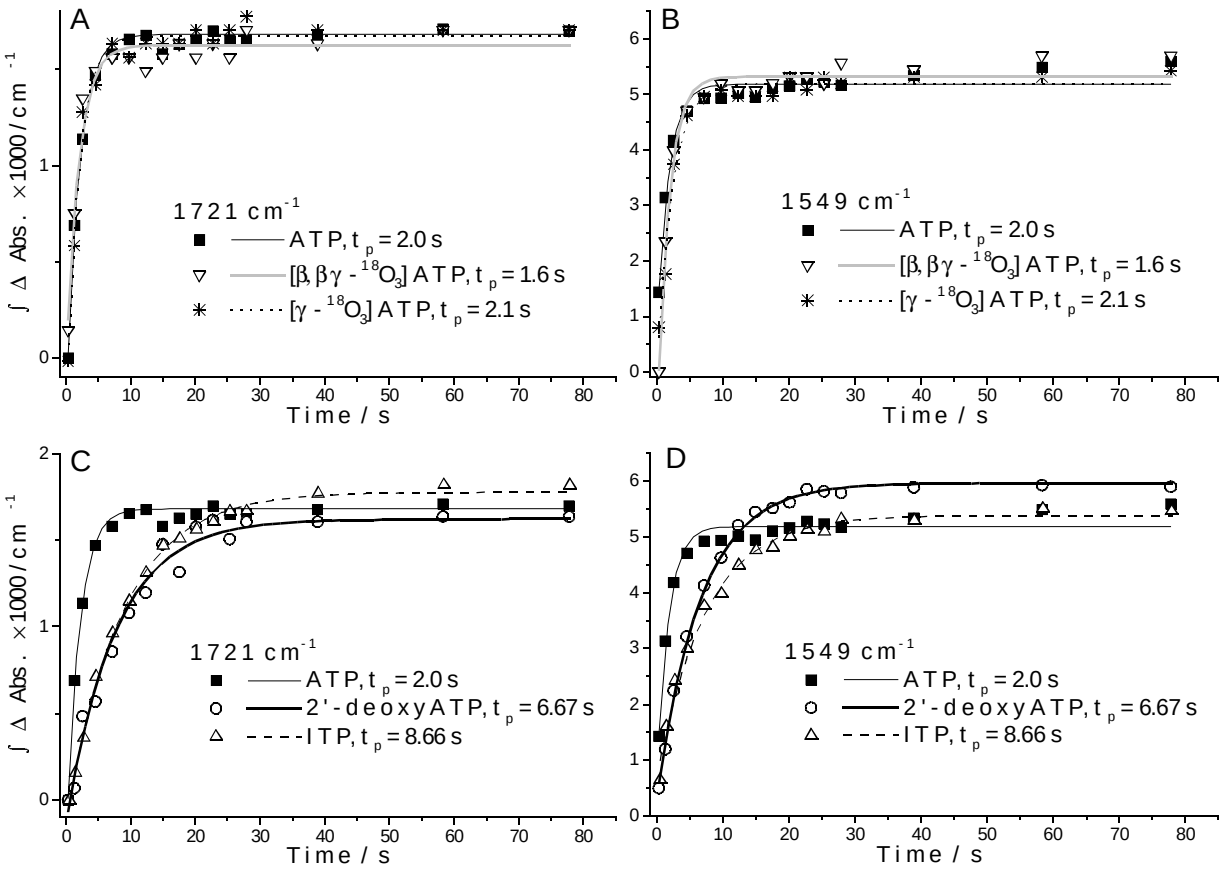

Fig. 3.3-4 Kinetics of ATPase phosphorylation with ATP, [β,βγ-$^{18}O_3$]ATP and [γ-$^{18}O_3$]ATP (A, B), 2'-deoxyATP and ITP (C, D) calculated with the bands at 1721 and 1549 cm^{-1}. The lines are obtained by fitting the bands with the first order exponential equation (Origin 5.0).

and 2'-deoxyATP as shown in Fig. 3.3-4 C and D has been observed before (de Meis et al., 1973; Kubo et al., 1990; Coan et al., 1993) but without specifying the rate for ATP.

With 3'-deoxyATP the ATPase seems not phosphorylated (see chapter 3.5). The band amplitude at 1721 cm^{-1} is only 40% of that with ATP, ITP and 2'-deoxyATP. The kinetics of the bands at 1721 and 1549 cm^{-1} was calculated to compare with the other ATP analogs and it displays

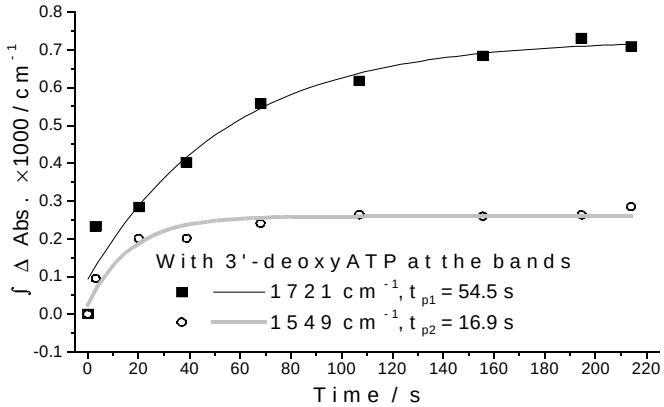

Fig. 3.3-5 Kinetics of the bands at 1721 and 1549 cm^{-1} in the 3'-deoxyATP samples. The lines are obtained by fitting the data with a first order exponential equation (Origin 5.0).

different characteristics. As shown in Fig. 3.3-5, the band at 1721 cm^{-1} evolves slower than that of 1549 cm^{-1}. One explanation is that the band at 1549 cm^{-1} obtained with 3'-deoxyATP samples is not related to the phosphorylation reaction. In line with this, the amplitude of this band is much smaller than that of the band at 1721 cm^{-1}, but with ATP, ITP and 2'-deoxyATP this band has larger amplitude than the band at 1721 cm^{-1}. Because the band at 1721 cm^{-1} has been assigned to the C=O vibration of phosphorylated Asp-351 and used as the marker band of phosphorylation reaction (Barth et al., 1996, 1998; Von Germar et al., 2000), the kinetic fitting result with this band was used for comparison with other ATP analogs. The time constant obtained with the band at 1721 cm^{-1} is 54.5 ± 13.4 s, which is much slower than the time constants of the enzyme phosphorylation obtained with ATP, ITP and 2'-deoxyATP. Slow phosphorylation with ATP analogs indicates the importance of these groups (2'- and 3'-OH, the adenine ring) for fast reaction and the effects on anchoring the γ-phosphate.

3.3.3 Kinetics of E2P formation and E2P hydrolysis

After nucleotide binding and phosphorylation, the next step in the reaction cycle of Ca^{2+} transport is phosphoenzyme conversion and Ca^{2+} release, as shown in Fig. 3.3-6. In this step, the phosphoenzyme changes the conformation from Ca_2E1P to E2P, and the Ca^{2+} ions are released from the ATPase at the same time (Barth et al., 1997b). Then E2P will be hydrolyzed and convert the conformation to the E2/E1 state.

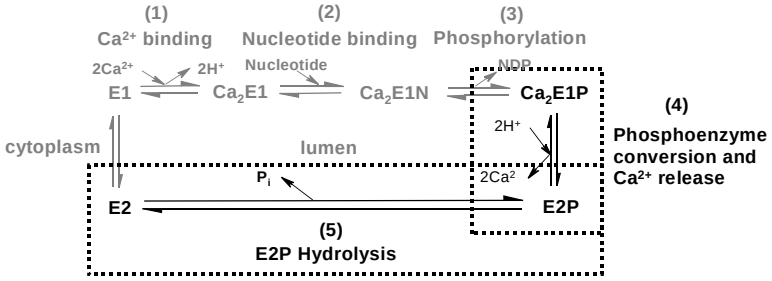

Fig. 3.3-6 Phosphoenzyme conversion, Ca^{2+} release and E2P hydrolysis in the Ca^{2+} transport reaction cycle.

With type II samples (see chapter 2.2.1), 3 mM ATP (one flash) or 6.6 mM ITP (three flashes) were released, and E2P was accumulated. The time constants of E2P formation and E2P hydrolysis with ATP and ITP were obtained by fitting the integral intensities of marker bands at 1711, 1689, 1653, 1571, and 1193 cm^{-1} (Barth et al., 1996) (see chapter 2.4.2).

Fig. 3.3-7 shows the time course of absorbance changes at four bands, which comprising the absorption regions of protonated carboxyl groups of Asp and Glu side chains (1711 cm^{-1}), of the amide I vibration (1689 cm^{-1}), of Asp/Glu carboxylate groups (1571 cm^{-1}), and of the phosphoenzyme phosphate group (1194 cm^{-1}). It is evident that the time course observed needs

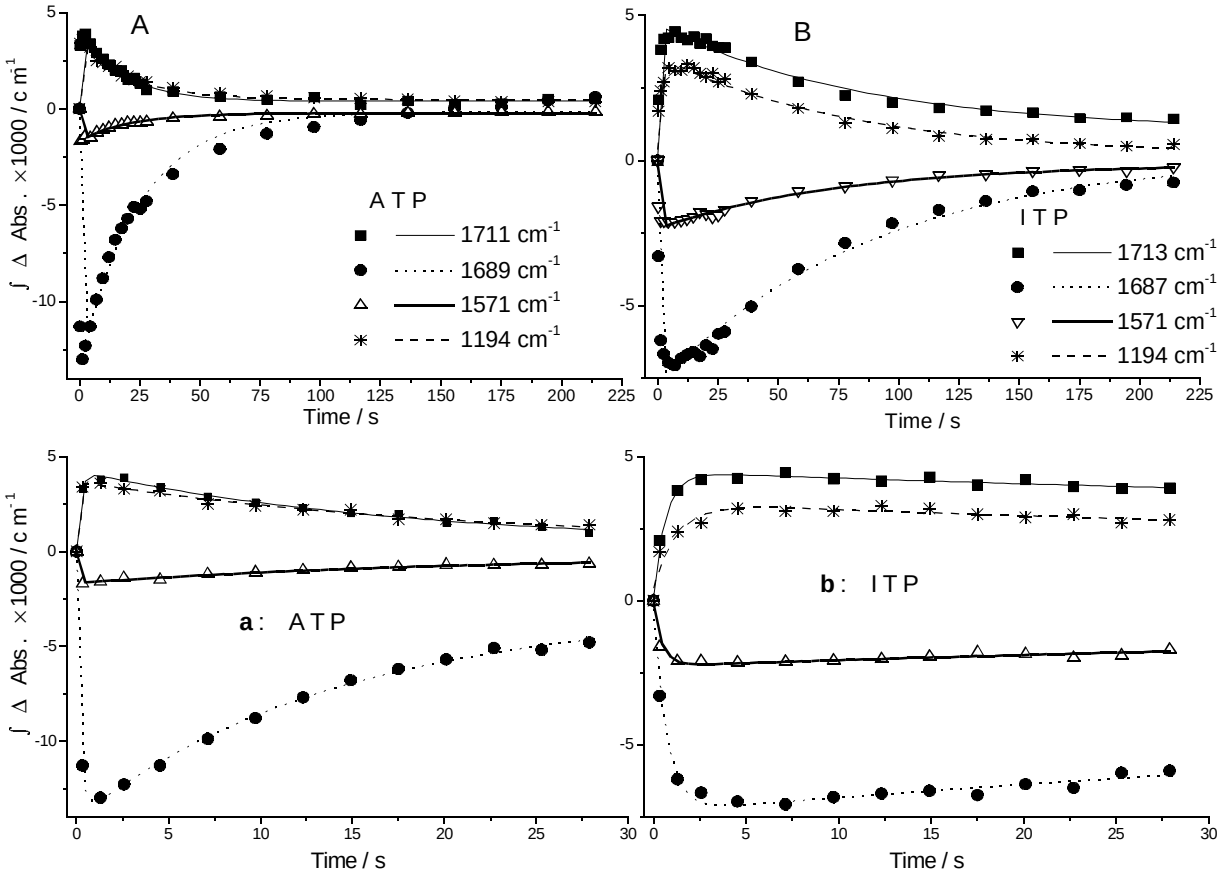

Fig. 3.3-7 Kinetics of E2P formation and E2P hydrolysis with ATP (**A** and **a**) and ITP **(B** and **b**) on different time scales. The lines are obtained by fitting the data with the second order exponential equation (Origin 5.0).

to be analyzed with two time constants. The fast reaction is associated with E2P formation, and the slow reaction is due to the hydrolysis of E2P to Ca_2E1. The time constants of E2P formation ($Ca_2E1 \rightarrow E2P$) and Ca^{2+} release with ATP and ITP are 0.10 s and 0.51 s, respectively, without significant difference. The time constants of the hydrolysis of E2P to Ca_2E1 are 23.7 ± 1.5 s and 89.3 ± 1.76 s with ATP and ITP, respectively. The hydrolysis of E2P with ITP is slower than that with ATP. Since more ITP was released than ATP, it may take longer for ITP to phosphorylate the ATPase.

3.4 Nucleotide binding to the SR Ca^{2+}-ATPase

Nucleotide binding reaction is shown in Fig. 3.4-1. After applying photolysis flash(es), nucleotide is released and binds to the ATPase.

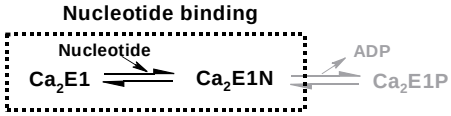

Fig. 3.4-1 The nucleotide binding reaction in the infrared samples.

Nucleotide binding to the ATPase were studied with ATP and ATP analogs (ADP, AMPPNP, ATP isotopomers, ITP, TNP-AMP, 2'- and 3'-deoxyATP, AMP, pyrophosphate, and ribose triphosphate). The spectra reflect the difference in absorbance between the initial nucleotide-free state Ca_2E1 and the nucleotide-ATPase complex Ca_2E1N. Negative bands are characteristic of Ca_2E1, positive bands of Ca_2E1N. Groups or structures not involved in the conformational change do not manifest in the difference spectra. The difference spectra reflect conformational changes of the protein backbone in the amide I (1700–1610 cm^{-1}) and amide II (1580–1500 cm^{-1}) region of the spectra. In addition, environmental and structural changes of side chains and nucleotide contribute in the entire spectral region shown. Except for ATP isotopomer binding, photolysis signals have been subtracted as described in chapter 2.4.4.

3.4.1 ATP, AMPPNP, ADP binding to the Ca^{2+}-ATPase

AMPPNP is unable to phosphorylate the ATPase with the -NH group between the β- and γ-phosphate group. The reaction between the ATPase and AMPPNP stops at the nucleotide binding step. Therefore, the spectrum observed after AMPPNP binding in Fig. 3.4-2 shows only the binding-induced conformational changes of the ATPase.

Fig. 3.4-2 shows that the ATP binding spectrum is in close agreement with the AMPPNP binding spectrum as noted before (Von Germar et al., 2000). Therefore it is attributed to nucleotide binding. In terms of the secondary structure changes shown in the amide I region, the positive band at 1653 cm^{-1} is characteristic of α-helical structure, the signals near 1693, 1682, 1641 and 1628 cm^{-1} are characteristic of β-sheets. Turn structures likely contribute to the high wavenumber signals near 1665 cm^{-1}. The spectrum suggests that α-helices, β-sheets and turns are affected by ATP binding in line with previous findings (Barth et al., 1996; Von Germar et al., 2000).

As shown in Fig. 3.4-2, the ADP binding-induced bands are generally smaller than the ATP

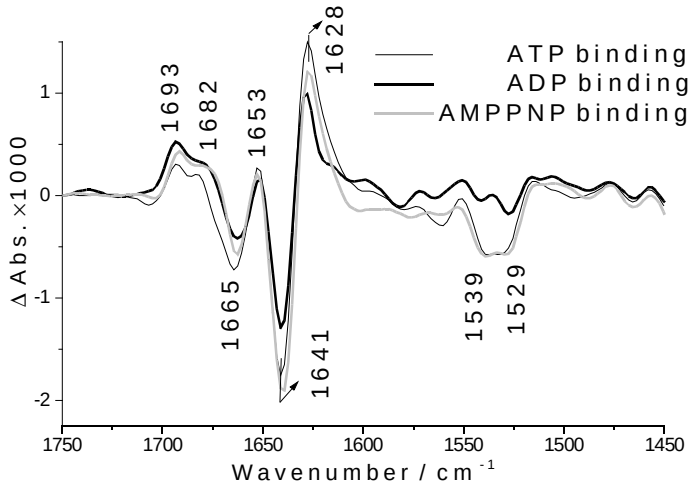

Fig. 3.4-2 Nucleotide binding spectra of ATP, ADP and AMPPNP (1°C, pH 7.5, 3 mM nucleotide, 1.2 mM ATPase and 10 mM Ca^{2+}).

binding-induced bands. Even smaller bands were obtained in a previous study (Von Germar et al., 2000) in which 3 mM ADP were released resulting in non-saturating ADP binding signals. Here up to twofold more ADP (8.75 mM) than ATP (3 mM) was released to obtain saturating ADP binding signals. The similar shape of the two binding spectra indicates that the conformational change induced by ADP and ATP binding is very similar, although the extent is different.

Judged from the band area of the difference bands in the amide I region, the conformational change with ADP is 80% of that with ATP. The residual 20% is the contribution of the γ-phosphate of ATP to the conformational change. The most obvious deviations between the ADP and ATP binding spectrum are shown at 1641 and 1628 cm^{-1} in the amplitudes and on the low wavenumber side of the band at 1628 cm^{-1} where the shoulder in the ATP binding spectrum is reduced in the ADP binding spectrum. The differences at these band positions indicate that γ-phosphate binding affects β-sheets.

Von Germar *et al.* have detected a different shape at 1680 cm^{-1} of the ATP and AMPPNP binding spectrum in a previous study (Von Germar et al., 2000) and suggested that a different protonation state of the γ-phosphate group of ATP and AMPPNP could cause this deviation, which results in ATP being more charged than AMPPNP. With ADP, the spectrum here is similar to that of AMPPNP, strengthening the argument that this region is sensitive to the γ-phosphate binding mode.

Difference between bound ATP and free ATP

To analyze the absorbance change below 1300 cm^{-1} induced by ATP phosphate groups in binding reaction, the ATP release spectrum obtained with control I samples in the absence of the

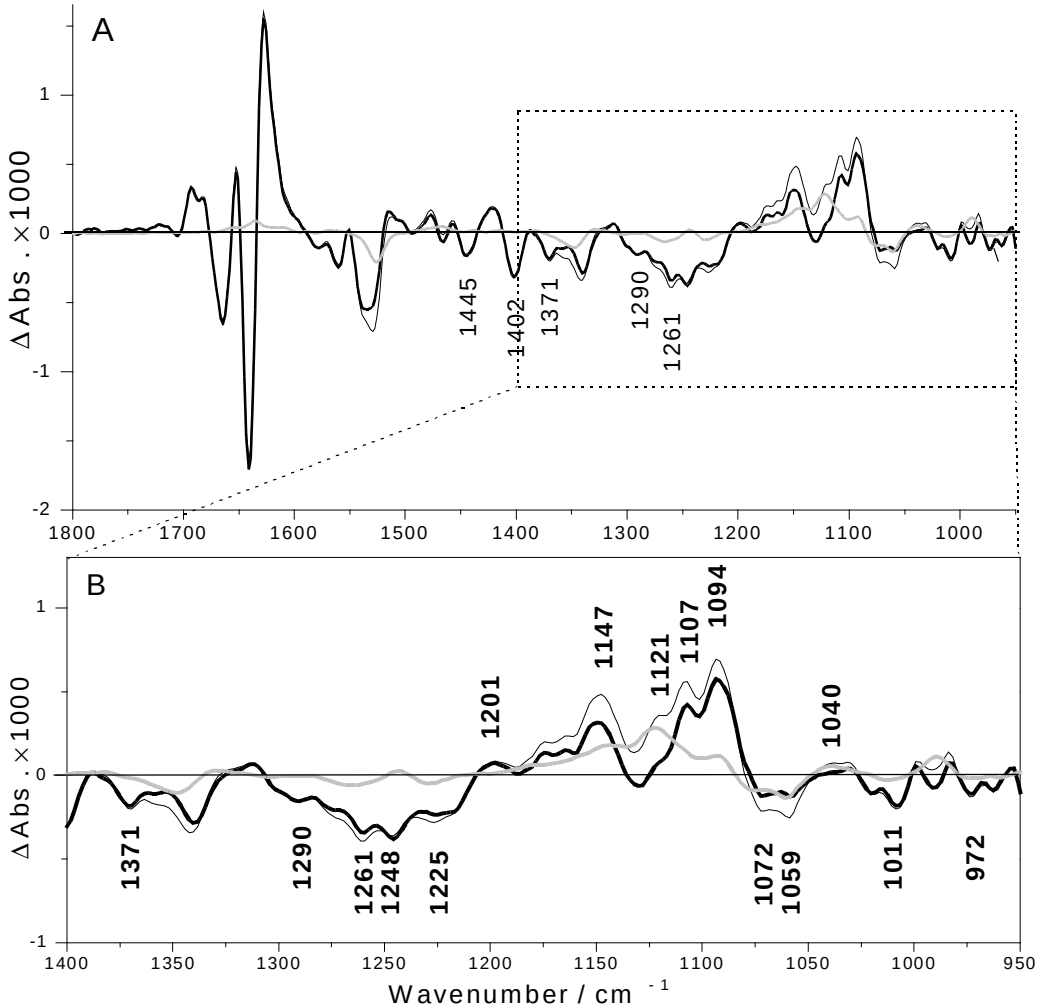

Fig. 3.4-3 Comparison of the raw ATP binding spectrum and the ATP release spectrum (1°C, pH 7.5, 3 mM ATP, 10 mM Ca^{2+}). **A**, spectra from 1800 to 950 cm^{-1}. **B**, spectra from 1400 to 950 cm^{-1}. *Black-thin* line, the raw ATP binding spectrum; *grey* line, the ATP release spectrum multiplied by a factor of 0.25; *black-bold* line, the raw ATP binding spectrum minus the ATP release spectrum the latter multiplied with a factor of 0.25. The labels refer to the raw ATP binding spectrum.

ATPase (see chapter 3.2.1) is used here to compare with the raw ATP binding spectrum (without subtraction of photolysis signals) in the presence of the ATPase and to study the interactions between the bound phosphate groups and the ATPase. Comparing the ATP release spectrum (caged ATP → ATP, *grey* line) with the raw ATP binding spectrum (Ca_2E1 + caged ATP → Ca_2E1ATP, *black-thin* line) in Fig. 3.4-3, phosphate groups of bound ATP and free ATP absorb at different wavenumbers below 1300 cm^{-1}. It was observed that phosphate groups of bound GTP (GTP binds to Ras) and free GTP absorb at different wavenumbers too (Cepus et al., 1998; Allin et al., 2001). Positive bands in the ATP release spectrum show the absorbance of free ATP, whereas in the raw ATP binding spectrum positive bands show the absorbance of bound ATP and possibly of little excess free ATP. In the presence of the ATPase, interactions between the ATPase and bound ATP change the electron density distribution of ATP, which results in changes of the vibrational frequencies of ATP, especially of phosphate groups

absorption, and of the coupling modes of the phosphate groups' vibration. Thus, the raw ATP binding spectrum and the ATP release spectrum differs considerably in the region of phosphate absorption. By subtracting the ATP release spectrum from the raw ATP binding spectrum with a suitable weighting factor, the signals of caged ATP photolysis can be subtracted and the double difference spectrum generated shows the absorbance difference between bound ATP and free ATP. The phosphate groups of ATP (bound or free) absorb below 1300 cm^{-1} and are likely to dominate the spectrum there because of their high absorption index or extinction coefficient. The subtraction factor was judged by the 1525 cm^{-1} region of the processed spectrum corresponding to that region in the spectrum obtained with [^{15}N]caged ATP (Von Germar et al., 2000), as discussed in chapter 2.4.4. According to this criterion a factor of 0.25 was used. By comparing the double difference spectrum with the subtraction factor of 0.25 (*black-bold* line) with the ATP release spectrum (*grey* line) as shown in Fig. 3.4-3B, it can be concluded that the positive

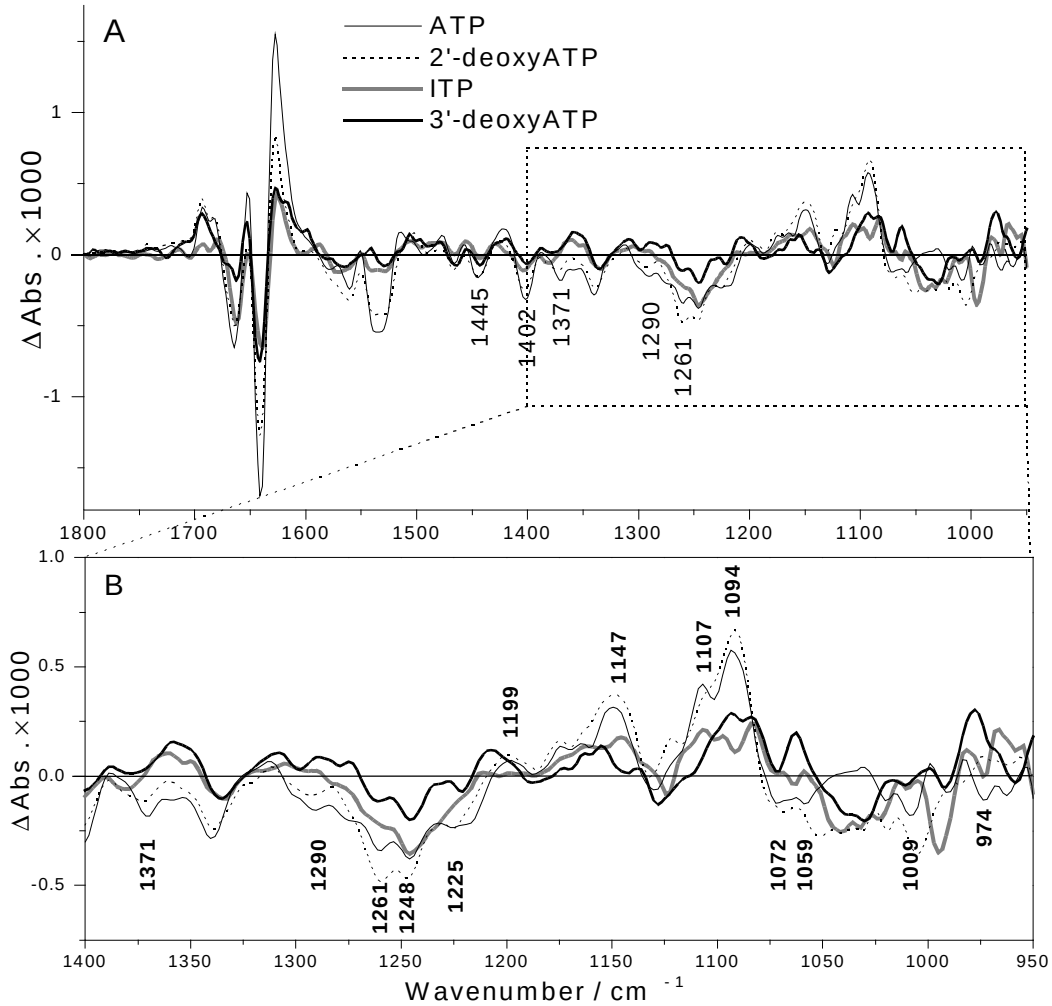

Fig. 3.4-4 Double difference spectra between the raw nucleotide binding spectra and the ATP photolysis release spectrum (1°C, pH 7.5, 10 mM Ca^{2+}). **A**, spectra from 1800 to 950 cm^{-1}. **B**, spectra from 1400 to 950 cm^{-1}. *Solid-thin* line, bound ATP minus free ATP the latter multiplied by a factor of 0.25; *dotted* line, bound 2'-deoxyATP minus free ATP the latter multiplied by a factor of 0.8; *solid-bold* line, bound 3'-deoxyATP minus free ATP the latter multiplied by a factor of 0.88; *grey* line, bound ITP minus free ATP the latter multiplied by a factor of 0.77. The labels refer to the spectrum of bound ATP minus free ATP.

bands around 1130–1100 cm^{-1} in the raw ATP binding spectrum are mainly from free ATP. In the range of 1210–1130 cm^{-1}, 1100–1080 cm^{-1}, and 1000–950 cm^{-1}, the signals of free and bound ATP overlap.

The amplitudes of negative bands in Fig. 3.4-3A between 1500 and 1350 cm^{-1}, for example the bands at 1445, 1402 and 1371 cm^{-1}, as well as of the bands in amide I region, are not affected by the subtraction. Therefore, these bands are attributed to structural changes of the protein. The negative bands between 1300 and 1200 cm^{-1}, and below 1080 cm^{-1} show mainly absorbance changes of caged ATP's phosphate groups.

Similar calculations were done with ITP and deoxyATPs to study the difference between bound nucleotide and free ATP as shown in Fig. 3.4-4. Above 1300 cm^{-1} IR signals are mainly due to the ATPase absorbance except for the photolysis bands at 1525 and 1345 cm^{-1}. Below 1300 cm^{-1}, the signals show mainly the absorbance of phosphate groups. In the photolysis spectra of ATP analogs the phosphate bands are expected to be similar to those of ATP below 1300 cm^{-1}. The positive bands below 1300 cm^{-1} show the absorbance of phosphate groups of bound ATP or bound ATP analogs. Similar positive bands were observed between bound 2'-deoxyATP and bound ATP as expected. The positive bands at ~1147 cm^{-1} and from 1110–1080 cm^{-1} observed with ATP and 2'-deoxyATP are not observed with ITP and 3'-deoxyATP. Since these regions show the absorbance of the γ-phosphate group (see chapter 3.4.5), the differences may indicate that the γ-phosphate of bound ITP and 3'-deoxyATP has different interactions with the ATPase compared with that of bound ATP.

3.4.2 Binding of deoxyATPs to the Ca^{2+}-ATPase

Fig. 3.4-5 shows IR absorbance changes induced by binding to the Ca^{2+}-ATPase of 2'- and 3'-deoxyATP. It is evident that the main difference among the binding spectra is the smaller conformational changes induced by deoxyATPs as compared with those by ATP. The lost of conformational changes are due to the substitution of 2'-OH and 3'-OH groups by hydrogen atom.

The 2'-deoxyATP binding spectrum has a very similar shape as the ATP binding spectrum, but only ~2/3 of the amplitude is obtained between 1670 and 1620 cm^{-1} in the amide I region and ~1/2 between 1550 and 1520 cm^{-1} in the amide II region. This indicates that interactions between the 2'-OH group and the ATPase affect the conformation of α-helix, β-sheets and turn structures when ATP binds. However, the bands at 1693 and 1682 cm^{-1} have the same amplitude. This demonstrates that the vibrational modes of these two bands may be less sensitive to the

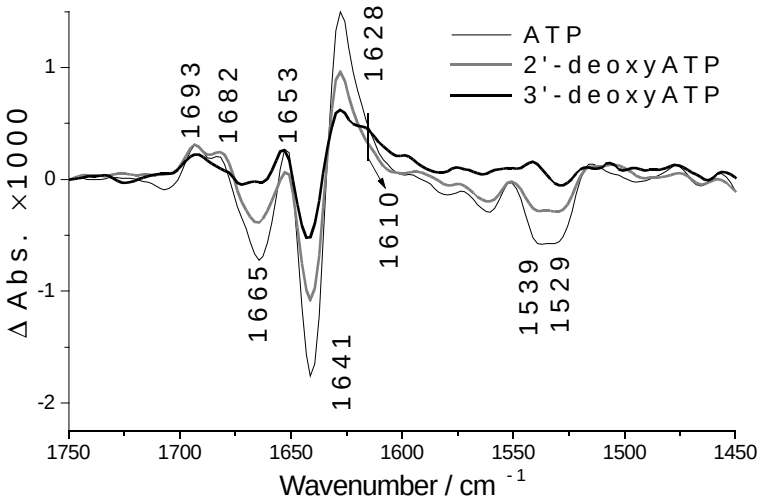

Fig. 3.4-5 Nucleotide binding spectra of ATP, 2'-deoxyATP and 3'-deoxyATP (1°C, pH 7.5, 3 mM nucleotide, 10 mM Ca^{2+}).

substitution of 2'-OH group by hydrogen atom than those of the bands at 1641 and 1628 cm^{-1}, which are all bands owing to the β-sheets changes.

The 3'-deoxyATP binding spectrum has much smaller band amplitudes than the ATP binding spectrum in the entire spectral region shown here, except at 1653 and ~1610 cm^{-1}. This spectrum indicates that smaller conformational changes of β-sheets and turns were induced with the substitution of hydrogen atom at 3'-position of the ribose ring. However, the similar band amplitude at 1653 cm^{-1} implies that the α-helical structures do not exhibit strong interaction with the 3'-OH group. The band at ~1610 cm^{-1} may be assigned to a side chain of the peptide since it is outside the amide I region.

As discussed above, it can be concluded that both 2'- and 3'-OH groups are important for acquirement of the full extent of binding-induced conformational changes. Dramatic effects were observed when 3'-OH is removed.

3.4.3 ITP binding to the Ca^{2+}-ATPase

ITP binding to the ATPase induces small conformational changes in the amide I region with only 1/3 of amplitude of the ATP binding spectrum as shown in Fig. 3.4-6, similar as 3'-deoxyATP binding. ITP binding does not affect amide II bands vibrations because there are no significant bands observed in the amide II region. The same result is observed for 3'-deoxyATP. The adenine moiety has been found to be prominent in ligand recognition by comparing the binding effect of ATP, ITP and GTP (de Meis et al., 1973; Mukohata et al., 1986).

ITP binding induces a band at ~1680 cm^{-1} different from ATP binding but similar to AMPPNP and ADP binding. As discussed before, this area is sensitive to the binding of γ-phosphate. The

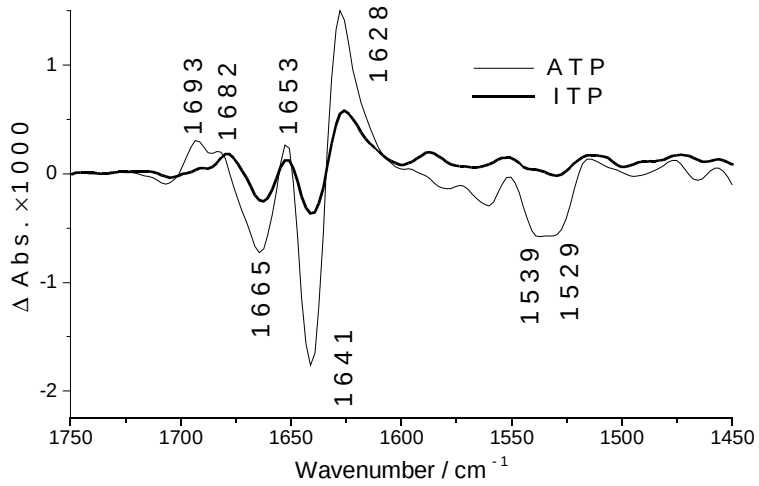

Fig. 3.4-6 Nucleotide binding spectra of ATP (3 mM) and ITP (6.6 mM) (1°C, pH 7.5, 1.2 mM ATPase, 10 mM Ca^{2+}).

difference here may indicate that the change in the adenine moiety at one end of ATP molecule could affect the binding of γ-phosphate at the other end of ATP molecule. The absence of the band at 1693 cm^{-1} indicates that interactions between the adenine ring and β-sheets become weaker or disappear when the adenine ring is substituted by the inosine ring, consistent with the much smaller bands at 1641 and 1628 cm^{-1}.

3'-deoxyATP and ITP both induce small conformational changes but the affinity of 3'-deoxyATP to the ATPase is higher for 3 mM 3'-deoxyATP gives saturating signals whereas for ITP 6.6 mM are needed. With 3 mM ITP, the binding signals are weaker (Fig. 3.1-1).

3.4.4 TNP-AMP binding to the Ca^{2+}-ATPase

As described above, nucleotide binding was triggered by photolytic release from caged nucleotides to detect the small infrared absorbance changes with high sensitivity. Unfortunately, a caged derivative of TNP-AMP is not available. Therefore TNP-AMP binding was investigated in a competition experiment, in which AMPPNP replaces TNP-AMP from the binding site as described in chapter 2.2.3 and 2.4.3. AMPPNP is released from caged AMPPNP and this triggers AMPPNP binding to the ATPase in the presence of TNP-AMP. AMPPNP is an excellent model for ATP because it induces very similar conformational changes (Fig. 3.4-2) and binds to the same site as ATP (Clore et al., 1982). AMPPNP as a non-phosphorylating analogue of ATP can also prolong the observation time for the nucleotide-ATPase complex compared with ATP and therefore enables a better signal-to-noise ratio of the nucleotide binding spectrum. From the comparison of AMPPNP binding in the presence and absence of TNP-AMP, a TNP-AMP binding spectrum can be constructed.

Competition between TNP-AMP and AMPPNP

TNP-AMP titration in TNP-AMP → AMPPNP competition experiments: In order to perform an experiment in which AMPPNP replaces TNP-AMP at the binding site of the Ca^{2+}-ATPase, the concentration of TNP-AMP necessary for saturating the nucleotide binding sites was first established. For this, different concentrations of TNP-AMP were used while the concentration of caged AMPPNP was 10 mM (3 mM released AMPPNP).

Fig. 3.4-7A shows the raw AMPPNP (3 mM) binding spectrum in the absence of TNP-AMP without subtraction of photolysis signals and the photolysis spectrum that was used for subtraction to obtain the "pure" AMPPNP binding spectrum. It is clear that the subtraction of the photolysis spectrum will affect neither the amplitude nor the band positions of the AMPPNP binding spectrum or the TNP-AMP → AMPPNP competition spectra in the amide I region.

Fig. 3.4-7B displays the AMPPNP binding spectrum and TNP-AMP → AMPPNP competition spectra obtained at different TNP-AMP concentrations. The associated absorbance changes cause negative and positive bands in the difference spectra, which are characteristic of the conformation of the enzyme before and after AMPPNP binding, respectively. As shown in Fig. 3.4-7B, increasing TNP-AMP concentration to 5 mM reduces the amide I signals considerably, which should be because TNP-AMP bound to the nucleotide binding site inhibits AMPPNP binding. The positions of the largest bands shift from 1640 and 1627 cm^{-1} in the AMPPNP binding spectrum (no TNP-AMP present) to 1639 and 1626 cm^{-1} in the competition spectra, which indicates that AMPPNP replaces TNP-AMP from its binding site. If AMPPNP binds to empty binding sites, no shifts in band position would be expected. No further shift in band position is observed at 10 and 30 mM TNP-AMP. Therefore 5 mM TNP-AMP seem to saturate the ATP binding sites. At higher TNP-AMP concentrations, the amplitude of the competition signals decreases further because less TNP-AMP was replaced by AMPPNP from the binding site. This experiment confirms that TNP-AMP and AMPPNP compete for the same binding site on the protein (Bishop et al., 1987; Suzuki et al., 1990), or at least that there is sufficient overlap between the binding sites to ensure efficient competition.

Fig. 3.4-7C shows the dependence of the fraction of ATPase bound with AMPPNP ($[EA]/[E_t]$, see chapter 2.4.6) on the concentration of TNP-AMP. The signals obtained with 2.5 mM TNP-AMP and 3 mM released AMPPNP are reduced to approx. 50% of that obtained with only 3 mM AMPPNP, which demonstrates similar affinities of the two nucleotides. The fit shown in Fig. 3.4-7C gave the ratio of the dissociation constants: $k_{AMPPNP} / k_{TNP\text{-}AMP} = 1.15$ (see chapter 2.4.6).

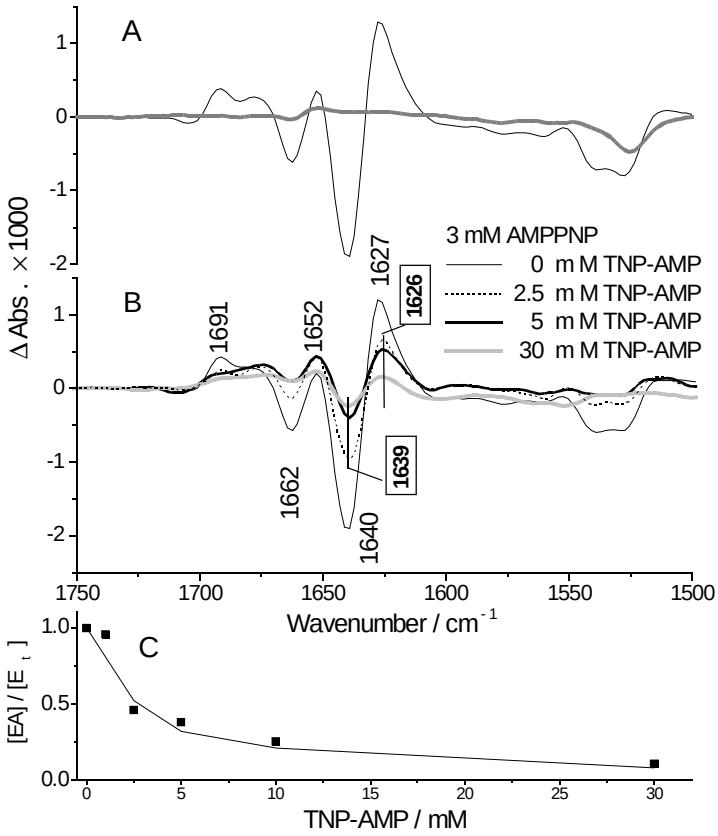

Fig. 3.4-7 Binding of 3 mM AMPPNP to the Ca^{2+}-ATPase in the presence of different amount of TNP-AMP (1°C, pH 7.5). Panel A and B are drawn to the same scale. **A**, effects of subtraction of the photolysis spectrum: the raw AMPPNP (3 mM) binding spectrum in the absence of TNP-AMP without subtraction of photolysis signals (*black* line), and the photolysis spectrum (*grey* line) multiplied by a factor of 0.37 which was used for subtraction. **B**, the AMPPNP binding spectrum and TNP-AMP→AMPPNP competition spectra. Labels in boxes show the band positions of competition spectra; the labels without box show the band positions of the AMPPNP binding spectrum (no TNP-AMP). Photolysis signals were subtracted. **C**, dependence of the fraction of ATPase bound with AMPPNP on the concentration of TNP-AMP, showing the inhibition of AMPPNP binding by TNP-AMP. The line shows the fit that gave the ratio of dissociation constants: $k_{AMPPNP} / k_{TNP\text{-}AMP} = 1.15$.

In samples with diluted SR vesicles, the dissociation constant of TNP-AMP is on the order of 10 nM for the Ca^{2+}-free enzyme E1 (Suzuki et al., 1990) and the Ca^{2+} loaded form Ca_2E1 (Bishop et al., 1987), whereas that of AMPPNP for E1 is in the low micromolar range, similar to that of ATP and AMPPCP (Mintz et al., 1995). These measurements have detected for the Ca^{2+}-free form a large distinction in affinities between TNP-AMP and AMPPNP. However, this work detected similar affinities of TNP-AMP and AMPPNP for Ca_2E1. A higher affinity of AMPPNP for Ca_2E1 than for E1 is possible and has been found in the presence of Mg^{2+}, as concluded from the lower half-saturating Ca^{2+} concentration in the presence of AMPPNP (Mintz et al., 1995). The discrepancy is the comparably high concentrations of protein and ligands used in the samples here, which may apparently reduce the affinity of the ATPase for nucleotides to the millimolar range. This was observed for ADP that 8.75 mM are necessary to obtain saturating binding-induced infrared signals here in spite of a dissociation constant in diluted samples in the 100 µM range (Pickart et al., 1984; Wakabayashi et al., 1990). The protein concentration used in the infrared experiments may be high if compared with other experiments, but corresponds to the high concentration of total proteins in cells that causes macromolecular crowding (reviewed in Ellis, 2001).

AMPPNP titration in TNP-AMP → AMPPNP competition experiments: Having identified the

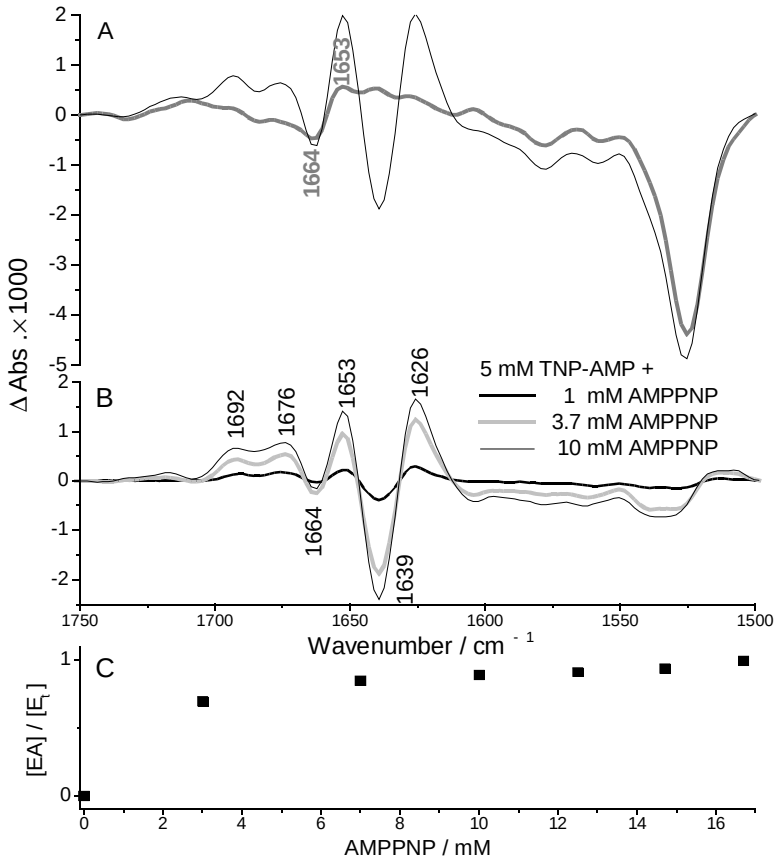

Fig. 3.4-8 TNP-AMP → AMPPNP competition spectra in the presence of 5 mM TNP-AMP (1°C, pH 7.5). **A**, effects of subtraction of the photolysis spectrum: the difference spectrum of 10 mM AMPPNP release in the presence of 5 mM TNP-AMP without subtraction of the photolysis spectrum (*black* line), and the photolysis spectrum multiplied by a factor of 1.64 which was used for the subtraction (*grey* line). **B**, TNP-AMP→ AMPPNP competition spectra of the titration with AMPPNP, the labels show the band positions of competition spectra. **C**, dependence of the fraction of ATPase with bound AMPPNP ([EA]/[E_t]) on the concentration of released AMPPNP in the presence of 5 mM TNP-AMP.

TNP-AMP concentration that saturates the binding site, the concentration of AMPPNP for a close to 100% exchange with TNP-AMP was established in a titration experiment. With a fixed concentration of 5 mM TNP-AMP, the concentration of released AMPPNP was increased by applying consecutive photolysis flashes (see chapter 2.4.3). Fig. 3.4-8A shows the spectrum upon release of ~10 mM AMPPNP in the presence of 5 mM TNP-AMP and the photolysis spectrum that was subtracted to obtain the "pure" competition spectrum with 5 mM TNP-AMP and 10 mM released AMPPNP in Fig. 3.4-8B. The small bands at 1664 and 1653 cm^{-1} in the photolysis spectrum may affect the amplitude but not the band positions of the TNP-AMP → AMPPNP competition spectra when the photolysis spectrum is subtracted from the raw difference competition spectrum. As shown in Fig. 3.4-8B, the signal amplitude of the competition spectra increases with the increasing amount of released AMPPNP showing that AMPPNP replaces TNP-AMP from the binding sites. In Fig. 3.4-8C the fraction of ATPases that bind AMPPNP ([EA] / [E_t]) is plotted against the concentration of released AMPPNP. The proportion of the AMPPNP-ATPase complex increases until ~10 mM AMPPNP is released and exhibits a plateau from 10 mM of released AMPPNP onwards. Therefore 10 mM of released AMPPNP nearly completely replace 5 mM TNP-AMP from the binding sites and give saturating TNP-AMP → AMPPNP competition signals.

TNP-AMP binding spectrum

According to Fig. 3.4-8C, releasing 10 mM AMPPNP is sufficient to nearly completely substitute 5 mM TNP-AMP from the binding sites of the ATPase. The respective TNP-AMP → AMPPNP competition spectrum shows similar band positions and band amplitudes as the AMPPNP binding spectrum. Both are shown in Fig. 3.4-9A. This similarity implies that AMPPNP binding causes similar conformational changes no matter whether TNP-AMP is initially bound to the ATPase or not. Therefore the conformation of the Ca_2E1TNP-AMP complex is similar to that of Ca_2E1. However, upon closer inspection, there are band shifts and amplitude differences between the competition spectrum (*black-thin* line) and the AMPPNP binding spectrum (*grey* line). For example, the bands at 1640 and 1627 cm^{-1} in the AMPPNP binding spectrum shift to 1639 and 1626 cm^{-1} in the competition spectrum; the amplitude of bands at 1692, 1675 and 1653 cm^{-1} in the competition spectrum is larger than that of bands at 1692, 1681 and 1652 cm^{-1} in the AMPPNP binding spectrum; the band at 1607 cm^{-1} is not present in the AMPPNP binding spectrum but is clearly negative in the competition spectrum. The difference between the two experiments is that the dissociation of TNP-AMP from the binding site contributes to the competition spectrum but not to the AMPPNP binding spectrum in which AMPPNP binds to the empty site. The subtle spectral differences between the spectra indicate that TNP-AMP dissociation from the binding site causes conformational changes.

By subtracting the competition spectrum from the AMPPNP binding spectrum (see chapter 2.4.3 and Fig. 2.4-3), the TNP-AMP binding spectrum (*black-bold* line in Fig. 3.4-9A) was obtained, which demonstrates the infrared absorbance changes associated with TNP-AMP binding. The bands in the amide I region of the TNP-AMP binding spectrum indicate that several secondary structure elements are involved in TNP-AMP binding to the ATPase. Structural changes of β-

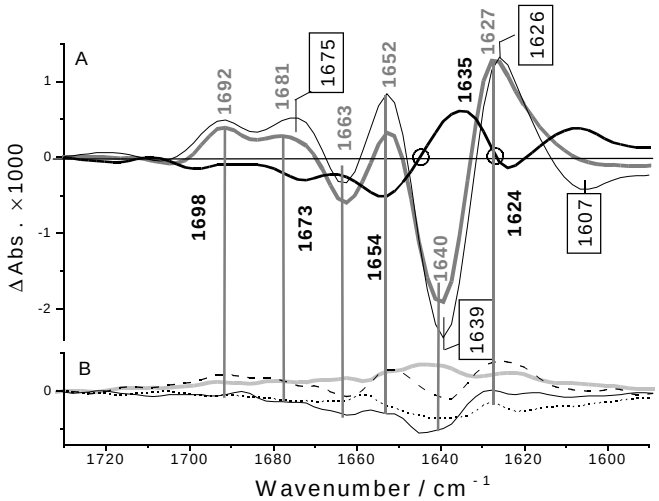

Fig. 3.4-9 A, Comparison of the AMPPNP binding spectrum (*grey* line, grey labels), the TNP-AMP → AMPPNP competition spectrum at 10 mM released AMPPNP (*black-thin* line, labels in a box), and the TNP-AMP binding spectrum (*black-bold* line, bold labels). **B**, the standard deviation of the AMPPNP binding spectrum (*grey* line) and three confidence level spectra (other lines, see chapter 2.4.3), drawn to the same scale of panel A.

sheet regions can induce the bands at 1635 and 1624 cm^{-1}, of α-helical regions that at 1654 cm^{-1}, and of turns that at 1673 cm^{-1}. In line with this, several residues of the ATPase in different secondary structures have been found to be involved in TNP-AMP binding. Thr-441 located in an α-helix is close to the surface of the nucleotide binding site and interacts with the TNP moiety (Toyoshima et al., 2000; Abu-Abed et al., 2002). Lys-515 in a β-strand region, Phe-487 and Arg-560 in loop regions between two β-strands interact with the adenine moiety (McIntosh, 2000; Toyoshima et al., 2000; Abu-Abed et al., 2002).

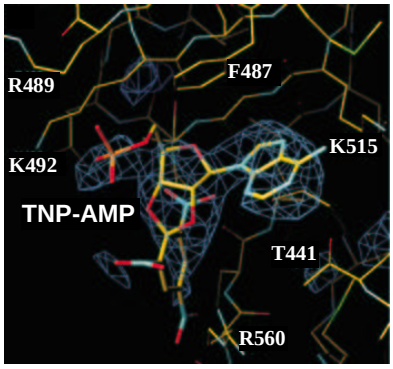

Fig. 3.4-10 Residues involved in TNP-AMP binding to the Ca^{2+}-ATPase, from Toyoshima *et. al. Nature*, 2000, **405**: 647-655. F, Phe; R, Arg; K, Lys; T, Thr.

This TNP-AMP binding spectrum is evidently distinct from the AMPPNP binding spectrum or the ATP binding spectrum, with considerably smaller bands often of opposite sign and at slightly different positions. This indicates that TNP-AMP binding induces smaller extent of conformational changes in a different mode compared with AMPPNP binding. The finding of relatively small conformational changes upon TNP-AMP binding is in agreement with the result (Toyoshima et al., 2000) that the structure of the ATPase with bound Ca^{2+} and TNP-AMP is not significantly different from that in the absence of TNP-AMP, whereas ATP binding to the ATPase causes a conformational change that destroys the crystals (other evidence as stated in chapter 1.2.2).

The TNP-AMP binding spectrum was obtained in a less direct way than the AMPPNP binding spectrum and the competition spectrum, because it is the subtraction between two normalized difference spectra obtained from two sets of experiments. Therefore, the significance of bands in the TNP-AMP binding spectrum is discussed below by assessing the variations of band amplitudes and band positions between different samples in the same set of experiments. Fig. 3.4-9B shows the standard deviation of the AMPPNP binding spectrum (obtained with OPUS 3.1) and the confidence level spectra drawn to the same scale as in Fig. 3.4-9A. Confidence level spectra assess the significance of bands in a double difference spectrum. They were calculated from the four AMPPNP binding spectra obtained with four samples as described in chapter 2.4.3. In these confidence level spectra, small bands at 1663, 1652, 1640, and 1627 cm^{-1} were

observed. These bands are caused by small deviations in band amplitude between the individual experiments. Therefore these bands in the confidence level spectra are usually observed at peak positions of the AMPPNP binding spectrum. Bands of the TNP-AMP binding spectrum are generally larger than those of the confidence spectra in the same spectral region and all bands labeled in bold in Fig. 3.4-9A were also observed in additional experiments in which the released AMPPNP was not enough to saturate the amplitude of the competition spectrum (data not shown). In spite of that the small bands above 1680 cm^{-1} are carefully attributed to a conformational change upon TNP-AMP binding because it is difficult to prove it rigorously. However, the bands at 1635 and 1624 cm^{-1} in the TNP-AMP binding spectrum reveal evidently real diversities between the TNP-AMP → AMPPNP competition spectrum and the AMPPNP binding spectrum. These bands cannot be explained by a different band amplitude in the difference spectra used in the subtraction. Instead their effect can be detected already upon comparing the AMPPNP binding and the competition spectrum, in which they lead to different band positions: peak positions vary for the AMPPNP binding spectra (1640/1627 cm^{-1}) of the four individual experiments from 1639.9 to 1640.4 cm^{-1} and from 1626.9 to 1627.3 cm^{-1} and for the competition spectra (1639/1626 cm^{-1}) of two individual experiments from 1639.2 to 1639.3 cm^{-1}. At 1625.9 cm^{-1} the competition spectra show the same peak position for both experiments. The two peak positions are therefore clearly different in the AMPPNP binding spectrum and the TNPAMP → AMPPNP competition spectrum. Also the 1654 cm^{-1} band of the TNP-AMP binding spectrum is observed at a position different from that at 1652 cm^{-1} in either the AMPPNP binding spectrum or the competition spectrum and the band at 1673 cm^{-1} leads to a clearly different shape in the AMPPNP binding spectrum and the competition spectrum. Subtraction of the photolysis spectrum hardly affects peak positions since it changes the peak position only in one case by 0.1 cm^{-1}. Therefore the different band positions in the AMPPNP binding and the competition spectrum are clear indications of spectral differences.

3.4.5 Binding of other nucleotides to Ca^{2+}-ATPase

AMP, pyrophosphate and ribose triphosphate were used to reveal the impact of the adenosine, β-phosphate and the ribose ring on nucleotide binding, respectively. The structures of these compounds are shown in Fig. 1.2-5. Photolysis of 10–30 mM caged AMP and caged pyrophosphate were used to trigger binding, whereas ribose triphosphate binding was investigated in a competition experiment as TNP-AMP binding because no caged derivative of this compound was available.

With up to 9 mM released AMP no binding signals were observed in the amide I and amide II

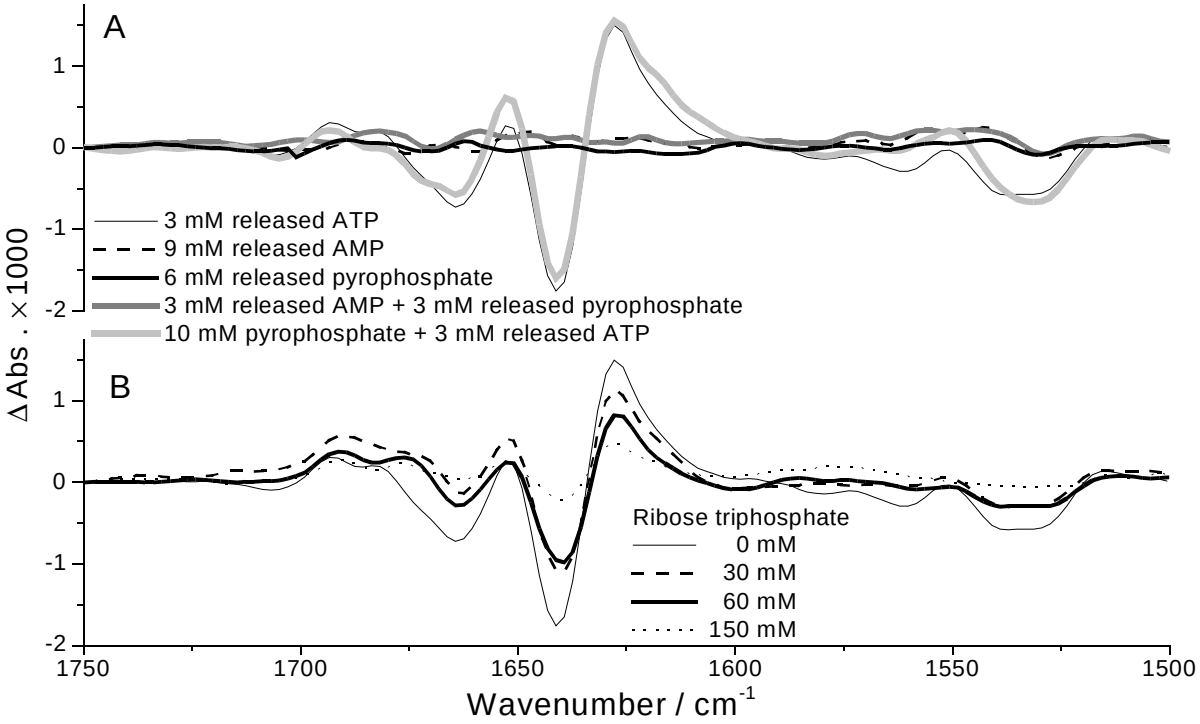

Fig. 3.4-11 AMP, pyrophosphate, and ribose triphosphate binding to the ATPase (1°C, pH 7.5, 10 mM Ca^{2+}). Photolysis signals were subtracted. **A**, spectra with ATP, AMP and pyrophosphate binding. **B**, competition spectra with different amount of ribose triphosphate and 3 mM released AMPPNP.

region (*dashed* line in Fig. 3.4-11A). This clarifies the importance of the β- and γ-phosphate in ATP binding: without the β- and γ-phosphate group the affinity of the ATPase for nucleotide decreases significantly. In line with this, the β-phosphate was thought to be important for anchoring the ATP molecule in the binding pocket (Arrondo et al., 1984; Moutin et al., 1994). A key role of the β-phosphate of GTP was observed with GTP binding to H-Ras p21 (Cepus et al., 1998; Allin et al., 2001).

With up to 6 mM released pyrophosphate no binding signals were observed (*black-bold* line in Fig. 3.4-11A). This indicates the indispensability of both the ribose ring and the adenine moiety to ATP binding to the ATPase. Samples were also prepared with both 10 mM caged AMP and 10 mM caged pyrophosphate (*grey* line in Fig. 3.4-11A), and no binding bands were obtained either. This demonstrates that AMP with pyrophosphate cannot bind to the ATPase as ATP, although the combination of pyrophosphate and AMP closely resembles ATP. The result indicates that it is important for binding to link all three phosphate groups to the adenosine moiety of ATP.

Samples with 10 mM pyrophosphate and 10 mM caged ATP were prepared in competition experiments. After photolysis of caged ATP, the competition spectrum (*light-grey* line in Fig. 3.4-11A) shows similar binding signals compared to the ATP binding spectrum (*black-thin* line

in Fig. 3.4-11A), which was obtained from the samples with only ATP (no pyrophosphate). This indicates that pyrophosphate at 10 mM does not bind to the ATPase, or does not induce significant conformational changes. Otherwise smaller signals would be observed in the competition spectra obtained with pyrophosphate and released ATP, owing to the competition between the two compounds. However, the subtle differences between these two spectra may indicate that there were weak interactions between pyrophosphate and the ATPase before ATP binding.

In the competition experiments with ribose triphosphate and caged AMPPNP, ribose triphosphate was added at concentrations from 30 to 150 mM. As shown in Fig. 3.4-11B, the signal amplitudes decrease with increasing amount of ribose triphosphate and the signals are smaller than those with only AMPPNP in the absence of ribose triphosphate. This elucidates there is competition between AMPPNP and ribose triphosphate binding to the ATPase, and ribose triphosphate binds to the ATPase at high concentrations.

3.4.6 Binding of ATP isotopomers to the Ca^{2+}-ATPase

Two ATP isotopomers, [β,βγ-$^{18}O_3$]ATP and [γ-$^{18}O_3$]ATP, were used for assigning and studying the vibrational modes of phosphate groups. Before discussing binding of ATP isotopomers, photolysis spectra with ATP isotopomers in the absence of the ATPase are investigated. These spectra reveal the bands induced by the β- and γ-phosphate group of caged ATP and free ATP. Then in the binding spectra in the presence of the ATPase, the bands of caged ATP can be distinguished which facilitates the discussion of the isotope effect on nucleotide binding spectra.

Photolysis of ATP isotopomers

Upon photolysis of ATP isotopomers, prominent downshifts of bands due to the isotope effect are expected. Here both the photolysis spectra and the double difference spectra were studied. The double difference spectra were obtained by subtracting the photolysis spectrum obtained with caged ATP from the photolysis spectra obtained with caged ATP isotopomers. The double difference spectra are helpful to understand band shifts. Because bands without shift will not be shown in the double difference spectra, the shifted bands will be highlighted. The double difference spectra are therefore named *isotope effect spectra* here. Fig. 3.4-12 shows how the band shifts are displayed in the isotope effect spectra. A positive band in the photolysis spectrum obtained with caged ATP ([^{16}O]) that downshifts with caged ATP isotopomers ([^{18}O]) in Fig. 3.4-12A, will be presented as a negative band at its original position in the isotope effect spectra in Fig. 3.4-12a; and there should be a positive band in the isotope effect spectra at the lower

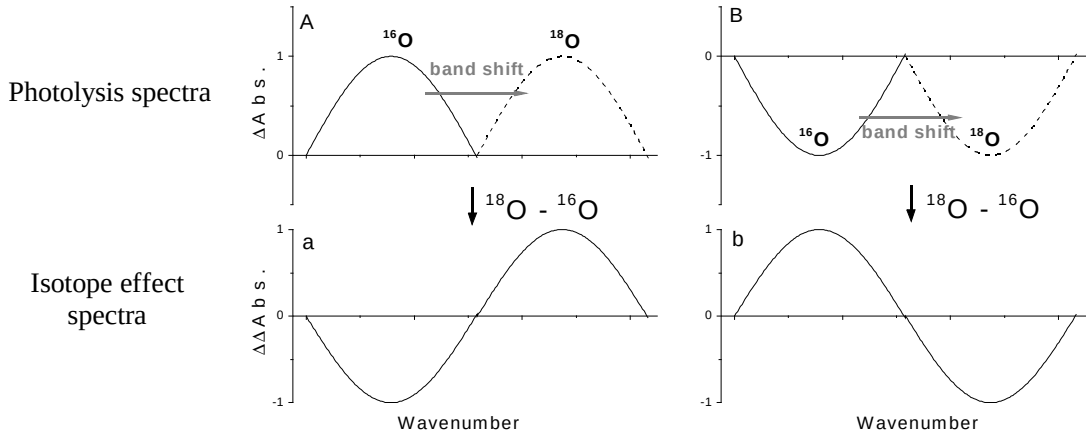

Fig. 3.4-12 Illustration of the positive band shift in the difference spectrum (**A**) and in the double difference spectrum (**a**), and the negative band shift in the difference spectrum (**B**) and in the double difference spectrum (**b**).

wavenumber corresponding to the shifted position for the isotopically labeled compound. A negative band in the photolysis spectrum obtained with caged [^{16}O]ATP that downshifts with caged ATP isotopomers ([^{18}O]) in Fig. 3.4-12B, will be presented as a positive band at its original position in the isotope effect spectra in Fig. 3.4-12b; and there should be a negative band in the isotope effect spectra at the lower wavenumber corresponding to the shifted position for caged isotopically labeled compound. However, in practice, one shifted band may be overlapped by another shifted band. Thus, the determination of band shifts needs to be done carefully. For example, in Fig. 3.4-13A the positive band at 1040 cm^{-1} in the photolysis spectrum obtained with caged unlabeled ATP was not observed with caged ATP isotopomers. This may be due to the overlapping of downshifted negative bands nearby but not due to an isotope effect on the 1040 cm^{-1} band itself.

For an isolated P-O oscillator, a downshift of 30–40 cm^{-1} is expected due to the mass effect on the vibration. Absorption bands of the phosphate groups of ATP and caged ATP observed in the range 1300–950 cm^{-1} can be assigned to the antisymmetric (ν_{as}) and symmetric stretching (ν_s) mode of the $-PO_2^-$ and $-PO_3^{2-}$ groups. The ν_{as} and ν_s mode of the $-PO_2^-$ groups absorb in the range 1270–1210 cm^{-1} and 1140–1060 cm^{-1}, which downshift to 1240–1180 cm^{-1} and 1120–1040 cm^{-1} upon isotope effects, respectively (Takeuchi et al., 1988; Barth et al., 1995, 1997a). The ν_{as} and ν_s modes of the $-PO_3^{2-}$ groups absorb at ~1130 and ~990 cm^{-1}, respectively, which downshift to ~1090 and 975 cm^{-1} upon isotope effect, respectively (Takeuchi et al., 1988; Barth et al., 1995). The three photolysis spectra in Fig. 3.4-13A were normalized using the amplitude of the band at 1526 cm^{-1} to correct the slightly different amount of ATP and ATP isotopomers release. After normalization, the subtraction between the photolysis spectra obtained with caged ATP isotopomers and caged ATP exhibits band shifts due to isotopic substitution as shown in Fig.

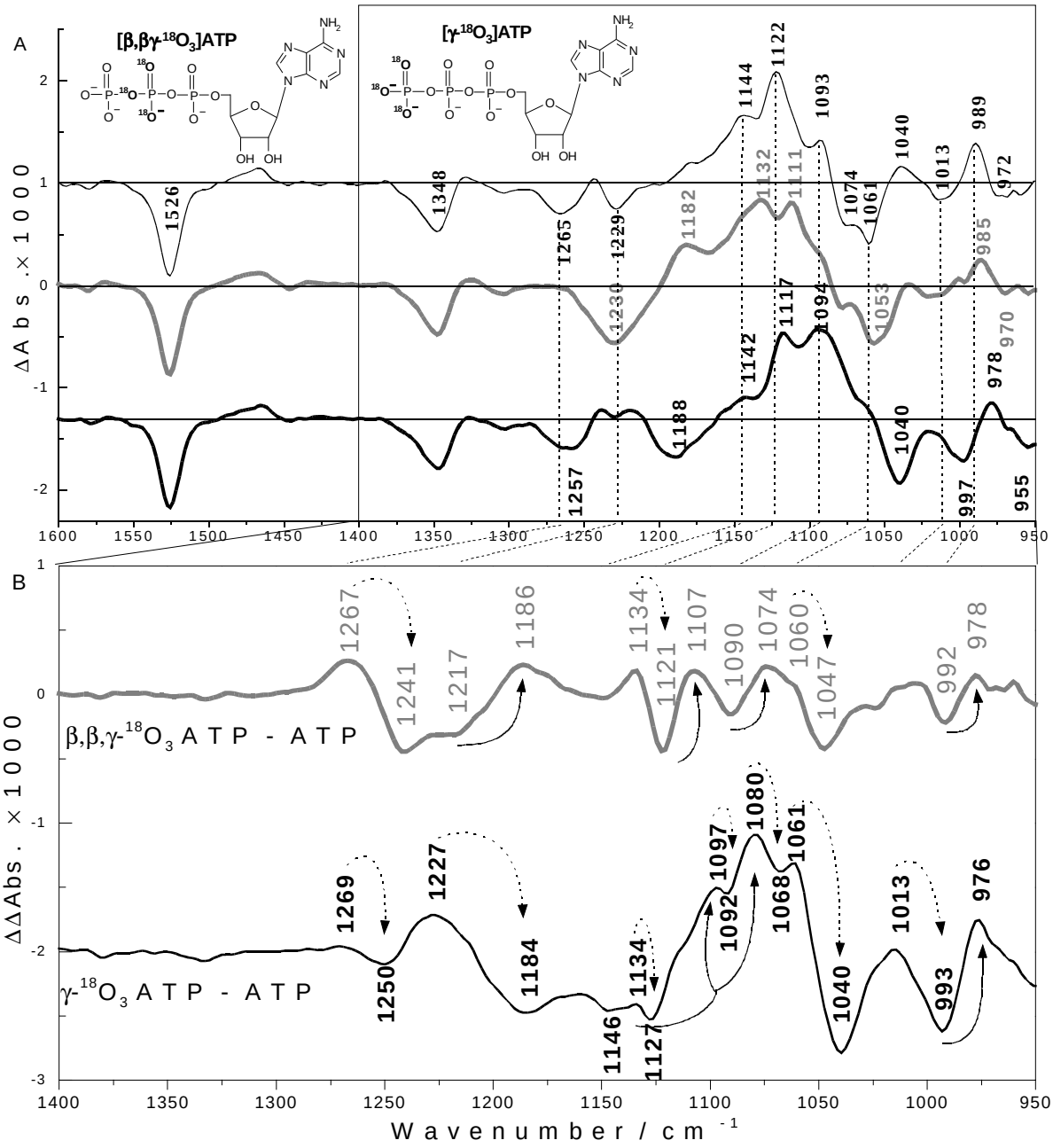

Fig. 3.4-13 A, photolysis spectra with ATP (upper), [β,βγ-$^{18}O_3$]ATP (middle) or [γ-$^{18}O_3$]ATP (lower) below 1600 cm^{-1} (1°C, pH 7.5). The structures of isotopically labeled ATPs are shown above the upper plot. **B**, double difference spectra below 1400 cm^{-1}: *Grey* line, the spectrum with [β,βγ-$^{18}O_3$]ATP minus that with ATP; *black* line, the spectrum with [γ-$^{18}O_3$]ATP minus that with ATP. The dotted arrows show the band shifts of caged ATP; the solid arrows show the band shift of free ATP.

3.4-13B. Band assignments obtained from comparison of the spectra in Fig. 3.4-13 are listed in Table 3-3. These band assignments are in line with (Takeuchi et al., 1988; Barth et al., 1995, 1997a).

Table 3-3 Band assignments of the spectra with ATP and ATP isotopomer release. Band positions refer to Fig. 3.4-13B. Bands are assigned in line with (Takeuchi et al., 1988; Barth et al., 1995, 1997a).

Band position / cm^{-1}	Assignments	Shifted observed with
1267 → 1241	$\nu_{as}(PO_2^-)$ mode of caged ATP, with a strong contribution from the β-phosphate.	[β,βγ-$^{18}O_3$]ATP
1269 → 1250	$\nu_{as}(PO_2^-)$ mode of caged ATP	[γ-$^{18}O_3$]ATP
1227 → 1184	$\nu_{as}(PO_2^-)$ mode of caged ATP	[γ-$^{18}O_3$]ATP
1217 → 1186	$\nu_{as}(PO_2^-)$ mode of free ATP	[β,βγ-$^{18}O_3$]ATP
1150-1120 → 1110-1050	$\nu_{as}(\gamma\text{-}PO_3^{2-})$ mode of free ATP	[γ-$^{18}O_3$]ATP
1134 → 1127/1121	$\nu_s(PO_2^-)$ mode of caged ATP	[β,βγ-$^{18}O_3$]ATP and [γ-$^{18}O_3$]ATP
1121 → 1107	$\nu_s(PO_2^-)$ mode of free ATP	[β,βγ-$^{18}O_3$]ATP
1097 → 1092	$\nu_s(PO_2^-)$ mode of caged ATP	[γ-$^{18}O_3$]ATP
1090 → 1074	$\nu_s(PO_2^-)$ mode of free ATP	[β,βγ-$^{18}O_3$]ATP
1080 → 1068	$\nu_s(PO_2^-)$ mode of caged ATP	[γ-$^{18}O_3$]ATP
1061 → 1047/1040	$\nu_s(PO_2^-)$ mode of caged ATP	[β,βγ-$^{18}O_3$]ATP and [γ-$^{18}O_3$]ATP
1013 → 997	$\nu_s(PO_2^-)$ mode of caged ATP	[γ-$^{18}O_3$]ATP
992 → 978	P_α-O-P_β backbone mode of free ATP	[β,βγ-$^{18}O_3$]ATP
993 → 976	coupled P-O-C and $\nu_s(\gamma\text{-}PO_3^{2-})$ mode of free ATP	[γ-$^{18}O_3$]ATP

Raw binding spectra obtained with ATP isotopomers

Raw binding spectra with these two ATP isotopomers are shown in Fig 3.4-14. Above 1300 cm^{-1} outside the absorption area of phosphate groups, the same band positions and very similar band amplitudes were obtained with ATP and ATP isotopomers. This demonstrates the excellent reproducibility of the IR spectra.

In Fig. 3.4-14A, the raw binding spectra are shown without subtraction of photolysis signals. Therefore, in the raw binding spectra the negative bands are characteristic of Ca_2E1 and caged ATP or caged ATP isotopomers, and the positive bands are characteristic of Ca_2E1ATP. The double difference spectra obtained with subtraction between them in Fig. 3.4-14B manifest the isotope effect. Thus, these double difference spectra are named *isotope effect spectra* of ATP binding to the ATPase. Except for a small band at ~1525 cm^{-1} that is due to a small difference in the amount of released ATP, these two isotope effect spectra in Fig. 3.4-14B show nearly zero amplitude above 1300 cm^{-1}. Small signals between 1400 to 1300 cm^{-1} beside the region of phosphate absorption indicate the limit of experimental reproducibility. Bands of similar amplitude in the region of phosphate absorption (below 1300 cm^{-1}) have to be assigned carefully.

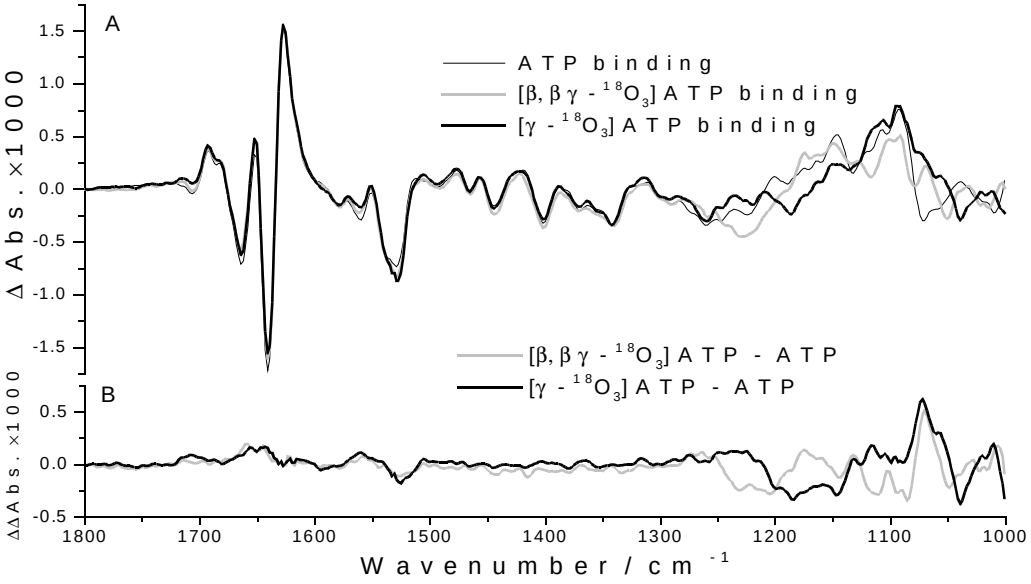

Fig. 3.4-14 A, raw binding spectra with ATP, [β, βγ-$^{18}O_3$]ATP and [γ-$^{18}O_3$]ATP (1°C, pH 7.5, 3 mM ATP), photolysis signals were not subtracted. **B**, the isotope effect spectra, *black* line, the raw [γ-$^{18}O_3$]ATP binding spectrum minus the raw ATP binding spectrum, *grey* line, the raw [β, βγ-$^{18}O_3$]ATP binding spectrum minus the raw ATP binding spectrum.

They are regarded as noise unless there is an obvious explanation.

Isotope effect spectra with [β,βγ-$^{18}O_3$]ATP and [γ-$^{18}O_3$]ATP

Fig. 3.4-15A gives the raw binding spectra below 1400 cm^{-1} on a larger scale to display the band shifts more clearly. Most of bands are at different positions in the three spectra. The significant differences are due to the band shifts caused by the isotopically labeled oxygen atoms on the β- and γ-phosphate group. It is not easy to assign these bands because of the complicated bands overlap and coupling of vibrational modes in this region. However, with the isotope effect spectra, only the shifted bands appear, and all bands that are not affected by labeling are subtracted. The isotope effect spectra below 1400 cm^{-1} are shown in Fig. 3.4-15B, giving the subtraction between the raw ATP isotopomer binding spectra and the raw ATP binding spectrum. The negative bands in the raw ATP binding spectrum in Fig. 3.4-15A are due to the vibrational modes of caged ATP. The shifts of these bands have been discussed above (see Fig. 3.4-13 and Table 3-3). As shown in Fig 3.4-15B top panel, the bands at ~1263, 1132, 1101 and 1060 cm^{-1} shift to 1232, 1118, 1094 and 1049 cm^{-1}, respectively, owing to the isotope effect of the β-phosphate of caged ATP; as shown in Fig. 3.4-15B bottom panel the bands at ~1230, 1132, 1058, and 1011 cm^{-1} shift to 1185, 1126, 1040 and 998 cm^{-1}, respectively, owing to the isotope effect of the γ-phosphate of caged ATP. The isotope effect spectra of ATP release in the absence of the ATPase (*dashed* lines) are also shown in Fig. 3.4-15B for comparison of bands induced by caged ATP, free ATP and bound ATP. The positive bands of the difference spectra

below 1300 cm^{-1} in Fig. 3.4-15A, mainly owing to bound ATP will be discussed here with the isotope effect spectra in detail. The band assignments are listed in Table 3-4.

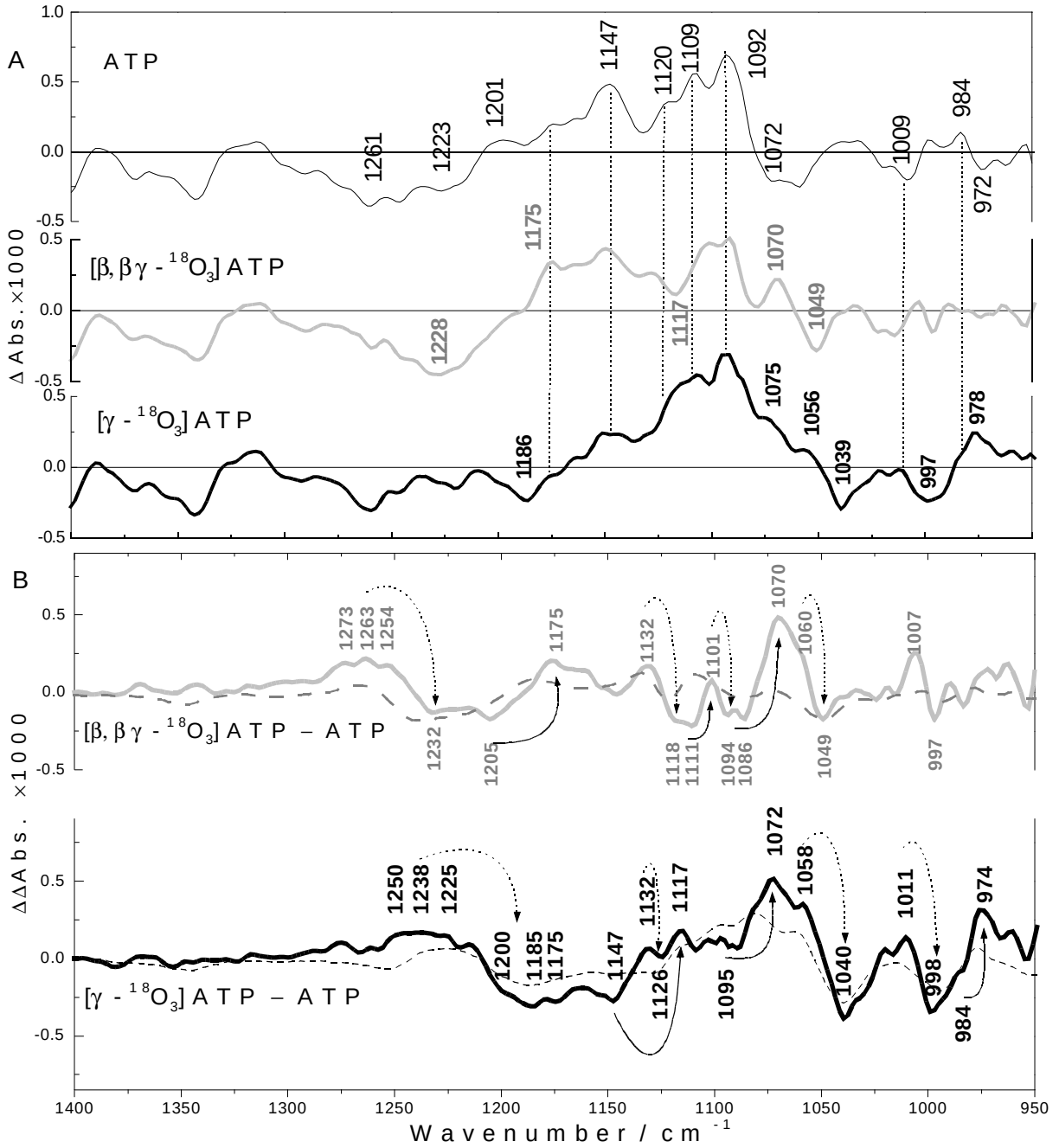

Fig. 3.4-15 **A**, raw binding spectra with ATP (upper), [β,βγ-$^{18}O_3$]ATP (middle) or [γ-$^{18}O_3$]ATP (lower) below 1300 cm^{-1} (1°C, pH 7.5, 3 mM ATP, 1.2 mM ATPase, 10 mM Ca^{2+}). **B**, isotope effect spectra below 1400 cm^{-1}: *grey* line, the spectrum with [β,βγ-$^{18}O_3$]ATP binding minus the spectrum with ATP binding; *black* line, the spectrum with [γ-$^{18}O_3$]ATP binding minus the spectrum with ATP binding. *Dashed* lines in plot B are the isotope effect spectra obtained with the ATPase-free samples in Fig. 3.4-5B. The dotted arrows show the band shifts of caged ATP; the solid arrows show the band shifts of bound ATP.

As shown in Fig. 3.4-15B, with [β,βγ-$^{18}O_3$]ATP the band at 1205 cm^{-1} shifts to 1175 cm^{-1} and can be assigned to the $\nu_{as}(PO_2^-)$ mode of β-phosphate of bound ATP (Barth et al., 1997a; Du et al., 2000; Allin et al., 2001). The band at 1111 cm^{-1}, which seems to shift to 1101 cm^{-1}, can be

assigned to the in-phase $\nu_s(PO_2^-)$ mode of bound ATP (Takeuchi et al., 1988); the band at 1086 cm^{-1}, which may shift to 1070 cm^{-1}, was tentatively assigned to the $\nu_s(\alpha,\beta\text{-}PO_2^-)$ modes of ATP (Barth et al., 1997a). These bands at 1205, 1111 and 1086 cm^{-1} are at similar position of 1217, 1121 and 1090 cm^{-1} in Fig. 3.4-13B in the ATPase-free samples, showing similar shifts to 1186, 1107 and 1074 cm^{-1}. In the ATPase-free samples they were assigned to the β-phosphate of free ATP. However, in the absence of the ATPase, the first two bands are at higher wavenumber (1217 and 1121 cm^{-1}). More partial charge on oxygen atoms of the β-phosphate due to the change of hydrogen bonding on the γ-phosphate after ATP binding to the ATPase may result in the downshifts of these bands. Similar results were observed for GTP binding to H-Ras protein (Allin et al., 2001) and the downshifts in the presence of the enzyme were attributed to a lowering of the bond order of the nonbridged P-O bonds of the β-phosphate. The bond order changes were explained by a shift of negative charges from oxygen atoms of the γ-phosphate to the β-phosphate, and such a shift may facilitate GTP hydrolysis.

Table 3-4 Band assignments of the raw binding spectra with ATP and its isotopomers. Band positions refer to Fig. 3.4-7B. Bands marked with * are assigned in line with (Takeuchi et al., 1988; Barth et al., 1995, 1996, 1997a). The other new assignments are obtained with this work.

Band position / cm^{-1}	**Assignments**	**Shift observed with**
*~1263 → 1232	$\nu_{as}(PO_2^-)$ mode of caged ATP, with a strong contribution from the β-phosphate.	[β,βγ-$^{18}O_3$]ATP
*~1225 → 1185	$\nu_{as}(PO_2^-)$ mode of caged ATP, with a strong contribution from the γ-phosphate.	[γ-$^{18}O_3$]ATP
*1205 → 1175	$\nu_{as}(PO_2^-)$ mode of bound ATP	[β,βγ-$^{18}O_3$]ATP
1147 → 1117	$\nu_{as}(\gamma\text{-}PO_3^{2-})$ mode of bound ATP	[γ-$^{18}O_3$]ATP
1132 → 1118/1126	$\nu_s(PO_2^-)$ mode of caged ATP	[β,βγ-$^{18}O_3$]ATP and [γ-$^{18}O_3$]ATP
*1111 → 1101	$\nu_s(PO_2^-)$ mode of bound ATP	[β,βγ-$^{18}O_3$]ATP
1101 → 1094	$\nu_s(PO_2^-)$ mode of caged ATP	[β,βγ-$^{18}O_3$]ATP
1095 → 1072	$\nu_{as}(\gamma\text{-}PO_3^{2-})$ mode of bound ATP	[γ-$^{18}O_3$]ATP
*1086 → 1070	$\nu_s(PO_2^-)$ mode of bound ATP	[β,βγ-$^{18}O_3$]ATP
*~1060 → 1049/1040	$\nu_s(PO_2^-)$ mode of caged ATP	[β,βγ-$^{18}O_3$]ATP and [γ-$^{18}O_3$]ATP
1011 → 998	$\nu_s(PO_2^-)$ mode of caged ATP	[γ-$^{18}O_3$]ATP
*984 → 974	coupled P-O-C and $\nu_s(\gamma\text{-}PO_3^{2-})$ mode of bound ATP	[γ-$^{18}O_3$]ATP

With [γ-$^{18}O_3$]ATP, as shown in Fig. 3.4-15B, positive bands at 1147, 1095 and 984 cm^{-1} shift to

1117, 1072 and 974 cm^{-1}. The positive band at 1147 cm^{-1} can be assigned to the $\nu_{as}(\gamma\text{-}PO_3^{2-})$ mode of bound ATP (Ca_2E1ATP). Similar studies were done with GTP binding to H-Ras (Du et al., 2000; Allin et al., 2001) and a band at ~1144 cm^{-1} was assigned to the $\nu_{as}(\gamma\text{-}PO_3^{2-})$ mode of GTP. In the raw [$\beta,\beta\gamma\text{-}^{18}O_3$]ATP binding spectrum, the amplitude of this band is smaller, which indicates that the β-phosphate has a slight effect on this band. The band shift from ~1095 to 1072 cm^{-1} shown in Fig. 3.4-15B might be assigned to the $\nu_{as}(\gamma\text{-}PO_3^{2-})$ mode of bound ATP. There may be band shifts from 1150–1110 cm^{-1} to 1100–1050 cm^{-1}, which can be assigned to the $\nu_{as}(\gamma\text{-}PO_3^{2-})$ mode of possibly excess free ATP (dashed line in the lower panel of Fig. 3.4-15B). The overlap of these two band shifts of bound and free ATP could result in no significant band at 1095 cm^{-1} in the lower panel of Fig. 3.4-15B. Compared with the broad band of the same $\nu_{as}(\gamma\text{-}PO_3^{2-})$ vibrational mode of free ATP (1150–1110 cm^{-1}), this band at 1095 cm^{-1} of bound ATP is at lower wavenumber. Less partial charge on oxygen atoms of the γ-phosphate due to the change of hydrogen bonding after ATP binding to the ATPase could result in the upshift of the γ-phosphate band. Here a band downshift was observed, which indicate that there may be other effects on the γ-phosphate of bound ATP. Less partial charge on the γ-phosphate may also help this group bind to Asp-351 with less repulsion. The band at 984 cm^{-1} assigned to the $P_\beta\text{-O-}P_\gamma$ backbone vibrational modes of bound ATP seems to shift to 974 cm^{-1}.

3.4.7 Comparison and discussion of nucleotide binding to the Ca^{2+}-ATPase

Comparison of the extent of conformational changes

The contour of the binding spectra in the amide I region obtained with ATP, ADP, AMPPNP, ITP, 2'-, and 3'-deoxyATP is similar, the main difference is the amplitude of the signals indicating various extents of conformational change. AMP and pyrophosphate at millimolar range do not bind to the ATPase, or the affinity of the ATPase for them is much lower than for other nucleotides used here. Ribose triphosphate binds to the ATPase also with rather low affinity (~100 mM). TNP-AMP binds to the ATPase in a distinct mode and will be discussed separately below.

As defined in chapter 3.1.2, a comparison was made with the signal amplitude termed maximum signal amplitude (MSA) that is the difference between the absorbance changes at 1628 and 1641 cm^{-1}. As shown in Fig. 3.4-16A, the largest binding-induced signals were obtained with ATP and AMPPNP (MSA $\approx 3 \times 10^{-3}$), medium size signals (MSA $\approx 2 \times 10^{-3}$) with ADP and 2'-deoxyATP, and the smallest signals (MSA $\approx 1 \times 10^{-3}$) with ITP and 3'-deoxyATP. The different amplitudes

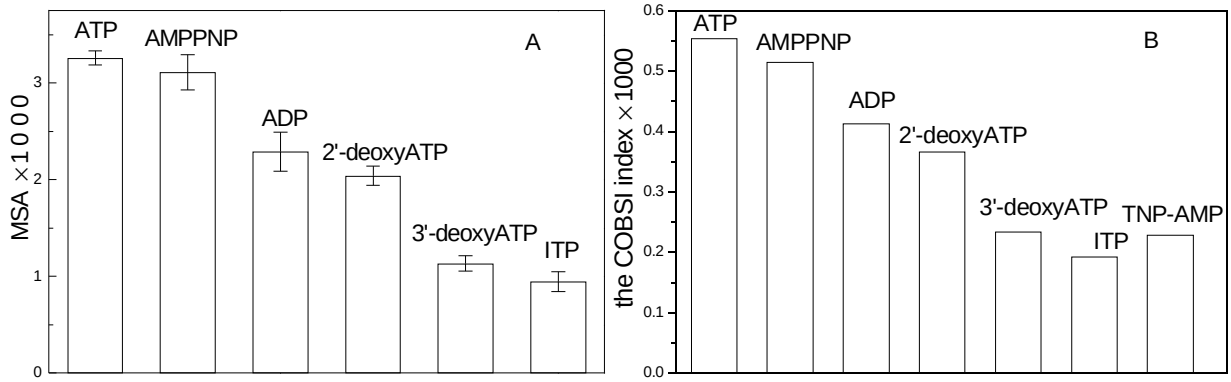

Fig. 3.4-16 A, Maximum signal amplitude (MSA) of the nucleotide binding spectra with standard deviation bars. MSA is the difference between the absorbance change at 1628 cm^{-1} and that at 1641 cm^{-1} in the nucleotide binding spectra. **B**, the change of backbone structure and interaction (COBSI) indices of ATP and ATP analogs (see chapter 2.4.5).

of the nucleotide binding spectra cannot be explained by incomplete binding to the ATPase because it has been verified that saturating signals have been obtained (see chapter 3.1.2) in the time intervals for nucleotide binding which were determined by the kinetic evaluation of marker bands (see chapter 3.3.1). Therefore, the difference should be due to the different extent of conformation changes of the ATPase upon nucleotide binding. MSA values for nucleotide binding spectra differ slightly from MSA values shown in Fig. 3.1-2 of the titration experiments, in which a time slot was evaluated when Ca_2E1P – not Ca_2E1N – was accumulated, because of conformational changes accompanying the phosphorylation reaction.

Another parameter was used to analyze the extent of conformational changes induced by nucleotide binding. It is the change of backbone structure and interaction (COBSI) index (Barth et al., 1996), as described in chapter 2.4.5. The index is calculated by the integral intensity of spectra in the amide I region (1700–1610 cm^{-1}) and shows the net change of the secondary structure during the reaction. This index is sensitive to secondary structure changes, changes in hydrogen bonding to peptide groups, and subtle structural changes within a given secondary structure. Only net changes are revealed. The index of COBSI with ATP binding is 5.5×10^{-4}, which is ~2 orders of magnitude smaller than COBSI index for a 100% secondary structure transition. This implies that the ATPase secondary structure is virtually not perturbed and only a few residues of the ATPase are involved in a net secondary structure change upon ATP binding. The COBSI indices in Fig. 3.4-16B present a similar relationship as MSA does. The COBSI index of TNP-AMP is larger than ITP, being more than 1/3 of that of ATP and AMPPNP, which may be due to the large TNP moiety.

Fig. 3.4-17 shows a model of the different extent of conformational changes induced by binding of ATP and ATP analogs. In the Ca_2E1 state (the second panel), the three cytoplasmic domains

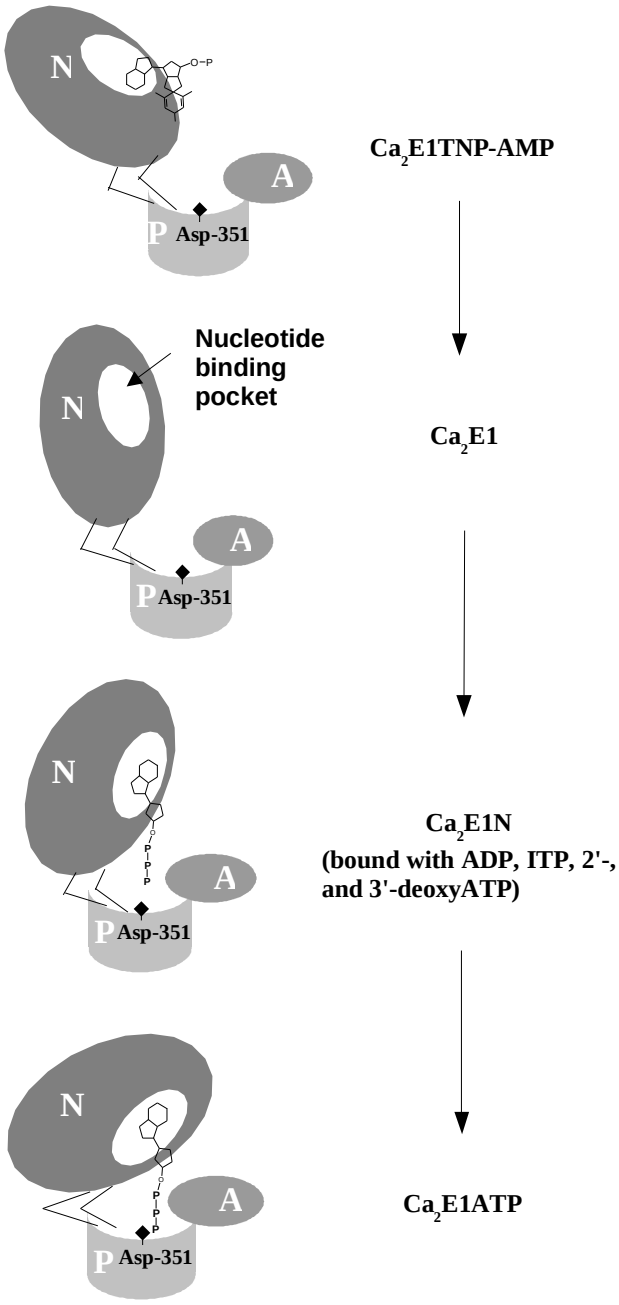

Fig. 3.4-17 Models of different extent of conformational changes of the ATPase with binding of ATP and ATP analogs, extended from Danko, *et. al. FEBS Letters*, **2001**, 505: 129-135. The first panel: the Ca_2E1TNP-AMP state, with larger distance among three cytoplasmic domains; the second panel: the Ca_2E1 state, with large distance among the three cytoplasmic domains of the ATPase; the third panel: the Ca_2E1N state with binding of ATP analogs, with some distance between the N and P domain and with the γ-phosphate group far away from Asp-351; the fourth panel: the Ca_2E1ATP state, with smaller distance between the N and P domain and with the γ-phosphate group close to Asp-351. N, the nucleotide binding domain; P, the phosphorylation domain; A, the actuator domain.

open to an extent which is smaller than those in the Ca_2E1 crystal structure (Toyoshima et al., 2000) with binding of TNP-AMP (the first panel). With binding of ATP, the cleft between N and P domain closes more than with ADP, ITP, 2'- and 3'-deoxyATP. The conformational change of the hinge domain is larger with ATP binding than with these ATP analogs, as discussed below in "The hinge movement between N and P domain".

Interaction between the ATPase and ATP

The results point out that modifications to ATP's amino, 2'-OH, 3'-OH, the β- and γ-phosphate group affect the binding-induced conformational change of the ATPase. These groups are therefore important for the interaction between ATP and the ATPase. The region near the amino

group and 3'-OH have the most significant influence on the induced-fit movement of the ATPase, because modification to either of these two groups reduces the extent of backbone conformational change seen by IR spectroscopy to only 1/3 of that obtained with ATP. They are therefore important groups of ATP that anchor ATP to the ATPase. The importance of the functional groups of ATP investigated here has been shown before in several partial steps of the ATPase reaction cycle (De Meis et al., 1973; Bodley et al., 1987; Coan et al., 1993). The new finding here is that modifications of the ATP molecule have a direct effect on the structure of the nucleotide-ATPase complex. This is valid not only for side chain orientation as often found (Davis et al., 1999) but also for backbone conformation: with some ATP analogues the binding-induced conformational change of the backbone seen by IR spectroscopy in the amide I region was found to be only 1/3 of that for ATP.

The effects of modifying ATP on nucleotide binding might have several causes: (i) a direct interaction of the modified group of ATP with the ATPase, (ii) a direct interaction of the introduced group of the ATP analog and (iii) an indirect effect on the interactions between protein and ATP via a change in electron density or conformation of ATP.

A direct interaction of the modified group of ATP with the ATPase is the most likely cause for the reduced extent of conformational change observed for deoxyATPs because (i) no sterical restrains are expected from the replacement of the hydroxyl groups by the smaller hydrogen atoms and (ii) effects on the equilibrium between sugar conformations of ATP in solution seem to be less relevant to the sugar conformation of bound ATP. 2'- or 3'-H substitution influences the sugar conformation in solution: according to the absorption spectra of ATP and deoxyATPs with deprotonated phosphate groups (chapter 2.3.4) in Fig. 3.4-18, the ratios of $C_{2'}$-*endo* (~830 cm^{-1}) and $C_{3'}$-*endo* (~814 cm^{-1}) puckering of these three nucleotides are 60:40, 80:20, and 70:30, respectively. This demonstrates that free ATP and deoxyATPs prefer $C_{2'}$-*endo* puckering, particularly deoxyATPs. Similar results for ATP and 2'-deoxyATP were obtained before (Schleich et al., 1972; Davies et al., 1974; Clore et al., 1982). NMR investigations demonstrate that $C_{2'}$- and $C_{3'}$-*endo* types of conformations are in rapid equilibrium in solution (Schleich et al., 1972) indicating only a small activation barrier between the two types of conformations. In spite of the predominant $C_{2'}$-*endo* puckering in solution, the ATPase seems to choose the $C_{3'}$-*endo* conformation for binding, as determined by NMR (Clore et al., 1982). Therefore the conformation of the nucleotide-ATPase complex will not depend on the predominant sugar puckering in solution and the effects of ribose OH substitution are best explained by direct interactions of the ribose hydroxyls with the ATPase.

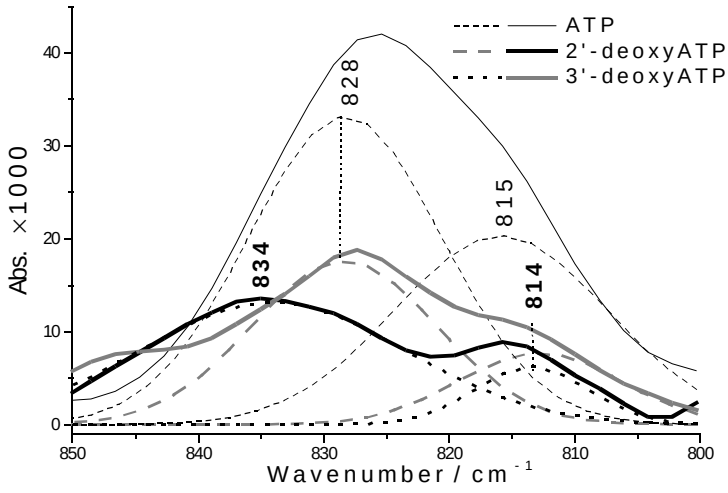

Fig. 3.4-18 Absorbance spectra of 500 mM ATP, 2'-deoxyATP and 3'-deoxyATP with 1500 mM KOH in puckering mode region from 850 to 800 cm^{-1}. *Black-solid-thin* line, the ATP absorbance spectrum; *black-dashed* lines, the fit results of the two bands at 828 and 815 cm^{-1} to the ATP absorbance spectrum. *Black-solid-bold* line, the 2'-deoxyATP absorbance spectrum; *black-dot* lines, the fit results of the two bands at 834 and 814 cm^{-1} to the 2'-deoxyATP absorbance spectrum. *Grey-solid* line, the 3'-deoxyATP absorbance spectrum; *grey-dotted* lines, the fit results of the two bands at 828 and 814 cm^{-1} to the 3'-deoxyATP absorbance spectrum.

It is less certain whether the reduced extent of conformational change found with ITP can be explained by a localized interaction between the amino group and the ATPase. In ITP the carbonyl group replaces the amino group of ATP and one of the two endocyclic nitrogen atoms is protonated. These alterations are not localized only on the amino group but will change the electron density distribution in the entire 6-membered ring and its hydrogen bonding pattern. Therefore the interaction seems to be located on the 6-membered ring of adenine. Because the most drastic alteration is at the amino group, it is likely but not mandatory that the results reflect a direct interaction of the ATPase with the amino group.

Concerted conformational change

The interactions between nucleotide and the protein induce a concerted conformational change upon nucleotide binding: they join forces to induce strain in the protein. If one of the interacting groups is modified to become a less effective binding partner, the interactions with the respective binding pocket are impaired, the strain is relieved and a smaller conformational change is produced. A weakened interaction therefore affects the conformational change as a whole instead of producing only local effects. This concept explains that the modifications of ATP studied reduce all bands in the amide I region of the difference spectrum. If an interaction between nucleotide and the ATPase had only local effects on the protein structure, a weakened interaction would selectively reduce the amplitude of difference bands associated with that conformational change, but not of all of the bands as observed here. Particularly interesting is functional groups of ATP that interact with different domains of the protein produce the same type of conformational change: the amino function is thought to interact with the N domain (McIntosh et al., 1996; Toyoshima et al., 2000; Hua et al., 2002), the γ-phosphate with the P domain (McIntosh et al., 1999; Clausen et al., 2001; Hua et al., 2002), as shown in the last panel

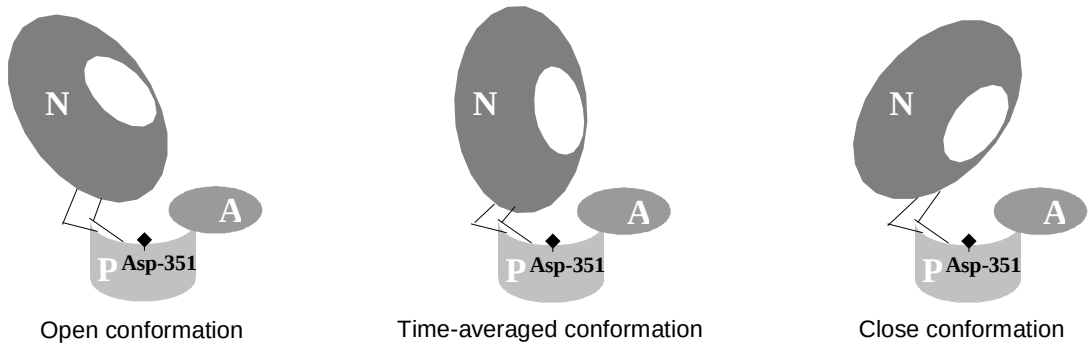

Fig. 3.4-19 A schematic model of the cytoplasmic region in the time-averaged conformation in solution, and the open and close conformation, adapted from Danko, *et. al*. *FEBS Letters*, 2001, **505**: 129-135. N, the nucleotide binding domain; P, the phosphorylation domain; A, the actuator domain.

of Fig. 3.4-17. In spite of that, the absence of the γ-phosphate in ADP or of the adenine amino group in ITP both reduce the amplitude of same bands. This gives evidence that the concerted conformational change detected here is caused by interactions of the nucleotide with different protein domains: the N and the P domain.

Nucleotide-specific conformation

The results suggest that nucleotide binding induces a conformation that is characteristic of the bound nucleotide, as proposed before from experiments that did not monitor the conformation of the nucleotide-ATPase complex directly (Rubtsov et al., 1988). In the light of the known flexibility of the N domain (Jona et al., 1990; Huang et al., 1998), this conformation might represent an average conformation. The open and close conformation of the N and P domain both exist in solution and what is observed in IR spectra is the time-averaged conformation, as indicated in Fig. 3.4-19. The average conformation adopted in the ATPase-nucleotide complex seems to be very sensitive to individual interactions between the ATPase and nucleotide because the extent of conformational change depends dramatically on the presence of individual functional groups of ATP.

The finding of a nucleotide-specific conformation of nucleotide-ATPase complexes is supported by previous reports, in which different effects of nucleotides were found on fluorescence properties (Kubo et al., 1990; Lacapere et al., 1990; Wakabayashi et al., 1990), partial reaction rates (Scofano et al., 1979; Hobbs et al., 1985; Champeil et al., 1988; Ferreira et al., 1988), protection against proteolysis (Danko et al., 2001b), effects of aromatic compounds (Petretski et al., 1989), nucleotide binding properties of mutants (McIntosh et al., 1999), and uncoupling (Fortea et al., 2000).

The structures of the nucleotide-ATPase complexes studied differ in two aspects: (i) the extent

of the conformational change induced by nucleotide binding differs as indicated by the different amplitudes of the amide I signals; (ii) structural details of the nucleotide-ATPase complex differ as shown by the subtle differences of band positions and spectral shape in the entire IR spectra observed among the nucleotide binding spectra.

The small conformational change upon ITP binding observed here suggests that soaking Ca_2E1 crystals with β,γ-iminoinosine 5'-triphosphate (IMPPNP) may not disrupt the crystals as ATP does (Toyoshima et al., 2000) because of the relatively small conformational change seen here for ITP. This may therefore enable the investigation of nucleotide binding at atomic resolution. The conformational change induced by ATP binding may then be extrapolated from the conformational change seen upon IMPPNP binding. This illustrates that infrared spectroscopy is helpful to search for the binding partners to obtain crystals in expected enzyme states.

The conformational change reflected in IR spectra

Conformational changes in two regions of the protein were proposed to occur upon nucleotide binding (Danko et al., 2001a, b): (i) movement of the N domain towards the P domain and (ii) movement of the A domain towards the P domain. The latter does not seem to contribute to a large extent to the IR spectra for the following reason. In the study of protection of the ATPase against proteolytic attack by various nucleotides (Danko et al., 2001a, b), the protection effect is thought to reflect a movement of the A domain. And no effect for ADP was observed, indicating that ADP does not promote significant movement of the A domain. The IR spectra of nucleotide binding however show that ADP binding induces a conformational change, the extent of which is 2/3 of that induced by ATP (Fig. 3.4-2). This elucidates that the conformational change of the A domain contributes not or only to a small extent to the IR difference spectra.

Instead, the anticipated hinge movement of the N and P domain upon ATP binding likely causes the amide I signals. The hinge movement will however not *directly* reflect in the spectra since highly mobile structural elements would give broad IR bands before and after the conformational change, which would largely cancel in the difference spectrum. Therefore IR spectroscopy will largely miss a conformational change in the mobile hinge region *itself*. In line with this, only small bands in a limited spectral region (1660–1680 cm^{-1}) can be assigned to mobile structures because they exchange their amide proton upon $^1H_2O/^2H_2O$ exchange (Von Germar et al., 2000). Instead, the nucleotide binding bands in the amide I region are caused by backbone stretches within well-defined and stable structures because they are hardly affected by $^1H_2O/^2H_2O$ exchange. In line with this finding of conformational changes in well-ordered regions, NMR

spectroscopy has detected changes of backbone conformation in the N domain upon AMP binding (Abu-Abed et al., 2002).

These conformational changes in well-ordered regions might report the hinge movement indirectly since a conformational change in the hinge region will also affect the connecting stretches. The more ordered these stretches become, the more they are incorporated into the domains and therefore give rise to distinct bands in the amide I region. In other words, a hinge movement will alter the relative orientation of the connecting amide groups and their hydrogen bonding and therefore affect their amide I signals. These considerations suggest that the spectra detect the hinge movement *indirectly* because it is reported by structured backbone stretches that link the hinge domain and the other domains.

The hinge movement between N and P domain

The hinge movement upon nucleotide binding seems to be less pronounced than anticipated in the structural models (Toyoshima et al., 2002; Xu et al., 2002). Fluorescence resonance energy transfer experiments suggest that distances between fluorescence labels in the N and the P domain do not change between Ca_2E1 and E2 conformation (reviewed in Bigelow et al., 1992). Of particular interest is the unchanged distance of two pairs of residues for which a change in distance is obtained from the two X-ray structures (Toyoshima et al., 2000, 2002). The distance between Cys-344 and Lys-515 increases from 46 Å in E2TG to 50 Å in Ca_2E1, and that between Cys-344 and Glu-439 changes from 38 Å in E2TG to 45 Å in Ca_2E1, as shown in 3.4-20. These distance changes should result in decreases in fluorescence energy transfer (calculated by the equation, $E = R^6 / (R^6 + r^6)$, when R is Foerster radius and r is the distance between the residues) by 33% and 41%, respectively, which are not observed (Mata et al., 1993; Stefanova et al., 1993).

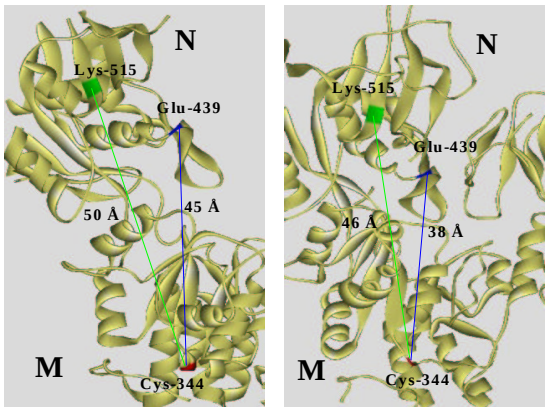

Ca_2E1 state **E2TG state**

Fig. 3.4-20 Distance between Cys-344 and Lys-515, Glu-439 in the crystal structures of the Ca_2E1 state and E2TG state (PDB file 1EUL and 1IWO). N, the nucleotide binding domain; M, the transmembrane domain.

The hinge movement can bring the N and P domain close together in the Ca_2E1 state as evidenced by crosslinked with glutaraldehyde (McIntosh, 1992). The crosslinked cleft of Ca_2E1 resembles that of the E2TG structure because the crosslinked residues Lys-492 and Arg-678 are only 5 Å apart in the E2TG structure but 21 Å in the Ca_2E1 structure. In line with these experiments, closure of the hinge could be modeled with the N and P domain structures of Ca_2E1 without sterical hindrance and this brings these two crosslinked residues as close as 4 Å (Xu et al., 2002). The mobility of the N domain (Jona et al., 1990; Huang et al., 1998) implies that it is likely to move rather independently from the rest of the protein and that the hinge angle might depend less on the Ca_2E1 and E2 state than expected from the crystal structures. The open cleft between the N and P domain in Ca_2E1 and the more closed conformation in E2TG of the crystal structures (Toyoshima et al., 2000, 2002) therefore most likely do not represent the average conformation of these states in solution. They are probably adopted in the crystals because of crystal contacts that are made possible by the mobility of the N domain in both states (Jona et al., 1990; Huang et al., 1998). In solution the average position of the N domain will be probably in between those observed in the two crystal structures as shown in Fig. 3.4-19. It is therefore plausible to assume that the cleft is less open for Ca_2E1 in solution than in the Ca_2E1 crystal structure and that upon nucleotide binding the hinge movement between the N and P domain will be smaller than anticipated from the crystal structure. The circular dichroism spectra of the ATPase in the E1 and E2 states are similar (Csermely et al., 1987), suggesting that the conformational coupling during E1-E2 transition occurs by a rearrangement of protein domains through the hinge domain or sliding motions, without major changes in secondary structure.

Discussion of TNP-AMP binding to the ATPase

TNP-AMP was chosen for the infrared study because it was the nucleotide with which binding could be observed in the ATPase crystals. The structure of the ATPase with bound Ca^{2+} and TNP-AMP is not significantly different from that in the absence of TNP-AMP (Toyoshima et al., 2000), whereas ATP binding to the ATPase causes a conformational change that destroys the crystals. In solution, a conformational change upon binding of TNP-AMP to the SR Ca^{2+}-ATPase was detected here that is smaller than that induced by binding of ATP or AMPPNP. Therefore, infrared spectroscopy has detected a difference in the structures of Ca_2E1 and Ca_2E1TNP-AMP that was not detected by X-ray crystallography (Toyoshima et al., 2000).

As discussed above, the conformational changes caused by nucleotide binding are proposed to be characteristic of the bound nucleotides. The binding mode for the other ATP analogs (AMPPNP, ADP, ITP, deoxyATPs) seems however to be similar to that of ATP, since the shape

of the spectra in the amide I region is similar: they all present bands of the same sign as ATP near 1627, 1640 and 1652 cm^{-1} and most of them also near 1662 and 1691 cm^{-1}. Table 3-5 compares the positions of bands and shoulders for these close ATP derivatives with those for TNP-AMP. It is evident that the character of the conformational change caused by TNP-AMP binding is largely opposite to that induced by the other nucleotides: positive bands in the spectra of close ATP derivatives (near 1680, 1652 and 1628 cm^{-1}) appear as negative bands at similar positions in the TNP-AMP binding spectrum (at 1673, 1654 and 1624 cm^{-1}); the largest negative band in the spectra of close ATP derivatives (near 1640 cm^{-1}) is positive at similar position in the TNP-AMP binding spectrum (at 1635 cm^{-1}). The opposite character of the TNP-AMP binding spectrum is particularly striking in the region of the largest bands below 1660 cm^{-1} (Fig. 3.4-9A), where all TNP-AMP bands have a sign opposite to that of bands of the other nucleotides investigated. If the conformational change upon binding is described by a one dimensional parameter, similar to a reaction coordinate, then the ATPase complexes with binding of TNP-AMP and ATP lie on opposite ends of the scale with the nucleotide-free state Ca_2E1 inbetween, but closer to the TNP-AMP-ATPase complex, as shown in Fig. 3.4-21.

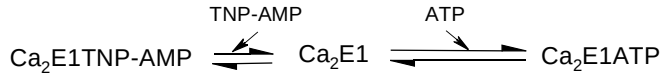

Fig. 3.4-21 The scheme of ATP and TNP-AMP binding to the ATPase described as a reaction coordinate.

The particular binding mode observed for TNP-AMP is most likely due to the bulky TNP group attached to the ribose moiety. This is because removal of single functional groups of ATP (2´-OH, 3´-OH, or γ-phosphate) leads mainly to a reduction in band amplitude compared with the ATP binding spectrum but retains most of the spectral shape. Thus, binding of the nucleotide moiety of TNP-AMP to the ATPase would lead to a further reduction in band amplitudes since it lacks four functional groups that are important for the conformational change of the Ca^{2+}-ATPase: the 2´-OH, the 3´-OH, the β- and γ-phosphate group. The lack of two phosphate groups result in a low affinity of the nucleotide moiety of TNP-AMP for the Ca^{2+}-ATPase (Lacapere et al., 1990). Therefore the high affinity of TNP-AMP and its particular binding mode detected here are attributed to the TNP moiety of the TNP-AMP molecule.

As discussed above, infrared spectroscopy detects indirectly the anticipated hinge movement between the N and P domain (Danko et al., 2001a, b). This hinge domain is thought to close the cleft between the N and P domain. Because the conformational changes upon TNP-AMP binding have an opposite character to those upon ATP binding, a working hypothesis was proposed that TNP-AMP binding opens the cleft as shown in Fig. 3.4-17. In line with the assumption, the cleft is wide open in the crystal structure of Ca_2E1 in the presence of TNP-AMP (Toyoshima et al.,

2000).

Caged AMPPNP binds to the ATPase when its concentration is higher than 10 mM (see chapter 3.2.4). This will not be a problem for samples used to study TNP-AMP → AMPPNP competition. In these samples although 30 mM of caged AMPPNP were used, the presence of 5 mM TNP-AMP and the high affinity of the ATPase for TNP-AMP ensure that TNP-AMP but not caged AMPPNP binds to the ATPase initially.

The TNP-AMP binding spectrum looks similar to the ADP-binding spectrum of mitochondrial creatine kinase induced by caged ADP photolysis with negative bands at 1651 and 1624 cm^{-1} and a positive band at 1640 cm^{-1} (Raimbault et al., 1996) which indicates a similar binding mode.

Table 3-5. Positions of bands and shoulders in the nucleotide binding spectra in the amide I region.

Nucleotide	**ATP**	**AMPPNP**	**ADP**	**2'-dATP**	**3'-dATP**	**ITP**	**TNP-AMP**
Band							1698(-)
Positions	1693(+)	1692(+)	1693(+)	1693(+)	1692(+)	1691(+)	
	1680(+)	1681(+)	1680(+, *s*)	1682(+)		1679(+)	
		1678(+, *s*)					
	1673(-, *s*)			1671(-, *s*)	1672(-, *s*)		1673(-)
	1664(-)	1663(-)	1663(-)	1665(-)	1664(-, *s*)	1663(-)	
	1652(+)	1652(+)	1652(+)	1652(+)	1653(+)	1652(+)	**1654(-)**
	1641(-)	1640(-)	1641(-)	1641(-)	1642(-)	1641(-)	**1635(+)**
	1628(+)	1627(+)	1628(+)	1628(+)	1628(+)	1626(+)	**1624(-)**
			1616(+, *s*)	1616(+, *s*)	1616(+, *s*)		
							1607(+)

Notes: *s*, shoulder; +, positive band or shoulder; -, negative band or shoulder. TNP-AMP bands with a sign opposite to ATP-binding binds are indicated in bold.

3.5 Ca_2E1P formation and phosphorylation of the Ca^{2+}-ATPase with different nucleotides

3.5.1 Ca_2E1P formation spectra with different nucleotides

After nucleotide binding, the Ca^{2+}-ATPase is phosphorylated and the ADP-sensitive phosphoenzyme Ca_2E1P is formed. The reaction is shown in Fig. 3.5-1. Here phosphorylation was studied with ATP, ITP, 2'-deoxyATP, 3'-deoxyATP and ATP isotopomers.

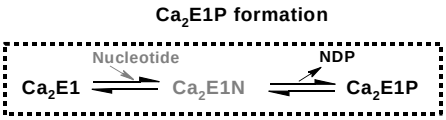

Fig. 3.5-1 Ca_2E1P formation reaction.

Ca_2E1P formation with ATP, ITP and 2'-deoxyATP

The Ca_2E1P formation spectra obtained with ATP, ITP and 2'-deoxyATP, i.e. the absorbance of Ca_2E1P minus the absorbance of Ca_2E1 ($Ca_2E1 \rightarrow Ca_2E1P$), are shown in Fig. 3.5-2A. Phosphorylation leads to the appearance of two bands at 1721 and 1549 cm^{-1} that serve as marker bands for the first phosphorylated intermediate Ca_2E1P (Barth et al., 1996, 1998). In this work, ATP, 2'-deoxyATP and ITP phosphorylate the ATPase at rates that are sufficiently high to observe accumulation of Ca_2E1P. 3'-deoxyATP seems not to phosphorylate the ATPase or phosphorylate the ATPase at a much lower rate with only ~40% amount of Ca_2E1P formation before the measurement finishes (see chapter 3.3.2). Therefore the Ca_2E1P formation spectrum with 3'-deoxyATP cannot be observed. However, the spectrum with ~40% amount of Ca_2E1P formation obtained with 3'-deoxyATP is shown in Fig. 3.5-3.

As found for nucleotide binding, the shape of the Ca_2E1P formation spectra obtained with 2'-deoxyATP and ITP is similar to that with ATP but the band amplitudes are different. With ITP and 2'-deoxyATP, smaller signals were obtained from 1670 to 1610 cm^{-1} in the amide I region and from 1540 to 1520 cm^{-1} in the amide II region. In contrast, the *same* amplitude is observed for the band at 1721 cm^{-1}. In this work, the amplitude (or the integral intensity) of the band at 1721 cm^{-1} was used to determine the concentration of phosphoenzyme, because this band has been assigned to the C=O vibration of Asp-351 formed upon phosphorylation (Barth et al., 1996, 1998; Von Germar et al., 2000). This local probe of phosphorylation reaction demonstrates that Ca_2E1P accumulates to the same extent with ITP and 2'-deoxyATP as with ATP. Therefore, the smaller signals in the amide I and II region obtained with the analogs cannot be explained by incomplete phosphorylation. Instead they are due to a smaller extent of

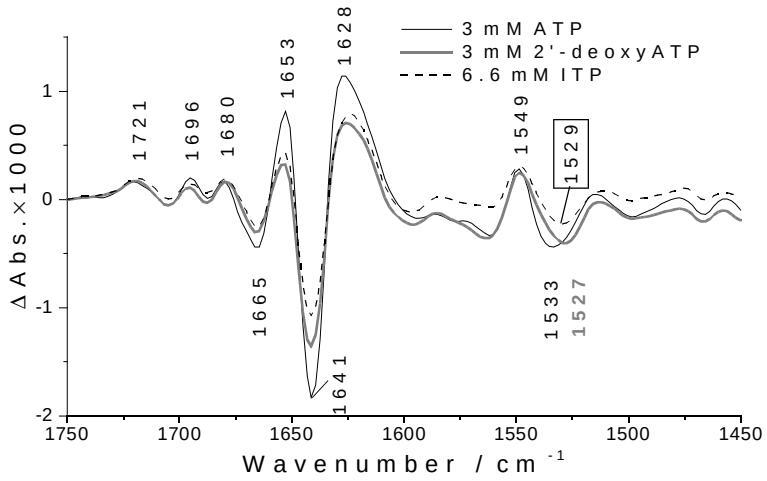

Fig. 3.5-2 Ca_2E1P formation spectra ($Ca_2E1 \rightarrow Ca_2E1P$) obtained with ATP, 2'-deoxyATP and ITP (1ºC, pH 7.5). The black labels refer to the band positions of the formation spectrum with ATP; the grey label refers to the spectrum with 2'-deoxyATP.

conformational changes showing that the conformation of Ca_2E1P depends on nucleotides used for Ca_2E1P formation. These results point out that 2'-OH and the 6-membered ring of the adenine moiety are important for full extent of conformational changes when Ca_2E1P forms, but their modifications do not affect the extent of Ca_2E1P accumulation.

The amplitude of Ca_2E1P formation spectrum obtained with ITP is larger than that of the ITP binding spectrum (Fig. 3.4-6). This will be more clear and discussed in the section of phosphorylation spectra later in chapter 3.5.2 (Fig. 3.5-10). Different band positions at 1527 cm^{-1} with 2'-deoxyATP and at 1529 cm^{-1} with ITP were observed. However this area is overlapped by the photolysis band at 1525 cm^{-1}. The subtraction of photolysis signals may affect the band position and amplitude at ~1525 cm^{-1}.

These two Ca_2E1P formation spectra obtained with ITP and 2'-deoxyATP have similar band amplitudes. However, their binding spectra in Fig. 3.4-5 and Fig. 3.4-6 have different band amplitudes. This reveals that the conformation with 2'-deoxyATP is similar to that with ITP in the Ca_2E1P state but not in the Ca_2E1N state.

As discussed above, Ca_2E1P accumulation cannot be observed completely with 3'-deoxyATP in this work. The spectrum averaged in the time interval of 165.4–224 s with 3'-deoxyATP samples is shown in Fig. 3.5-3. The shape of this spectrum is different from that of the Ca_2E1P formation spectrum obtained with ATP, with much smaller band amplitudes and different band positions. The marker band at 1721 cm^{-1} that was assigned to the phosphorylated Asp-351 is nearly invisible with 3'-deoxyATP. However, the band at 1707 cm^{-1} might be induced by the C=O of phosphorylated Asp-351. In conclusion, it cannot be confirmed whether the ATPase is phosphorylated with 3'-deoxyATP. The conformational change is probably due to the

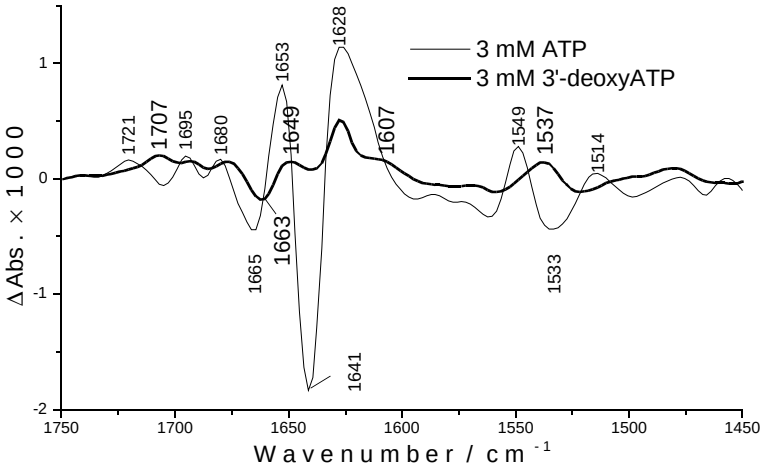

Fig. 3.5-3 Comparison of Ca_2E1P formation obtained with ATP and 3'-deoxyATP (1°C, pH 7.5). The small labels are for the spectrum of ATP, the large labels are for the spectrum of 3'-deoxyATP.

reorganization of the 3'-deoxyATP-ATPase complex, or the spectrum shows only further absorbance changes induced by 3'-deoxyATP binding. This demonstrates that 3'-OH in the ribose ring is important for ATP phosphorylating the ATPase and Ca_2E1P formation. Previous findings revealed a low phosphoenzyme concentration for both 2'- and 3'-deoxyATP (Coan et al., 1993). This discrepancy is likely due to the different buffers used because the associated conformational change depends on the composition of the medium as discussed in chapter 3.1.1.

<u>Ca_2E1P formation with ATP and ATP isotopomers</u>

The raw Ca_2E1P formation spectra obtained with ATP, [β,βγ-$^{18}O_3$]ATP and [γ-$^{18}O_3$]ATP are shown in Fig. 3.5-4A. Positive bands show the absorbance of the ATPase in the Ca_2E1P state, ADP and possibly excess ATP. Negative bands show the absorbance of caged ATP and Ca_2E1.

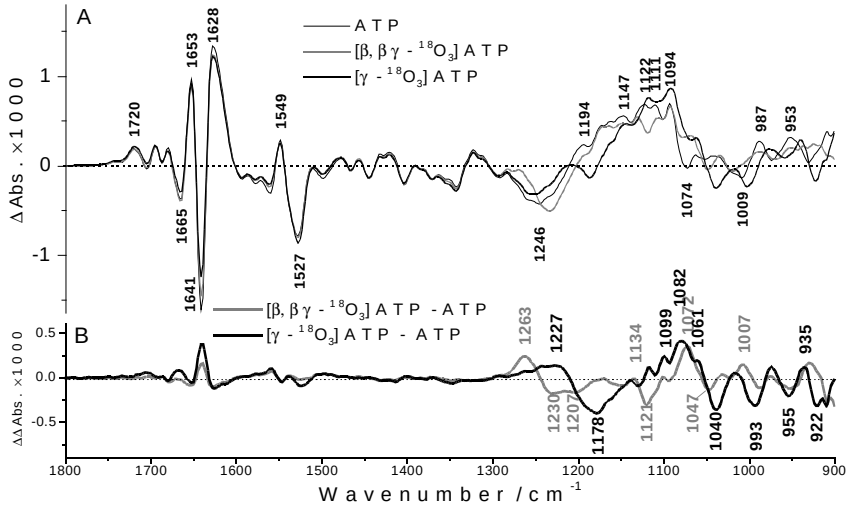

Fig. 3.5-4 A, Raw Ca_2E1P formation spectra (Ca_2E1 → Ca_2E1P) obtained with ATP, [β,βγ-$^{18}O_3$]ATP and [γ-$^{18}O_3$]ATP (1°C, pH 7.5). The labels indicate the band positions of the spectrum obtained with ATP. **B**, double difference spectra of Ca_2E1P formation. Grey labels refer to the *grey* line, black labels refer to the *black* line.

Above 1300 cm^{-1} outside the region of phosphate groups absorption, the raw Ca_2E1P formation spectra ATP isotopomers show the same band positions and similar band amplitudes as expected. The small differences in the amide I and II region, as more clearly shown in Fig. 3.5-4B, may be due to the subtle difference of different samples.

Band shifts due to isotope effects of the oxygen atoms on the β- and γ-phosphate are shown in the spectra below 1300 cm^{-1}. The phosphate groups of caged ATP, ADP, and the phosphoenzyme phosphate all absorb below 1300 cm^{-1} and result in negative and positive bands. The complicated overlap of these phosphate bands makes it difficult to assign the bands. The phosphate bands induced by caged ATP can be discussed by comparing the band shifts induced by caged ATP in the Ca_2E1P state to those obtained with the ATPase-free samples and with binding of ATP and ATP isotopomers in Fig. 3.4-8B. The isotope effect spectra in Fig. 3.5-5 show the phosphate band shifts of caged ATP photolysis observed in the absence and presence of the ATPase. In Fig. 3.5-5A the bands at 1263, 1130 and 1072 cm^{-1} always shift to 1230, 1120 and 1047 cm^{-1} with caged [β,βγ-$^{18}O_3$]ATP. In Fig. 3.5-5B the bands at 1227, ~1138, 1061 and 1016 cm^{-1} always shift to 1178, 1130, 1040 and 993 cm^{-1} with caged [γ-$^{18}O_3$]ATP. The identical shifts strengthen the assignments of these bands to caged ATP as discussed in chapter 3.4.6.

The band shifts due to the isotopically labeled β-phosphate of ADP and the isotopically labeled phosphoenzyme phosphate transferred from ATP are also shown in Fig. 3.5-4. However, as a result of the overlap with photolysis bands, these bands shift will be discussed below in chapter 3.5.3 of phosphorylation spectra, in which the photolysis signals were not shown.

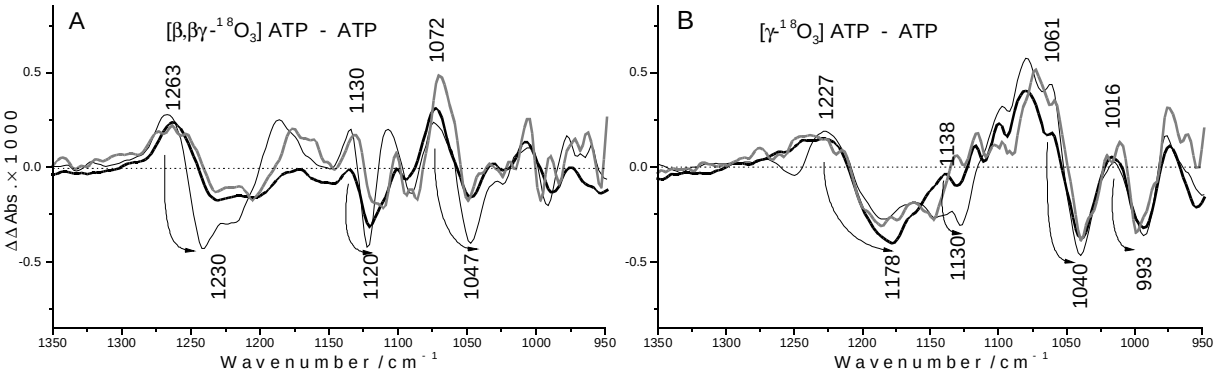

Fig. 3.5-5 Bands induced by caged ATP, obtained by comparison of band shifts of the isotope effect spectra with the ATPase-free samples (*black-thin* lines), with binding of ATP and ATP isotopomers binding (*grey* lines), and with Ca_2E1P formation (*black bold* lines). Labels are for the Ca_2E1P formation spectra. **A**, for [β,βγ-$^{18}O_3$]ATP; **B**, for [γ-$^{18}O_3$]ATP.

In Fig. 3.5-6 the difference spectra were obtained by subtracting the ATP of ATP isotopomers released spectra in the absence of the ATPase from the raw Ca_2E1P formation spectra obtained with ATP or ATP isotopomers in the presence of the ATPase, respectively. Therefore, the

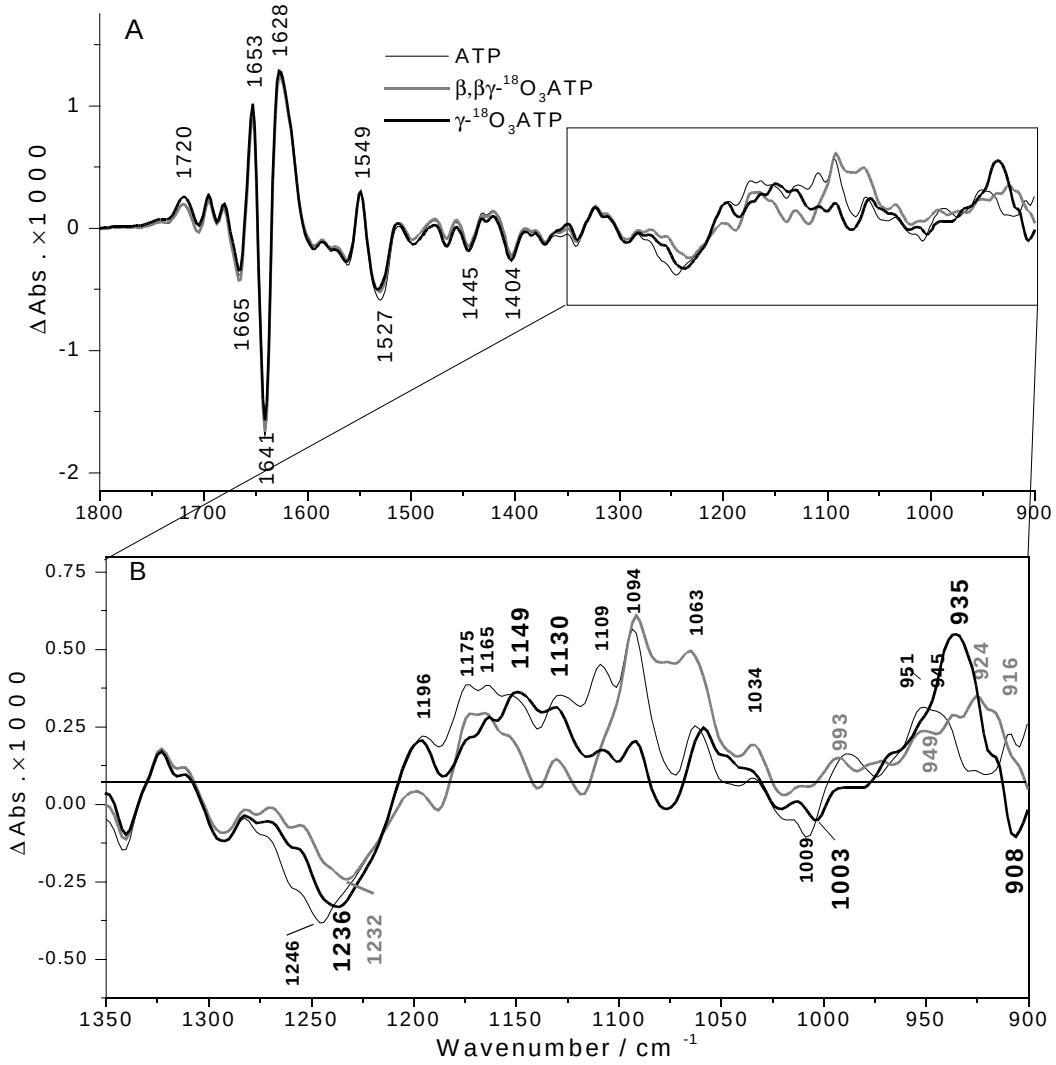

Fig. 3.5-6 Difference spectra obtained by subtracting the ATP/ATP isotopomers release spectra from the raw Ca_2E1P formation spectra obtained with ATP, [β,βγ-$^{18}O_3$]ATP and [γ-$^{18}O_3$]ATP (1°C, pH 7.5). **A**, from 1800 to 900 cm^{-1}; **B**, from 1350 to 900 cm^{-1}.: the small black labels refer to the *black-thin* line, the grey labels refer to the *grey* line, the large black labels refer to the *black-bold* line.

photolysis signals induced by caged ATP were subtracted. The phosphate bands induced by ADP and the phosphoenzyme phosphate from 1300 to 1000 cm^{-1} will be discussed in chapter 3.5.3. The bands at 987 and 953 cm^{-1} in the raw Ca_2E1P formation spectrum obtained with ATP in Fig. 3.5-4 are discussed here. After subtraction of photolysis signals, the band at 987 cm^{-1} disappears in Fig. 3.5-6, which shows this band is induced by excess free ATP. In Fig. 3.5-6B with [γ-$^{18}O_3$]ATP the band at 945 cm^{-1} may not shift and the band at 951 cm^{-1} may shift to ~935 cm^{-1}. The overlay of these two bands results in large band amplitude at 935 cm^{-1}. Therefore, the band at 951 cm^{-1} may be assigned to the phosphoenzyme phosphate group. With [β,βγ-$^{18}O_3$]ATP, the band amplitudes at 951 and 945 cm^{-1} decrease and these two bands shift to 924 and 916 cm^{-1}. Therefore, these two bands can be tentatively assigned to the β-PO_3^{2-} of ADP. The band at 951 cm^{-1} may have two components, one owing to ADP and the other owing to the phosphoenzyme phosphate, since the band shift was observed with both ATP isotopomers.

3.5.2 Phosphorylation spectra with different nucleotides

The phosphorylation reaction is shown in Fig. 3.5-7. After nucleotide binding and conformational changes of the ATPase, the γ-phosphate is transferred to Asp-351 of the ATPase. At the same time ADP forms.

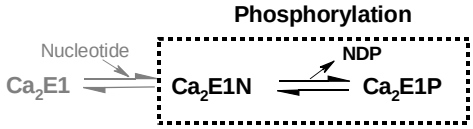

Fig. 3.5-7 Phosphorylation of the ATPase after nucleotide binding.

Phosphorylation of the Ca^{2+}-ATPase with ATP and ATP isotopomers

Phosphorylation with ATP - ATP phosphorylates the ATPase and induces the phosphorylation spectrum ($Ca_2E1ATP \rightarrow Ca_2E1P + ADP$) as shown in Fig. 3.5-8. Negative bands are characteristic of the ATP-ATPase complex Ca_2E1ATP, and positive bands are characteristic of the ADP-sensitive phosphoenzyme Ca_2E1P and ADP. The spectra below 1000 cm^{-1} may be disturbed because of the absorption of CaF_2 windows and the band assignments 1000 cm^{-1} will not be discussed in detail. The amplitude of IR signals induced by ATPase phosphorylation is much smaller than that induced by ATP binding and Ca_2E1ATP formation. This indicates that the conformational changes during phosphorylation ($Ca_2E1ATP \rightarrow Ca_2E1P$) are smaller than those upon ATP binding ($Ca_2E1 \rightarrow Ca_2E1ATP$), in line with previous observations (Barth et al., 1996, 1998). This is also consistent with the finding with a different method (Danko et al., 2001a, b) showing that Ca_2E1ATP and Ca_2E1P have similar patterns of susceptibility to proteinase K and V8 but distinctly different from Ca_2E1 and E2P. The phosphorylation spectrum obtained with ATP has similar band amplitude and band positions as observed before (Barth et al., 1996, 1998) which demonstrates the excellent reproducibility of IR spectroscopy. Subtle differences may be due to the different buffer conditions.

Most of bands in phosphorylation spectrum obtained with ATP in Fig. 3.5-8 can be assigned as in ref. (Barth et al., 1994, 1998), of which the band assignments are shown in Table 3-6. The band at 1719 cm^{-1} was assigned to the ν(C=O) mode of Asp-351 phosphate. Changes of secondary structure are evident in the amide I (1700–1610 cm^{-1}) and amide II (1580–1500 cm^{-1}) region. The bands below 1300 cm^{-1} mainly show the changes of phosphate groups. In this work with [β,βγ-$^{18}O_3$]ATP and [γ-$^{18}O_3$]ATP, new assignments or corrections in the region of phosphate group absorption were made as shown in Table 3-7 and as discussed below.

Table 3-6. Band assignments of the phosphorylation spectrum obtained with 6 mM released ATP in ref. (Barth et al., 1994, 1998).

Band positions (cm^{-1})	Assignments
1719	C=O group of Asp-351 phosphate
1657	Amide I mode of α-helical structures
1689, 1635, 1628, 1616	Amide I mode of β-sheets
1595	ν_{as} mode of the COO^- groups of Asp / Glu residues
1547	Amide II mode of the peptide backbone
1241	$\nu_{as}(PO_2^-)$ mode of bound ATP
1173	Rearrangement of the phosphate groups during the phosphorylation
1147	side reaction of thiol reagents with photolysis byproducts
1130	PO_3^{2-} group of ADP and the phosphoenzyme phosphate group
1086	$\nu_s(PO_2^-)$ mode of bound ATP
1067	$\nu_s(\alpha\text{-}PO_2^-)$ mode of ADP

Table 3-7. Band assignments of the phosphorylation spectrum obtained with 3 mM ATP.

Band positions (cm^{-1})			Assignments
ATP	[β,βγ-$^{18}O_3$]ATP	[γ-$^{18}O_3$]ATP	
1239[a]	-	-	$\nu_{as}(\alpha\text{-}PO_2^-)$ mode of bound ATP
1205[b]	1175[b]	-	$\nu_{as}(PO_2^-)$ mode of the β-phosphate of bound ATP
1190[a]	-	-	$\nu_{as}(PO_2^-)$ mode of ADP
1147[a]	1159[b]	1115[b]	$\nu_{as}(PO_3^{2-})$ mode of the γ-phosphate of bound ATP
1131[b]	-	1099-1086	$\nu_{as}(PO_3^{2-})$ mode of the phosphoenzyme phosphate group
1126[b]	1094[b]	-	β-PO_3^{2-} group of ADP
1099[b]	-	1070[b]	γ-PO_3^{2-} group of bound ATP
1086[b]	1069[b]	1070-1051[b]	β-PO_2^- group of bound ATP, affected by the γ-phosphate group
951[c]	924-916[c]	937[c]	β-PO_3^{2-} group of ADP and the phosphoenzyme phosphate group
945[c]	924-916[c]	-	β-PO_3^{2-} group of ADP

Notes: The band labeled by [a] and [b] refer to Fig. 3.5-9A and Fig. 3.5-9B, respectively. The bands labeled by [c] have been discussed in Fig. 3.5-6. - means no band shifts observed.

Phosphorylation with ATP isotopomers – The phosphorylation spectra obtained with [β,βγ-$^{18}O_3$]ATP and [γ-$^{18}O_3$]ATP are shown in Fig. 3.5-8. These two phosphorylation spectra are very similar to that obtained with ATP above 1300 cm^{-1}.

Below 1300 cm^{-1} where signals are mainly due to the phosphate groups, significant differences were observed as shown in the phosphorylation spectra and respective isotope effect spectra (subtraction between the phosphorylation spectrum obtained with ATP isotopomers and with

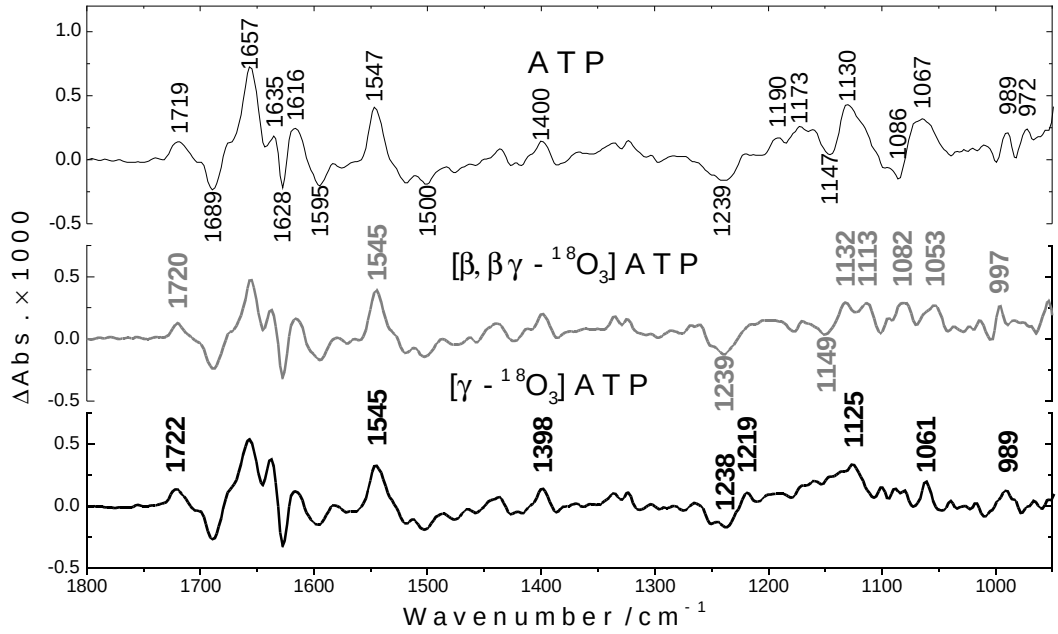

Fig. 3.5-8 Phosphorylation spectra (1°C, pH 7.5) obtained with ATP (upper), [β,βγ-$^{18}O_3$]ATP (middle) and [γ-$^{18}O_3$]ATP (lower).

unlabeled ATP) in Fig. 3.5-9. In the isotope effect spectra only the shifted bands show up and all bands that are not affected by labeling are subtracted, as illustrated in Fig. 3.4-12 of chapter 3.4.6.

The band at 1239 cm^{-1} in Fig. 3.5-9A was assigned as an $\nu_{as}(PO_2^-)$ mode of bound ATP (Barth et al., 1996) due to the loss of one PO_2^- group in ATP converting to ADP. Here no shift was observed with [β,βγ-$^{18}O_3$]ATP. Therefore, this band may be assigned as the $\nu_{as}(\alpha\text{-}PO_2^-)$ mode of bound ATP. The band at 1219 cm^{-1} in the bottom panel of Fig. 3.5-9A might be assigned to the $\nu_{as}(PO_2^-)$ mode of ADP. In the upper panel of Fig. 3.5-9A with unlabeled ATP this band is not observed, which may be due to the overlap with a negative band of bound ATP. The shift from 1205 to 1175 cm^{-1} with [β,βγ-$^{18}O_3$]ATP in Fig. 3.5-9B can be assigned to the $\beta\text{-}PO_2^-$ group of bound ATP, in line with the observation in the binding spectra in Fig. 3.4-15B. An overlap with a positive band nearby may be the reason of this band only shown in the isotope effect spectrum. The band at 1190 cm^{-1} in Fig. 3.5-9A can be assigned to $\alpha\text{-}PO_2^-$ of ADP because no band shift was observed with [β,βγ-$^{18}O_3$]ATP.

The assignment of the band at 1147 cm^{-1} is corrected here to the γ-phosphate of bound ATP. This band seems to shift to 1115 cm^{-1} in the phosphorylation spectrum obtained with [γ-$^{18}O_3$]ATP as shown in Fig. 3.5-9B. A similar shift was observed in the ATP binding spectra (Fig. 3.4-15B). This strengthens that this band is due to the γ-phosphate of bound ATP. The band at

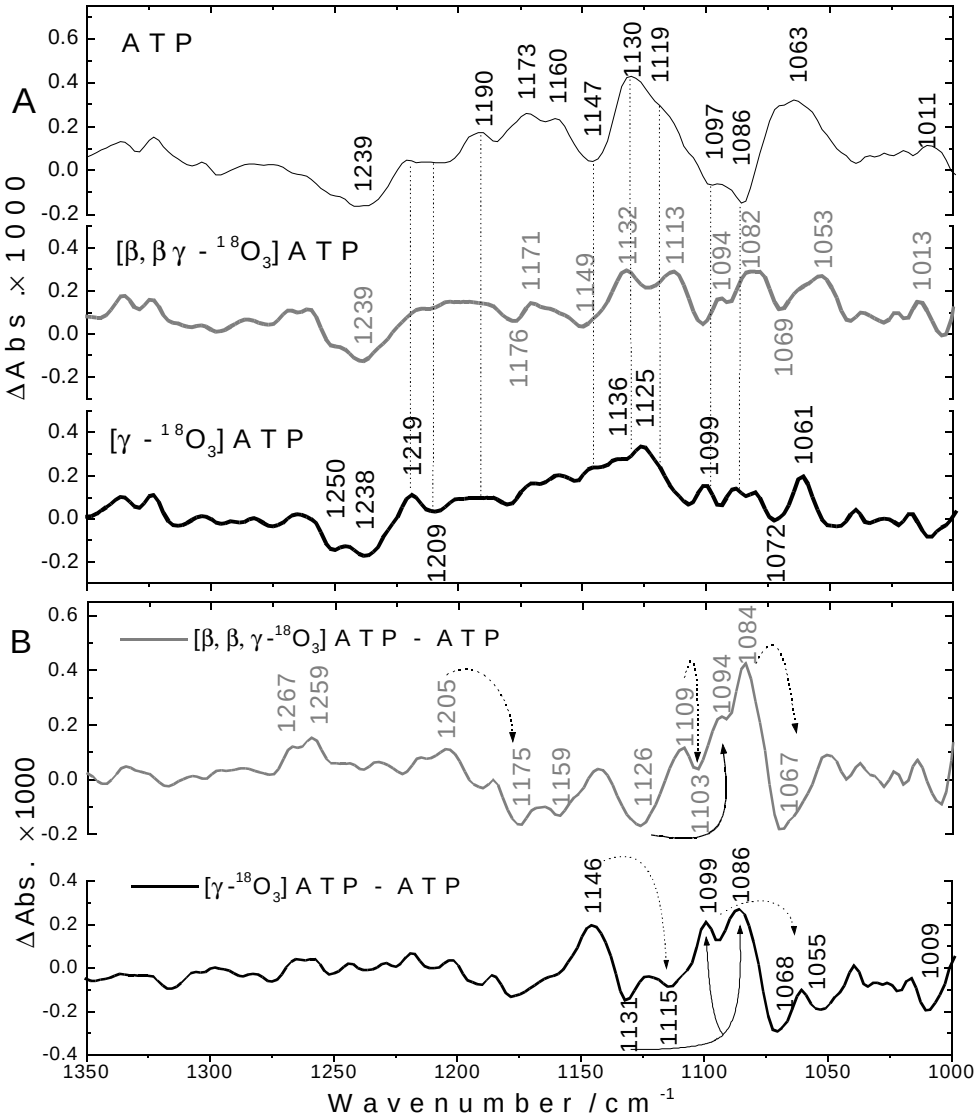

Fig. 3.5-9 A, Phosphorylation spectra obtained with ATP (upper), [β,βγ-$^{18}O_3$]ATP (middle) and [γ-$^{18}O_3$]ATP (lower) below 1350 cm^{-1} (1°C, pH 7.5, 3 mM ATP). **B**, isotope effect spectra below 1350 cm^{-1}. The dotted arrows show the band shifts of bound ATP; the solid arrows show the band shift of ADP.

1131 cm^{-1} in the lower panel of Fig. 3.5-9B is assigned to the phosphoenzyme phosphate group, because this band shifts to ~1099 or 1086 cm^{-1} in the isotope effect spectrum obtained with [γ-$^{18}O_3$]ATP, but does not shift with [β,βγ-$^{18}O_3$]ATP.

The positive shoulder at ~1119 cm^{-1} of the phosphorylation spectrum obtained with ATP in Fig. 3.5-9A can be assigned to the β-PO_3^{2-} group of ADP. Due to ATP conversion to ADP, the β-PO_2^- group of ATP is transformed to a β-PO_3^{2-} group of ADP. In the phosphorylation spectrum obtained with [β,β,γ-$^{18}O_3$]ATP in Fig. 3.5-9A, this band seems to shift to ~1094 cm^{-1}, whereas with [γ-$^{18}O_3$]ATP this shoulder is at 1125 cm^{-1} and no shift was observed. In the isotope effect spectrum of [β,βγ-$^{18}O_3$]ATP in the upper panel of Fig. 3.5-9B, this band shift is shown as a

negative band at 1126 cm^{-1} and a positive band at 1094 cm^{-1}. A similar band shift was observed with GTP phosphorylating Ras (Allin et al., 2001).

As shown in Fig. 3.5-9B, the band at 1099 or 1086 cm^{-1} in the isotope effect spectrum with [γ-$^{18}O_3$]ATP shifting to 1068 cm^{-1} can be assigned to the γ-PO_3^{2-} group of bound ATP. Similar band shifts were observed in the binding spectra as shown in Fig. 3.4-15B. The band at 1086 cm^{-1} in the isotope effect spectrum of [β,βγ-$^{18}O_3$]ATP could be also assigned to the β-phosphate of bound ATP because it shifts to 1067 cm^{-1} as shown in Fig. 3.5-9B. A similar shift from 1086 to 1070 cm^{-1} was observed in the binding isotope effect spectrum with [β,βγ-$^{18}O_3$]ATP in Fig. 3.4-15B. Therefore, the band at 1086 cm^{-1} may be due to a coupled vibration of the γ-PO_3^{2-} and β-PO_2^- group. In ref. (Barth et al., 1998) without using [β,βγ-$^{18}O_3$]ATP the shift of 1086 cm^{-1} was thought to be only due to the overlap by the shifted positive bands. A band shift from 1086 cm^{-1} to 1055 cm^{-1} with [γ-$^{18}O_3$]ATP in Fig. 3.5-9B is possible but not supported by the binding isotope effect spectra in Fig. 3.4-15B.

Phosphorylation of the Ca^{2+}-ATPase with 2'-deoxyATP

The phosphorylation spectrum obtained with 2'-deoxyATP shown in Fig. 3.5-10A was obtained by subtracting the 2'-deoxyATP binding spectrum from the Ca_2E1P formation spectrum obtained with 2'-deoxyATP. The phosphorylation spectrum obtained with 2'-deoxyATP shows similar signals as that obtained with ATP except for the bands at ~1643, 1241 and 1115 cm^{-1}. The difference at ~1640 cm^{-1} in the amide I region is possibly due to the different conformational changes of β-sheets of peptide backbone during phosphorylation with 2'-deoxyATP. The band at 1241 cm^{-1} has been assigned as the nucleotide $\nu_{as}(PO_2^-)$ mode (Barth et al., 1998). The conversion of nucleoside triphosphate (NTP) to nucleoside diphosphate (NDP) results in a loss of -PO_2^- group in the samples and generates a negative band here. The larger amplitude in the phosphorylation spectrum obtained with 2'-deoxyATP may imply faster conversion of 2'-deoxyATP to 2'-deoxyADP. One explanation is that there is an uncoupling reaction branch in the reaction cycle to hydrolyze more 2'-deoxyATP without Ca^{2+} transport. A larger amplitude of this band was observed in the phosphorylation spectrum obtained with ITP, too. It will be discussed in detail in chapter 3.5.3. The band at 1115 cm^{-1} may be due to phosphate groups of 2'-deoxyADP.

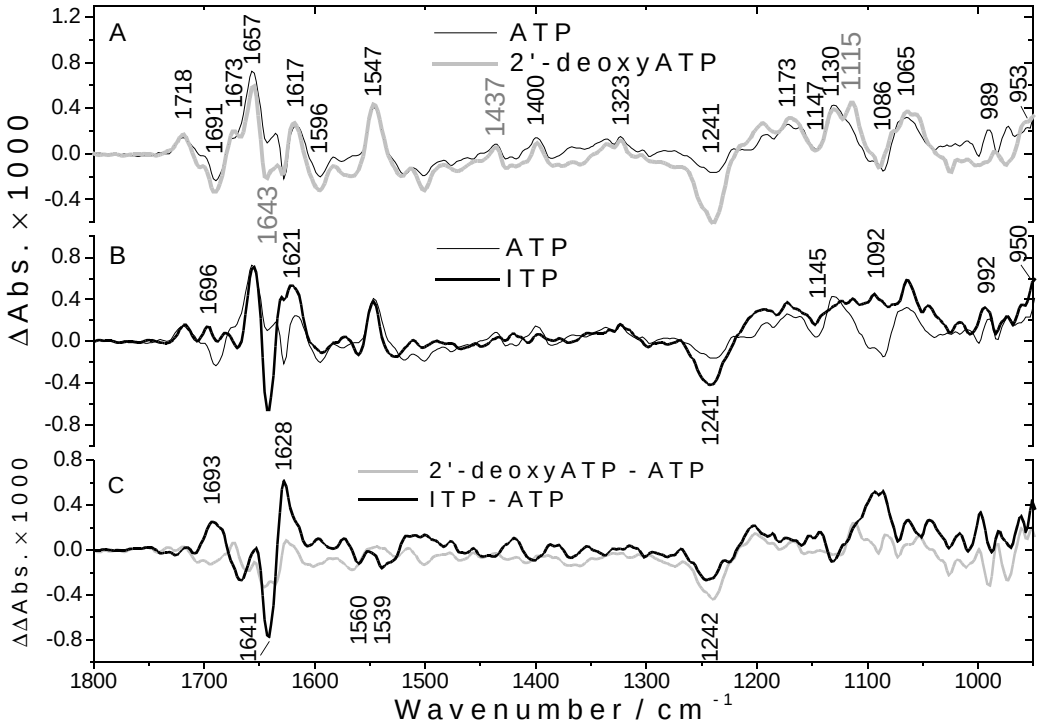

Fig. 3.5-10 A, phosphorylation spectra obtained with 3 mM ATP and 2'-deoxyATP (1°C, pH 7.5). The black labels are for the spectrum with ATP and grey labels are for the spectrum with 2'-deoxyATP. **B**, phosphorylation spectra obtained with 3 mM ATP and 6.6 mM ITP (1°C, pH 7.5). The black labels are for the spectrum with ITP. **C**, double difference phosphorylation spectra of (2'-deoxyATP – ATP) and (ITP – ATP). The black labels are for the spectrum of (ITP – ATP).

Phosphorylation of the Ca^{2+}-ATPase with ITP

The phosphorylation spectrum obtained with ITP is different from those obtained with ATP and 2'-deoxyATP, especially in the amide I region as shown in Fig. 3.5-10B. The signals at 1696 and ~1691 cm^{-1} are different from those in the phosphorylation spectra obtained with ATP and 2'-deoxyATP, which indicates the conformational changes of β-sheets with ITP phosphorylating the ATPase are different. The larger amplitude of bands at 1642 and 1621 cm^{-1}, and of the shoulder at 1628 cm^{-1} indicate that relatively large conformational changes take place upon enzyme phosphorylation with ITP. The amplitudes of these bands in Fig. 3.5-10B are larger than those in the ITP binding spectrum. This indicates that larger changes are induced by ITP phosphorylation of the ATPase than by ITP binding. This makes the Ca_2E1P formation spectrum obtained with ITP more similar to that with ATP, whereas the ITP binding spectrum is less similar to the ATP binding spectrum. The bands at 1642 and 1621 cm^{-1} are close to the marker bands at 1641 and 1628 cm^{-1} in the nucleotide binding spectrum. It could indicate that ITP binds slowly to the enzyme and induces conformational changes that overlap in time with those of the phosphorylation reaction. However, incomplete nucleotide binding is not the reason for this phenomenon because the kinetic analysis manifests that ITP binding (Fig. 3.3-2) and

phosphorylation (Fig. 3.3-4) are well separated in time. Moreover, the kinetics of the bands at 1642 and 1621 cm^{-1} is the same as that of phosphorylation. They are therefore associated with phosphorylation. Therefore, the signals in the phosphorylation spectrum obtained with ITP in Fig. 3.5-10B do only show enzyme phosphorylation with ITP.

In ITP samples, 6.6 mM ITP was released, 3.6 mM more than that in ATP samples. As shown in Fig. 3.5-10 the increasing amplitude in the amide I region of the Ca_2E1P formation spectrum with ITP could be due to the extra amount of ITP interacting with the ATPase in the phosphorylation reaction. However, in the samples with 3 mM released ITP, the increase of amplitude in the phosphorylation reaction exists too (data not shown). One possibility is that there are another regulatory site for ITP binding in the ATPase. The binding of ITP to this site induces conformational changes of the peptide backbone only during phosphorylation ($Ca_2E1ITP \rightarrow Ca_2E1P$) but not during ITP binding to the catalytic site ($Ca_2E1 \rightarrow Ca_2E1ITP$). However, this possibility asks for higher affinity of the regulatory site for ITP than for ATP that seems not convincing. Another possibility is that more conformational changes are needed for phosphorylation with ITP, as discussed in the first paragraph of this section, which is more convincing. Previous fluorometric studies of N-acetyl-N'-(5-sulfo-1-naphthyl)ethylenediamine attached to Cys-674 with binding of ATP, AMPPNP, ITP, GTP and CTP to the ATPase (Suzuki et al., 1987; Kubo et al., 1990; Kanazawa et al., 1995) found that the conformational change in nucleotide binding reaction is essential for the phosphoenzyme formation because this conformational change become rate-limiting for phosphoenzyme formation when it is slow at low ATP concentration. There may be a minimum conformational change required for phosphorylation, most of which occurs by ATP upon binding. ITP induces only part of this minimum conformational change in the binding reaction and this residual change has to occur upon phosphorylation.

As shown in Fig. 3.5-10B, the negative band at 1145 cm^{-1}, assigned to the γ-phosphate of bound ATP as discussed above, has smaller amplitude in the phosphorylation spectrum obtained with ITP compared with the band at 1147 cm^{-1} in phosphorylation spectra obtained with ATP and 2'-deoxyATP. This may indicate that the interaction of ITP's γ-phosphate with the ATPase is different from that of the γ-phosphate of ATP and 2'-deoxyATP, which points out that the modification in the 6-membered ring of adenine moiety in one end of ATP molecule may affect the interaction between the ATPase and the γ-phosphate group in the other end of ATP molecule. Besides, the negative band at 1086 cm^{-1} in the phosphorylation spectrum obtained with ATP is not observed in the spectrum with ITP. This band was assigned as a phosphate group

band of bound ATP in chapter 3.4.6. The disappearance of this band may indicate the phosphate groups of bound ITP interact differently with the ATPase compared with those of bound ATP. The band at 1092 cm^{-1} in Fig. 3.5-10B may be due to the phosphate groups of IDP.

Interactions between 3'-deoxyATP and the Ca^{2+}-ATPase after binding reaction

As discussed in chapter 3.3.2, with 3'-deoxyATP less accumulation of Ca_2E1P intermediate and slower reaction kinetics of the band at 1721 cm^{-1} were observed. Ca_2E1P formation with 3'-deoxyATP cannot been observed completely in this work. Therefore, the pure phosphorylation spectrum with 3'-deoxyATP is not available. However, by subtracting the 3'-deoxyATP binding spectrum from the spectrum averaged from 165.4 to 224 s measured with 3'-deoxyATP, the generated spectrum as shown in Fig. 3.5-11A provides some information about the phosphorylation reaction with 3'-deoxyATP. Except for bands at 1718 and 1674 cm^{-1}, most of the bands in the generated spectrum obtained with 3'-deoxyATP show different band positions and band amplitudes compared with the phosphorylation spectrum obtained with ATP. Therefore, as discussed in the section of Ca_2E1P formation, the phosphorylation with 3'-deoxyATP is unsure. The signals of the generated spectrum obtained with 3'-deoxyATP are possibly due to the reorganization of the 3'-deoxyATP-ATPase complex.

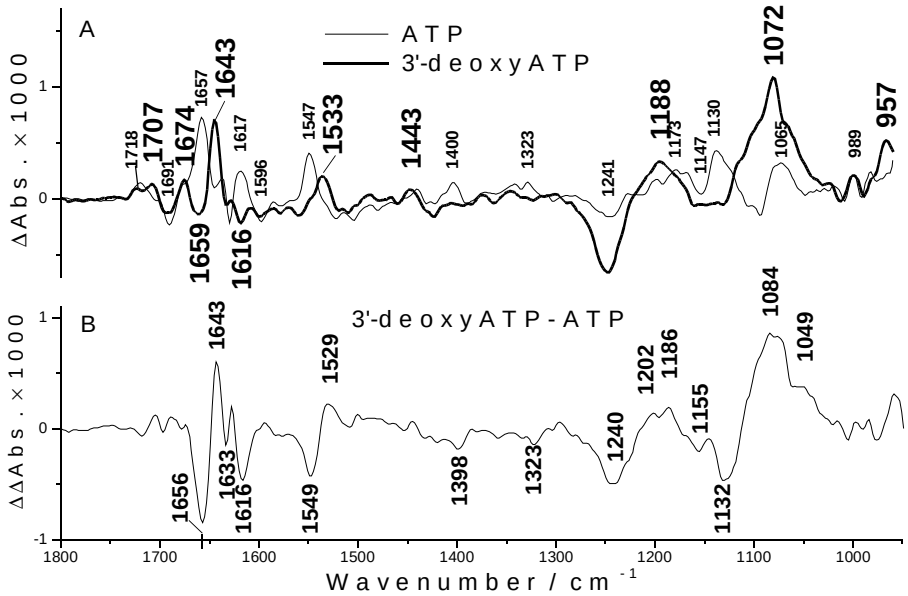

Fig. 3.5-11 A, comparison of the phosphorylation spectrum obtained with ATP and the spectrum obtained with 3'-deoxyATP by subtracting the 3'-deoxyATP binding spectrum from the spectrum averaged from 165.4 - 224 s. The small labels are for the spectrum with ATP and larger labels for the spectrum with 3'-deoxyATP. **B**, double difference spectrum obtained by subtraction between the phosphorylation spectrum obtained with ATP and the spectrum with 3'-deoxyATP in panel A (the *black-bold* line).

3.5.3 Comparison and discussion of the Ca^{2+}-ATPase phosphorylation

As shown above, phosphorylation of the Ca^{2+}-ATPase can be observed with ATP, ITP and 2'-deoxyATP but not with 3'-deoxyATP under the experimental conditions here. Phosphorylation reaction with ITP and 2'-deoxyATP is slower than that with ATP. The conformational change occurred during phosphorylation with ITP is larger than that with ATP and 2'-deoxyATP. Fast conversion from NTP to NDP seems occur with ITP and 2'-deoxyATP during phosphorylation than with ATP. With these results, it can be concluded that the functional groups of ATP, 2'-OH, 3'-OH and the adenine ring, are important for inducing the conformational change of the ATP-ATPase complex that is competent for phosphoryl transfer. This is shown by the dependence of the phosphorylation rate and the extent of the enzyme conformational changes on the modification of 2´-OH, 3´-OH and the adenine amino group. Therefore, interactions distant from the phosphate groups contribute to approaching the γ-phosphate to the residue Asp-351 or to forming the phosphate binding pocket. Therefore, phosphorylation is an interactive process in which the formation of interactions of a given functional group of ATP is reinforced by interactions of other groups, which can be at the opposite end of the ATP molecule.

Relationships between nucleotide binding and phosphoenzyme formation

A smaller amplitude in the nucleotide binding spectra and Ca_2E1P formation spectra was obtained with 2'-deoxyATP and ITP compared to that with ATP. However, the same amount of Ca_2E1P accumulated with ATP, 2'-deoxyATP and ITP. This shows that phosphorylation does not strictly depend on the full extent of the conformational change achieved by ATP binding. This is in line with the observation that pseudo substrates like acetyl phosphate are able to produce the same kind of phosphoenzyme as ATP (Bodley et al., 1987) although they are not expected to induce the same conformational change as ATP because their structures are even more different from ATP than those of the nucleotides investigated here.

There is no simple link between the extent of conformational change upon nucleotide binding and the ability to form the phosphoenzyme: (i) the extent is larger for 2'-deoxyATP than for ITP (Fig. 3.4-5 and Fig. 3.4-6) but the apparent phosphorylation rates are very similar (Fig. 3.3-4), (ii) the extent is similar for 3'-deoxyATP and ITP (Fig. 3.4-5 and Fig. 3.4-6) but significant phosphorylation is only observed for ITP.

If the conformational change detected in nucleotide binding spectra and the distance between γ-phosphate and phosphorylation site Asp-351 were correlated, a smaller conformational change would place the γ-phosphate further away from Asp-351 than a larger one and result in slower

phosphorylation. Then phosphorylation with ITP should be much slower than that with 2'-deoxyATP. This is not observed. Therefore the conformational change seen in the spectra seems to be not or only weakly correlated with the distance between γ-phosphate and Asp-351. This finding is in line with models in which the γ-phosphate in the nucleotide-ATPase complex is still some distance away from the phosphorylation site, as proposed by Hua et al. (Hua et al., 2002) for the Ca^{2+}-ATPase and Ettrich et al. for the Na^+, K^+-ATPase (Ettrich et al., 2001). Then, the γ-phosphate arrives at the catalytic site only after nucleotide binding. The γ-phosphate transfer could take place during the conformational change after nucleotide binding that has been identified as the rate-limiting step for phosphorylation (Petithory et al., 1986). The γ-phosphate in some distance to the phosphorylation site provides a possibility of binding a regulatory ATP molecule to the phosphoenzyme at the same site (Bishop et al., 1987).

Characteristic conformation of the phosphoenzyme

An enzyme structure characteristic of the nucleotide is inferred not only for the nucleotide-ATPase complex, but also for the Ca_2E1P state in which the conformation of the phosphoenzyme depends on the nucleotide that was used for phosphorylation.

The differences of the phosphorylation spectra obtained with ITP and 2'-deoxyATP compared with that with ATP are listed in Table 3-8 and are more clearly shown in the double difference spectra of the phosphorylation spectrum obtained with ITP or with 2'-deoxyATP minus that with ATP in Fig. 3.5-10C. Between ATP and 2'-deoxyATP, the differences are less and mainly shown by the $\nu_{as}(PO_2^-)$ mode of NTP conversion to NDP. This demonstrates that 2'-OH is not essential for ATP phosphorylating the ATPase. However, this group is important for fast phosphorylation, because the substitute of 2'-H slows down the phosphorylation reaction 5 times.

Another explanation for these bands is that more ITP binding is necessary for ITP phosphorylation. There seems to be a minimum extent of conformational changes required for the enzyme phosphorylation. In the first step of the reaction cycle, ITP binding-induced conformational changes are not enough to close the cleft between the N and P domain. Then during phosphorylation more ITP has to bind to the ATPase and induce more conformational changes for moving the γ-phosphate of bound ITP closer to the residue Asp-351. In Fig. 3.5-10C the double difference spectrum between the phosphorylation spectra obtained with ITP and ATP shows bands at 1693, 1641 and 1628 cm^{-1}. These bands were observed in the ATP binding spectrum. This may indicate that the extra conformational change upon interactions between ITP

and the ATPase during phosphorylation is similar to that upon ATP binding, which is required for subsequent phosphorylation.

Table 3-8. Differences in the band amplitudes and positions among ATP and ATP analogues in phosphorylation spectra.

Band Positions /cm^{-1}	**Assignments**	**Nucleotide with differences**
1696-1690	Amide I mode of β-sheet	ITP
1673	Amide I mode of turn	ITP
1645-1620	Amide I mode of β-sheet	2'-deoxyATP, ITP
1241	$\nu_{as}(PO_2^-)$ mode of bound nucleotide	2'-deoxyATP, ITP
1147	$\nu_{as}(PO_3^{2-})$ mode of γ-phosphate of bound nucleotide	ITP
1115-1113	In-phase $\nu_s(PO_2^-)$ mode of IDP and 2'-deoxyADP	2'-deoxyATP, ITP
1085	Phosphate groups of IDP	ITP

Different effects of ITP on phosphorylation of the ATPase have been observed before (Scofano et al., 1979; Kubo et al., 1990). Kubo et al. found that the effect of ITP, GTP and CTP binding on the conformational change around Cys-674 shown from the drop of fluorescence of I-EDANS was different with or without Ca^{2+}; however with ATP there was nearly no difference. This demonstrates the importance of the adenine moiety of ATP to the phosphoenzyme formation. Interestingly, Scofano et al. observed an overshoot of phosphorylation with 1 mM ITP but not with 5 µM ATP (pH 7.4, room temperature, 0.1 mM $CaCl_2$, 1.0 mg/ml leaky vesicles). However, similar steady state level of phosphoenzyme was obtained with 5 µM ATP and 1 mM ITP. This is partly consistent with the results here. In this instance the accumulation of Ca_2E1P state with 6.6 mM ITP and 3 mM ATP is similar but the conformational changes during phosphorylation with ITP is larger, which indicates extra interactions between ITP and the ATPase. However, an overshot of phosphorylation is not observed with ITP because the amplitude of the marker band at 1721 cm^{-1} in the phosphorylation spectrum obtained with ITP is the same as that with ATP.

3'-OH in the ribose ring is essential for ATP phosphorylating the ATPase, because with 3'-deoxyATP the time constant of the marker band at 1721 cm^{-1} is ~25 times slower than with ATP. At the same time, the spectrum averaged from 165.4 to 224 s obtained with 3'-deoxyATP (Fig. 3.5-3) is dramatically different from the Ca_2E1P formation spectra obtained with ATP, 2'-deoxyATP and ITP. It seems that the enzyme is not phosphorylated. The spectral changes may be only due to further rearrangement of the 3'-deoxyATP-ATPase complex.

ITP and 3'-deoxyATP show significant different properties from ATP with different spectra in both binding and phosphorylation, which demonstrates the importance of the adenosine ring and the 3'-OH group on the interactions between ATP and the ATPase. The changes at these two functional groups affect the transfer of γ-phosphate of ATP molecule.

Coupling between Ca^{2+} transport and ATP → ADP conversion

Besides the differences in amide I region, another important difference among the three phosphorylation spectra is the band at 1241 cm^{-1}. This band is due to a loss of one PO_2^- group upon phosphorylation as shown in Fig. 3.5-12. The larger amplitude of this band observed with ITP and 2'-deoxyATP during phosphorylation can be attributed to additional conversion from ITP to IDP and 2'-deoxyATP to 2'-deoxyADP. The kinetic evaluation of the 1241 cm^{-1} band obtained by fitting its integral intensity is shown in Fig. 3.5-13 and Table 3-9.

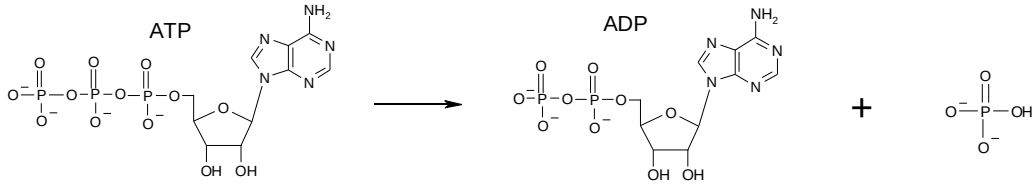

Fig. 3.5-12 Hydrolysis of ATP involving the net transformation of a PO_2^- group into a PO_3^{2-} group.

Fig. 3.5-13 shows the kinetic change of the band at 1241 cm^{-1} from 0 to 225 s. The negative integral intensity of this band increases during the measurements showing the extent of conversion from NTP to NDP. By comparing the time constants and amplitudes of ATPase phosphorylation and nucleotide conversion obtained in data fitting, it can be investigated whether ITP and 2'-deoxyATP convert more and faster to IDP and 2'-deoxyADP than ATP converts to ADP. As shown in Fig. 3.5-13 and Table 3-9, the kinetics of the band at 1241 cm^{-1} with ATP shows only the characteristic of phosphorylation, and ATP conversion to ADP is over when the phosphoenzyme is formed. The amplitude of the band observed with ATP is therefore solely attributed to the transfer of the γ-phosphate to the protein. With ITP and 2'-deoxyATP, two time constants in the second order exponential equation must be used to obtain good fitting results. The second constant and the larger amplitude of the band intensities show that more 2'-deoxyATP and ITP hydrolyze after the phosphoenzyme is formed. ITP conversion to IDP seems complete faster than 2'-deoxyATP conversion to 2'-deoxyADP. It is hypothesized that there is a branch reaction, which is much slower than ATPase phosphorylation with these two ATP analogs and results in uncoupling between NTP conversion to NDP and Ca^{2+} transport. With 3'-deoxyATP, the kinetics of the 1241 cm^{-1} band is the same as that of the 1721 cm^{-1} band.

However, the larger amplitude of the band intensity with 3'-deoxyATP may also indicate the uncoupling between 3'-deoxyATP conversion to 3'-deoxyADP and Ca^{2+} transport, which may explain the significant differences between the Ca_2E1P formation spectrum obtained with ATP and the spectrum averaged from 165.4 to 224 s obtained with 3'-deoxyATP (Fig. 3.5-3).

The branch reaction may uncouple conversion of ITP and 2'-deoxyATP to IDP and 2'-deoxyADP from Ca^{2+} transport through the membrane. Uncoupling of nucleotide conversion from NTP to NDP and Ca^{2+} transport was observed with UTP (Fortea et al., 2000). Branching reactions were found before with ITP and GTP (De Meis et al., 1974) that the SR Ca^{2+}-ATPase is phosphorylated by $[^{32}P]P_i$ through two different reactions: one is strongly inhibited by Ca^{2+} and is not modified when ITP, GTP or acetyl phosphate is added to the assay medium; the other reaction is observed in the presence of Ca^{2+} and requires ITP, GTP or acetyl phosphate as cofactors. The two reactions have a different pH profile and are inhibited by ATP and ADP to different extents. If there is a branch reaction in the formation of the ADP-insensitive phosphoenzyme in the presence of ITP, then it is also possible that there is a branch reaction in the formation of the ADP-sensitive phosphoenzyme with 2'-deoxyATP and ITP. The larger positive bands at 1115 and 1092 cm^{-1} in Fig. 3.5-10A and B may show the extra amount of 2'-deoxyADP and IDP, produced in uncoupled conversion from 2'-deoxyATP and ITP.

Table 3-9 Kinetic results of the band at 1241 cm^{-1} by fitting with exponential equations (Origin 5.0). t_p and A_p, t_b and A_b, are the time constants and the amplitudes of phosphorylation and of the branch reaction obtained by fitting, respectively.

Nucleotide	**ATP**	**ITP**		**2'-deoxyATP**		**3'-deoxyATP**
Time constants and amplitudes obtained by fitting	t_p = 2.0 s A_p = 3.3989	t_p = 8.66 s, A_p = 6.0335	t_b = 34.1 s A_b = 2.848	t_p = 6.67 s A_p = 6.19315	t_b = 76.7 s A_b = 4.6905	t_p = 54.5 s A_p = 6.7924

Another possible explanation for the different amplitude at the 1241 cm^{-1} band may be the presence of adenylate kinase in the samples of ATP and 2'-deoxyATP. Adenylate kinase was added in the samples of ATP and 2'-deoxyATP for removing the generated ADP or 2'-deoxyADP from the sample medium (see chapter 2.2.1). The reaction of adenylate kinase catalyzing ADP or deoxyADP and forming ATP/AMP or deoxyATP/deoxyAMP induces broad positive bands at 1230, 1080, ~980 cm^{-1} and negative bands at 1200 cm^{-1} (the author and A. Barth, unpublished observation). The band at 1230 cm^{-1} may overlap with the 1241 cm^{-1} band, which is due to conversion from NTP to NDP. If the smaller amplitude at 1241 cm^{-1} in the phosphorylation spectrum obtained with ATP was caused by the overlap of the adenylate kinase

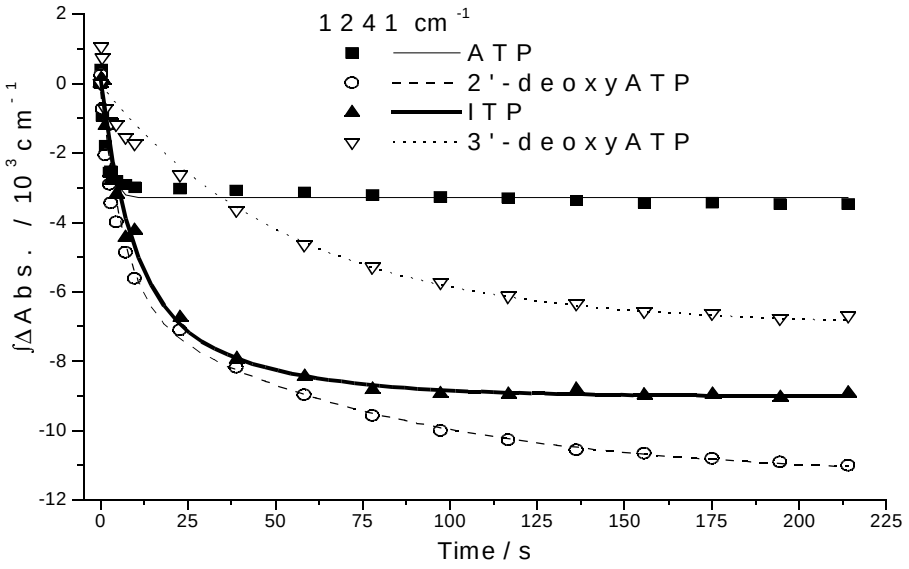

Fig. 3.5-13 Kinetics of the band at 1241 cm^{-1} of ATP and ATP analogs. The lines are obtained by fitting the bands with the first order exponential equation for ATP and 3'-deoxyATP, with the second order exponential equation for ITP and 2'-deoxyATP (Origin 5.0).

reaction band at 1230 cm^{-1}, then this band should be also smaller in the phosphorylation spectrum obtained with 2'-deoxyATP. This is not observed. If the band at 1230 cm^{-1} of adenylate kinase reaction affects the spectra in different ways with ATP and 2'-deoxyATP, then the band at ~1080 cm^{-1} should also be affected differently by the adenylate kinase reaction and the band shape at ~1080 cm^{-1} should look different. This is not the observed either. If AMP is produced, there will be a band between 990 and 980 cm^{-1}. A band at ~989 cm^{-1} was observed in the phosphorylation spectra obtained with ATP and ITP but not 2'-deoxyATP. Adenylate kinase was only added in the samples of ATP and 2'-deoxyATP. The band at ~989 cm^{-1} is therefore not due to AMP. A band at ~950 cm^{-1} in the phosphorylation spectra obtained with ATP, 2'-deoxyATP and ITP can be assigned to ADP, deoxyADP and IDP. This shows that not AMP, 2'-deoxyAMP and IMP but ADP, deoxyADP and IDP were produced. Therefore, the different amplitude here between phosphorylation spectra obtained with ATP and 2'-deoxyATP can not be explained by the effect of adenylate kinase reaction, but owing to different extent conversion from 2'-deoxyATP to 2'-deoxyADP as compared with ATP. At the same time, adenylate kinase catalyzes the reaction of forming ATP and AMP from ADP very slowly at 1°C, which could not be observed during the measurements (N. Bezlyepkina's unpublished results).

3.6 E2P formation and E2P hydrolysis of the Ca^{2+}-ATPase with different nucleotides

After nucleotide binding and phosphorylation, the ADP-insensitive phosphoenzyme E2P forms, and Ca^{2+} ions are released at the same time (Barth et al., 1997b), as shown in Fig. 3.6-1. Under physiological conditions, E2P is hydrolyzed rapidly, then the enzyme adopts an equilibrium between E1 and E2. In this work with type II samples (see chapter 2), hydrolysis of E2P was inhibited by the addition of DMSO, so that E2P accumulated and was hydrolyzed only slowly.

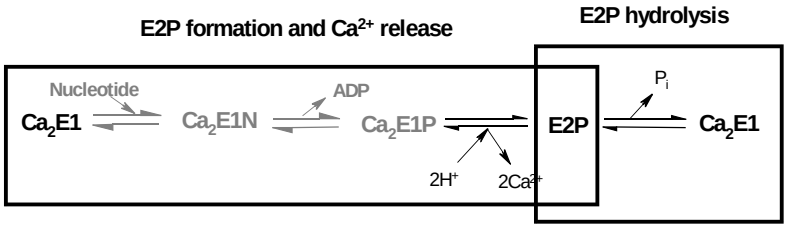

Fig. 3.6-1 E2P formation and Ca^{2+} release reaction, and the subsequent E2P hydrolysis.

3.6.1 E2P formation with ATP and ITP

<u>The E2P formation spectrum obtained with ATP</u>

According to the kinetic results of chapter 3.3.3, E2P formation spectra were obtained by averaging spectra from 0.32 s to 2.54 s after the photolysis flash(es) for ATP, and from 1.51 s to 16.3 s for ITP. The spectra are shown in Fig. 3.6-2A. Photolysis signals have not been subtracted. Therefore, positive bands show the absorbance of the enzyme in the E2P state, ATP and ADP, and negative bands show the absorbance of the Ca_2E1 state and caged nucleotide.

In the upper panel of Fig. 3.6-2A is the E2P formation spectrum obtained with ATP observed in methylimidazole buffer at pH 7.5 and 25°C, which has similar shape and amplitude to the E2P formation spectrum observed in (Barth et al., 1996) under different conditions (2-3 mM ATP, imidazole buffer, pH 7.0 and 1°C). The band amplitudes in the amide I region are larger than those in the ATP binding spectrum and the Ca_2E1P formation spectrum obtained with ATP. This indicates that the conformation of E2P is more different from that of Ca_2E1 than those of Ca_2E1ATP and Ca_2E1P, which is in line with recent observations (Danko et al., 2001a, b) found in a limited proteolysis study that the three domains of cytoplasmic region close compacter in the E2P state than in the Ca_2E1ATP and Ca_2E1P state when the three domains in Ca_2E1 state open loosely. In the amide I region, the bands at 1688, 1643 and 1630 cm^{-1} are characteristic of β-sheets, at 1653 cm^{-1} of α-helical structure. The bands at 1670 and 1662 cm^{-1} may show conformational changes of turns. The shape of this spectrum is very different from that of the

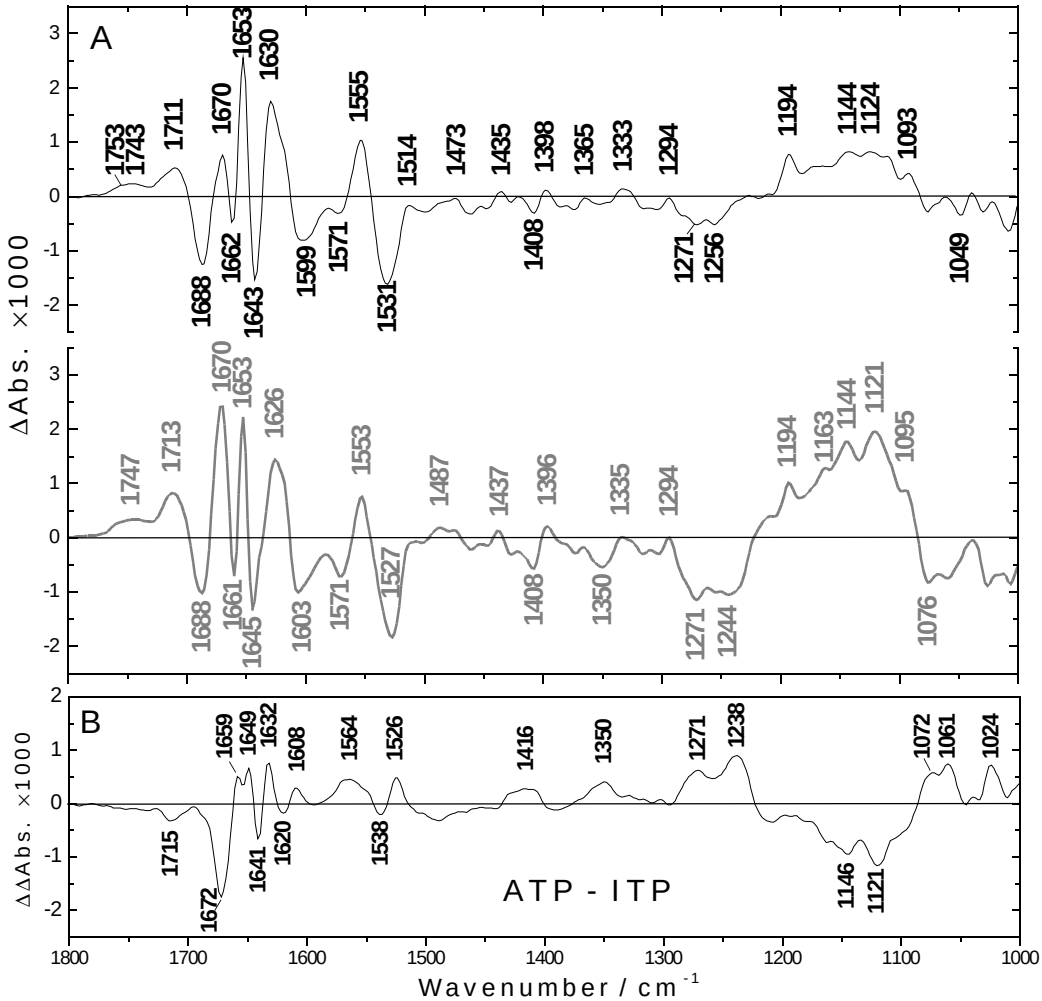

Fig. 3.6-2 A, E2P formation spectra with ATP and ITP (25°C, pH 7.5). The *black* line, with ATP; the *grey* line, with ITP. **B**, double difference spectrum of the E2P formation spectrum with ATP minus the E2P formation spectrum with ITP.

ATP binding spectrum and the Ca_2E1P formation spectrum obtained with ATP. In the amide I region, the differences are revealed in larger band amplitudes observed at 1688 and 1653 cm^{-1}, different band positions at 1643 and 1630 cm^{-1}, and opposite sign at 1670 cm^{-1}.

Some band assignments have been discussed in (Barth et al., 1994, 1996, 1997b; Barth, 1999). The bands at ~1750 and 1711 cm^{-1} can be assigned to the protonation of at least two Ca^{2+} chelating carboxylate groups of Asp/Glu side chains (Barth et al., 1996, 1997b). The bands at 1643 and 1630 cm^{-1} were assigned to the amide I modes of β-sheet structures or the C=O group of Asn/Gln residues (Chirgadze et al., 1975; Barth et al., 1994; Barth, 1999). The band at 1621 cm^{-1} was assigned to β-sheets, or to the imide group of a Pro residue in a helical or unordered conformation (Barth, 1999), or to COO^- side chain groups not interacting with water (Barth, 1999). Side chains of Arg, $HisH^+$, and Lys (Chirgadze et al., 1975; Venyaminov et al., 1990; Hienerwadel et al., 1997) can also absorb in the amide I region (1700–1610 cm^{-1}). The band at 1599 cm^{-1} may be attributed to a Pro imide group or COO^- side chain groups not interacting with

water (Doyle et al., 1971; Barth, 1999). The band pairs at 1571/1555 cm^{-1} and 1408/1398 cm^{-1} have been assigned to the $\nu_{as}(COO^-)$ and $\nu_s(COO^-)$ mode of Ca^{2+} chelating Asp/Glu carboxylate groups and of Ca^{2+} free Asp/Glu carboxylate groups (Barth et al., 1996), respectively, partially shielded from the aqueous environment (Barth et al., 1994; Barth, 1999). The band at 1514 cm^{-1} assigned to the ring mode of protonated Tyr residue (Chirgadze et al., 1975; Venyaminov et al., 1990; Hienerwadel et al., 1997; Barth, 1999) is nearly invisible here. This may de due to different sample conditions in this work compared with those in the literature. The band at 1365 cm^{-1} was assigned to the $\delta_s(CH_3)$ mode of aliphatic side chains (Barth, 1999). The band at 1333 cm^{-1} may be induced by the changes of turn structures of amide III modes (Goormaghtigh et al., 1994a, b), or the δ(COH) mode of Ser, Asp, or Glu with a weakly bonded OH group (Barth et al., 1994; Barth, 1999). The negative band at 1342 cm^{-1} induced by the nitro group of caged ATP is expected but not observed. There may be an overlap of positive bands nearby induced by conformational changes of the enzyme. The band at 1294 cm^{-1} was assigned to the ν(C-O) mode of Tyr or a Trp mode (Takeuchi et al., 1986) (Tyr-763 is involved in the cytoplasmic gate to Ca^{2+} binding sites (Andersen, 1995). The band at 1194 cm^{-1} was assigned to the E2P phosphate group (Barth et al., 1996; Barth, 1999). In the Ca_2E1P formation spectrum obtained with ATP, the phosphoenzyme phosphate group shows a band at ~1130 cm^{-1}. A possible reason for the different positions where the phosphoenzyme phosphate group absorbs is that the phosphate group in the E2P state absorbs differently from that in the Ca_2E1P state. In the E2P state, the environment around the phosphoenzyme phosphate group is hydrophobic, whereas in the Ca_2E1P state, the environment is hydrophilic. This will result in different absorption. The bands at 1531, 1271 and 1256 cm^{-1} can be assigned to the photolysis of caged ATP (Barth et al., 1990, 1994, 1996). A component of the band at ~1531 cm^{-1} shows also a conformational change of the protein as discussed below in chapter 3.6.2.

The E2P formation spectrum obtained with ITP

The E2P formation spectrum with ITP is shown in the lower panel of Fig. 3.6-2A. The spectral shape and band positions are similar to those of the spectrum with ATP. This indicates that the conformation of E2P formed with ITP is similar to that with ATP. However, small variations in band amplitudes and band positions are noticeable particularly in the amide I region which are highlighted in the double difference spectrum.

The double difference spectrum obtained from the E2P formation spectrum with ATP minus that with ITP is shown in Fig. 3.6-2B. The differences between the two E2P formation spectra are mainly observed at the bands in the amide I region (1672, 1659, 1649, 1641 and 1632 cm^{-1}), the

amid II region (1564, 1538 and 1526 cm^{-1}), and phosphate group bands (1271, 1238, 1146, 1121, 1072, 1062 and 1024 cm^{-1}). And subtle differences exist in the entire spectral region revealing absorbance changes of side chains. The differences in the amide I region indicate that structural changes of β-sheets or turns (1670, 1641, 1632 and 1620 cm^{-1}) and α-helix (1659 and 1649 cm^{-1}) upon E2P formation with ITP are different from those with ATP.

It was found before (Barth et al., 1996) that some bands' characteristics for the Ca_2E1P state phosphorylated with ATP are still present in E2P state. This was observed with both ATP and ITP here, which is obvious for the bands at 1653, 1641, and 1630 cm^{-1}. With ITP, the sustained characteristics of signals was also observed at 1238 cm^{-1}. More ITP hydrolysis was observed in Ca_2E1P formation with type I samples (see chapter 3.4). Therefore, the larger amplitude of bands at 1238 cm^{-1} in Fig. 3.6-2B should be induced by more ITP hydrolysis when the Ca_2E1P state was formed, and these changes are still present in E2P state, as discussed below in chapter 3.6.2. The larger amplitude below 1300 cm^{-1} with ITP is also due to the more release amount of ITP (6.6 mM) than that of ATP (3 mM). The bands at 1144, 1121 and 1093 cm^{-1} in the E2P formation spectrum obtained with ITP show the absorption of ITP.

The extent of conformational changes of E2P formation with ITP is similar to that with ATP, which is different from the results of conformational changes in nucleotide binding and Ca_2E1P formation. This may be because the conditions of type II samples are more favorable for ITP interacting with the ATPase than those of type I samples. In type II samples, Ca_2E1P cannot be accumulated and this may reduce the extent of the branch reaction of ITP, which uncouples ITP hydrolysis and Ca^{2+} transport. This reduction can result in more ITP hydrolysis coupling with Ca^{2+} transport and cause larger conformational change when E2P forms than in type I samples.

Similar experiments were done with ITP but at 1°C (data not shown). E2P formation was observed but seemed not complete because the amplitudes of bands are smaller than the spectrum with ITP shown in Fig. 3.6-2B. E2P hydrolysis was not observed at 1°C. This shows that the low temperature is favorable for observing E2P accumulation with ITP and high temperature is favorable for E2P hydrolysis.

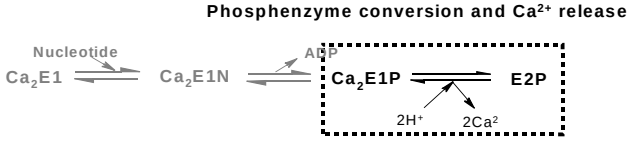

Fig. 3.6-3 Reaction of phosphoenzyme conversion and Ca^{2+} release.

Fig. 3.6-3 shows the phosphoenzyme conversion from Ca_2E1P to E2P, and the Ca^{2+} ions released from the ATPase at the same time (Barth et al., 1997b). They cannot be observed with

type II samples at 25°C, because Ca_2E1P formation is too fast to be observed. Therefore, the phosphoenzyme conversion spectra ($Ca_2E1P \rightarrow E2P$) cannot be obtained. Similar studies about phosphoenzyme conversion were done at 1°C (Barth et al., 1996, 1998).

3.6.2 Spectral changes during measurements with type II samples

Spectral changes with ATP in type II samples

E2P formation and Ca^{2+} release were studied in time-resolved FTIR kinetic measurements at 25°C. Fig. 3.6-4A shows a sequence of spectra obtained with ATP averaged in different time intervals after one photolysis flash. The reaction between ATP and the ATPase was fast and the E2P state was observed in the first two spectra in Fig. 3.6-4A. After that E2P was hydrolyzed and the ATPase converts to the Ca_2E1 state. This is confirmed by the decrease of signal amplitudes in the amide I region during the measurement. The last spectrum averaged from 204.4 - 223.8 s shows very small bands in the amide I region. This indicates that the final state of ATPase secondary structure is similar to the initial state Ca_2E1. The small signals of the last spectrum above 1300 cm^{-1} (except for the bands at 1526 and 1342 cm^{-1}) may be due to the incomplete hydrolysis of E2P.

The bands at 1526 and 1342 cm^{-1} in the last spectrum averaged from 204.4 to 223.8 s can be assigned to the ν_{as} and ν_s modes of the nitro group of caged ATP which were lost upon photolysis (Barth et al., 1990, 1995). The amplitude of the band at 1526 cm^{-1} in the last spectrum is likely the true amplitude of photolysis signals, and the larger amplitude in the first three spectra indicates a conformational change. This conformational change seems not to be induced by the amide II mode of the protein backbone because this band does not show the strong sensitivity toward $^1H \rightarrow {}^2H$ exchange (Barth, 1999). Side chains of residues may absorb in this region.

The bands below 1300 cm^{-1} arise predominantly from phosphate groups. The band at 1256 cm^{-1} can be assigned to ATP hydrolysis because the β-PO_2^- of caged ATP becomes the β-PO_3^{2-} of ADP. This band may also show photolysis of caged ATP. The band at 1194 cm^{-1} has been assigned to the phosphate group of E2P (Barth et al., 1996; Barth, 1999). This band was not observed in the last spectrum that confirms E2P hydrolysis and Ca_2E1 formation in the final state. The band at 1173 cm^{-1} in the last spectrum averaged from 204.4 to 223.8 s may be due to the hydrolyzed phosphoenzyme phosphate group. It is reasonable that the 1194 cm^{-1} band downshifts to 1173 cm^{-1} after the phosphate group in the bound state is hydrolyzed to be in the free state.

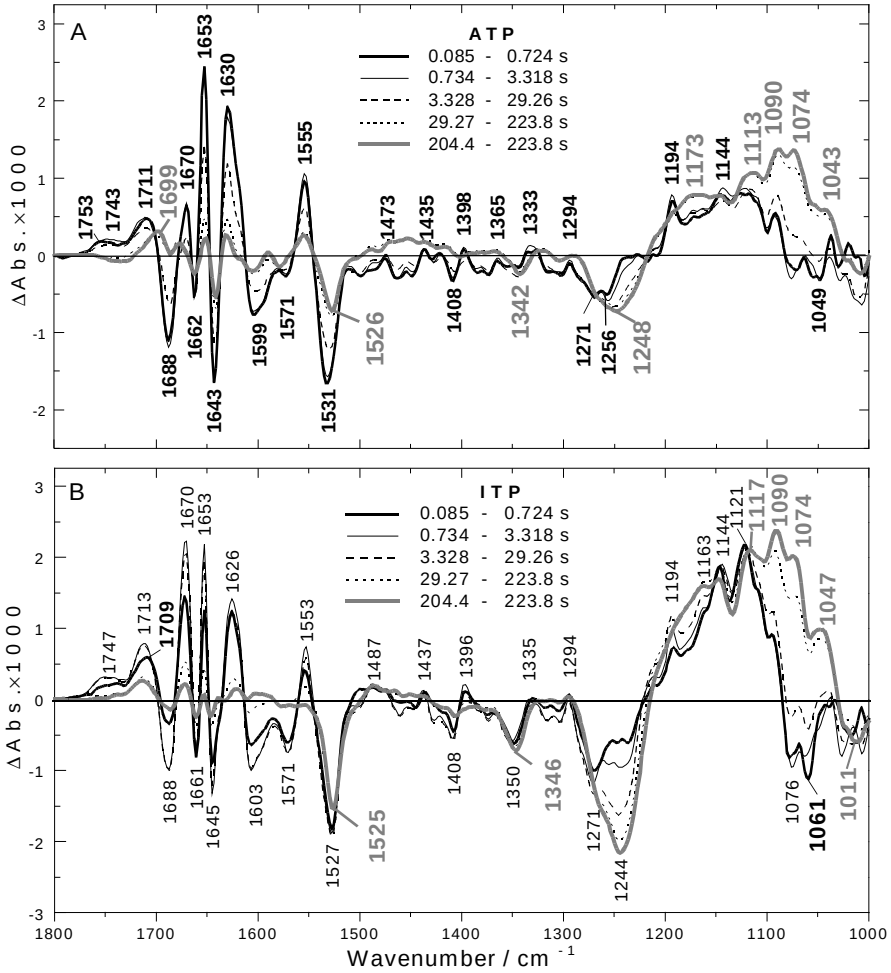

Fig. 3.6-4 Spectra averaged in different time intervals obtained with nucleotide interacting with the ATPase in type II samples for observing E2P formation and E2P hydrolysis (25°C, pH 7.5). Time intervals for spectra are shown in the plot. **A**, with ATP: black-bold labels refer to the first two spectra averaged from 0.085–0.724 s and 0.734–3.318 s; grey labels refer to the last spectrum averaged from 204.4–223.8 s. **B**, with ITP: black-bold labels refer to the first spectrum averaged from 0.085–0.724 s; black-thin labels refer to the spectra averaged from 0.734–3.318 s and 3.328–29.26 s; grey labels refer to the last spectrum averaged from 204.4–223.8 s.

The bands at 1113 and 1090 cm^{-1} may be assigned to the β-PO_3^{2-} of ADP. This band is at lower wavenumber compared with the band in the Ca_2E1P formation spectrum (1126 cm^{-1} in Table 3-7 and Fig. 3.5-9B), which may be due to the different experimental conditions. The band at 1074 cm^{-1} in the last spectrum may be due to the $\nu_{as}(PO_3^{2-})$ mode of the liberated phosphate group (Deng et al., 1998). The smaller amplitude or invisibility of the bands at 1113, 1092 and 1074 cm^{-1} in the first three spectra may indicate that there are absorbance changes of the ATPase when E2P forms and these changes cause negative bands at these positions; or these bands are lifted up by the hydrolysis bands. Another explanation for these three bands may be that sharp negative bands of caged nucleotide in the region 1120–1070 cm^{-1} superimpose with a broad positive photolysis band in this region, and these three bands are originally one broad band.

Spectra with ITP in type II samples

As shown in Fig. 3.6-4B, E2P formation and hydrolysis with ITP in type II samples are much slower than that with ATP. The amplitudes of bands in the amide I region first increase (the first two spectra) and then decrease (the last three spectra). However, the last spectrum averaged from 204.4–223.8 s obtained with ITP shows similar band amplitudes as that with ATP. This shows that E2P hydrolysis is nearly complete with both ATP and ITP in the final spectra.

The amplitude of the band at 1709 cm^{-1} increases first and then decreases during measurements and the band position moves to 1713 cm^{-1} at the end. In contrast, with ATP, the band was first observed at 1711 cm^{-1} and then at 1699 cm^{-1} in the final spectrum. This may indicate that the carboxylate groups of Asp/Glu side chains in ITP samples are different from those in ATP samples.

The bands below 1300 cm^{-1} in Fig. 3.6-4B obtained with ITP show mainly changes of phosphate groups. The bands are at similar positions as spectra obtained with ATP in Fig. 3.6-4A, but with larger amplitudes that are due to more ITP release and hydrolysis. The amplitude of the band at 1244 cm^{-1} increases significantly during the measurement. Compared with the band at ~1248 cm^{-1} with ATP in Fig. 3.6-4A, the band obtained with ITP samples is much larger, which indicates that more ITP was hydrolyzed. The same phenomenon was observed in the Ca_2E1P formation experiments and was explained by more hydrolysis of ITP uncoupled from Ca^{2+} transport in a branch reaction (see chapter 3.5.3). The bands from 1117 to 1090 cm^{-1} may be originally one broad band,which may be assigned to the β-PO_3^{2-} of IDP. The overlap of the broad positive band with sharp negative photolysis bands of caged ITP may result in the appearance of two sharp bands here. The band at 1074 cm^{-1} in the last spectrum may be due to the $\nu_{as}(PO_3^{2-})$ mode of the liberated phosphate group after ITP hydrolysis.

3.6.3 The E2TG spectrum obtained with TG, EGTA and ATP

E2TG samples were prepared as described in chapter 2.2.5. 0.6 mM EGTA are enough to chelate free Ca^{2+} ions in the samples but not enough to chelate completely the bound Ca^{2+} ions from the ATPase, and therefore the ATPase was in Ca_2E1 state.

After the photolysis flash, the spectrum obtained in the time interval of ATP binding (0.46–0.91 s) shows binding signals (data not shown) very similar to those of the ATP binding spectrum. The subsequent enzyme phosphorylation is very fast and the marker band of phosphorylation at 1721 cm^{-1} was not observed (data not shown). This indicates that under the experimental

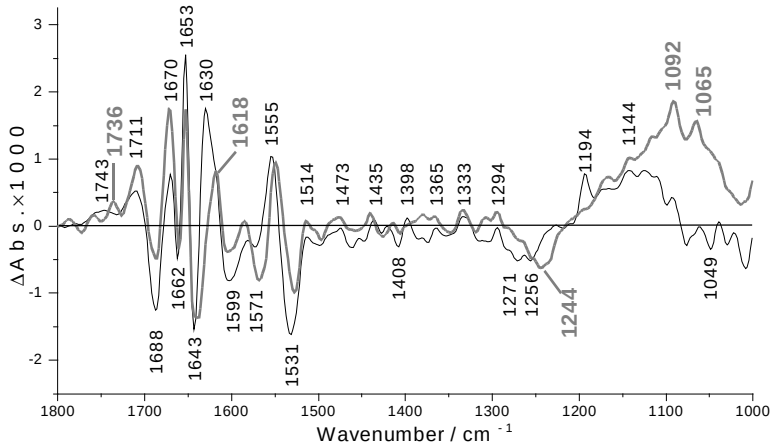

Fig. 3.6-5 Comparison of the E2P formation spectra obtained with ATP type II samples at 25°C (*black* line) and the spectrum obtained with 0.6 mM EGTA, 4.8 mM TG and 3 mM ATP at 1°C averaged from 204–224 s (*grey* line).

conditions here, nucleotide binding is the rate-limiting step compared with phosphorylation. The ATPase was trapped by TG in a dead-end complex E2TG leading to total inactivation (Kijima et al., 1991; Sagara et al., 1991, 1992). The spectrum obtained in the time interval of 204–224 s shows signals similar to E2P formation spectra, as shown in Fig. 3.6-5. The marker band at 1194 cm^{-1} for E2P formation was not observed in the spectrum obtained with EGTA and TG. This band was not observed in spectra of earlier time intervals either. Therefore, E2P did not accumulate but only existed transiently because the reaction of E2P hydrolysis would be accelerated by TG binding to E2. The enzyme will accumulate in the E2TG state. The large amplitudes of the spectrum (*grey* line in Fig. 3.6-5) illustrate the conformational differences between Ca_2E1 and E2TG. In line with this, the E2TG crystal structure shows significant movements of the cytoplasmic domains and rearrangement of the α-helices in the membrane domain, compared with the Ca_2E1 crystal structure (Toyoshima et al., 2000, 2002).

4. Conclusion

The results of this work demonstrate that IR spectroscopy can be used to map ligand-protein interactions and may become an important tool for research as well as for drug and herbicide optimization.

In the particular case of ATP binding to the SR Ca^{2+}-ATPase, modifications of the β- and γ-phosphate group, 2'-OH, 3'-OH and the adenine moiety of ATP reduce the induced-fit movement of the Ca^{2+}-ATPase, with the 6-membered ring of adenine, the 3'-OH of ribose ring and phosphate groups exerting key interactions.

Nucleotide binding seems to be a flexible and interactive process: the conformation of the complex is characteristic of the bound nucleotide, and the interactions between a given ligand group of ATP and the ATPase depend on interactions between other ligand groups of ATP and the ATPase. If binding of an ATP analog induces a conformation that is characteristic of only that analog, results with different analogs are not necessarily comparable and do not necessarily reflect the effects of ATP binding. Therefore it is proposed that some of the conflicting results can be explained by the different conformations of the complexes obtained with different analogs.

Modifications of ATP's 2'-OH, 3'-OH and adenine moiety affect the phosphorylation of the Ca^{2+}-ATPase, with the 3'-OH of ribose ring performing crucial roles. The conformation of the ADP-sensitive phosphoenzyme Ca_2E1P is also characteristic of the bound nucleotide with smaller conformational changes upon phosphoenzyme formation observed for ATP analogs. With ITP and 2'-deoxyATP full extent of phosphoenzyme Ca_2E1P accumulation is achieved although smaller conformational changes of the ATPase after phosphorylation were observed.

Modifications of 2'-OH and the adenine moiety of ATP result in accelerated hydrolysis of ATP analogs, which may be due to a branch reaction uncoupling of nucleotide hydrolysis and Ca^{2+} transport. However, with 3'-deoxyATP, definite phosphorylation was not observed, which demonstrates the key role of 3'-OH of the ribose ring for the γ-phosphate transfer to the phosphorylated residue Asp-351 of the ATPase. The time constant of ATPase phosphorylation is also affected by modifications to these groups by slowing down the ATPase phosphorylation.

Modification of the 6-membered ring of the ATP adenine moiety affects the formation of the ADP-insensitive phosphoenzyme E2P but the effects are weaker than those observed in the binding and phosphorylation reaction. Conformational changes in E2P formation are larger than those due to the formation of the nucleotide-ATPase complex and Ca_2E1P.

By comparing spectra obtained with ATP and isotopically labeled ATP ([β,βγ-$^{18}O_3$]ATP and [γ-$^{18}O_3$]ATP), band assignments of the β- and γ-phosphate group were analyzed. The band at 1147 cm^{-1} is found to be an important marker band for γ-phosphate binding. The band at 1205 cm^{-1} is assigned to the β-phosphate of bound ATP.

Four conformational states of the ATPase were observed, Ca_2E1N, Ca_2E1P, E2P, and E2TG. Significant differences were observed between the Ca_2E1 state and the Ca_2E1N, Ca_2E1P, E2P, E2TG state. The conformational differences between Ca_2E1 and Ca_2E1N, Ca_2E1P, E2P shown in IR difference spectra are larger and larger in the course of Ca^{2+} transport.

From a methodological point of view, it is demonstrated here that binding competition experiments (TNP-AMP → AMPPNP, pyrophosphate → ATP, and ribose triphosphate → AMPPNP,) can be performed using infrared spectroscopy, from which relative dissociation constants can be obtained without the need to develop a binding assay. It is confirmed that different binding modes of ligands can be detected with IR spectroscopy as shown before (White et al., 1990; Murray et al., 1994; Ryan et al., 1999). Applications like this will soon gain importance in fundamental and applied research when mixing devices become commercially available, which makes these experiments just as easy to perform in the infrared spectral region as in the visible spectral range. The advantage of infrared spectroscopy as a marker-free technique that directly observes protein and ligand can then be fully exploited.

Zusammenfassung

Das Binden von Liganden an Proteine kontrolliert eine enorme Anzahl zellulärer Prozesse und ist von großem wissenschaftlichen und ökonomischen Interesse. Die Flexibilität von Protein und Ligand ist ein wichtiger Bestimmungsfaktor der Wechselwirkung und führt oft zu Lingandenbindungsweisen, die nicht aus den Strukturen anderer Liganden vorhergesagt werden können. Zur Untersuchung von Enzym-Liganden-Wechselwirkungen wurde in dieser Arbeit die Infrerotspektroskopie eingesetzt, um unterschiedliche Liganden zu untersuchen, die an dasselbe Enzym binden. Diese Herangehensweise ist auf dem Gebiet der Liganden-Protein Erkennung sehr willkommen, da aufschlußreiche Techniken wie Kernspinresonanz (NMR) und Röntgenkristallographie aufwändig sind und problematisch für manche Systeme. Methoden wie Fluoreszenz und Lumineszenz benötigen geringeren Aufwand, stellen aber weniger molekulare Information zur Verfügung. Diese Technologielücke kann durch die Infrarotspektroskopie überbrückt werden.

Die Infrarotspektroskopie, eine der Schwingungsspektroskopiemethoden, hat mehrere Vorteile für die Aufklärung molekularer Mechanismen von Proteinen wie eine hohe Zeitauflösung, allgemeine Anwendbarkeit auf kleine lösliche Proteine bis hin zu großen Membranproteinen unter nahezu physiologischen Bedingungen und bei hohem molekularen Informationsgehalt, kombiniert mit einer Empfindlichkeit, die groß genug ist, um eine Änderung in der Umgebung eines einzelnen Atoms eines großen Proteins zu erfassen (Barth et al., 2002). Arbeiten, die in neueren Übersichtsartikeln zusammengefaßt sind (Carey et al., 1995; Deng et al., 1999; Barth et al., 2000; Wharton, 2000) haben gezeigt, dass sich das Schwingungsspektrum auf charakteristischer Weise ändert, wenn ein Ligand an das Protein bindet. Dies bietet die direkte Beobachtung des Ligandenbindens – keine Markersubstanz muss wie bei vielen anderen Methoden eingeführt werden, um den Bindungsprozess zu beschreiben. Vorangegangene Arbeiten haben sich hauptsächlich auf einzelne Wechselwirkungen zwischen einem Liganden und einem Protein konzentriert, indem der Einfluß der Proteinumgebung auf die Schwingungsfrequenz einer bestimmten Ligandengruppe mit Hilfe identifizierender Isotopenmarkierungen kontrolliert wurde (Belasco et al., 1980; Baenziger et al., 1993; Cepus et al., 1998).

Diese Arbeit benutzt einen anderen Ansatz, um die Rolle einzelner funktioneller Gruppen eines Liganden bei der Wechselwirkung mit dem Protein zu untersuchen: mit Hilfe der

Infrarotspektroskopie werden die Konformationsänderung eines Proteins verfolgt, die durch das Binden eines Analogons des nativen Ligandens induziert werden. Diese Analogons wurden an spezifischen Gruppen des Liganden modifiziert. Dies ermöglicht die Identifizierung derjenigen funktionelle Gruppen, die für die Wechselwirkung mit dem Protein wichtig sind. Struktur-Wechselwirkungs- Beziehungen werden erhalten, ähnlich den Struktur-Aktivitäts-Beziehungen in der Medikamentenentwicklung, welche die chemische Struktur von Komponenten ihrer pharmazeutischen Aktivität in Beziehung setzen.

In dieser Arbeit wurde die zeitaufgelöste Fouriertransform-Infrarot Spektroskopie angewendet. Der Nachweis von den kleinen IR-Absorptionsänderungen im Schwingungsspektrum, die im allgemeinen mit Proteinreaktionen verbunden sind, benötigen die hohe Empfindlichkeit der FTIR Spektroskopie und müssen direkt in der IR-Küvette ausgelöst werden, wofür die photolytische Nucleotidfreisetzung aus photolabilen Derivaten, zum Beispiel P^3-1-(2-nitrophenyl)ethyl Nucleotide (blockierte Nucleotide) eingesetzt wurde (Kaplan et al., 1978).

Die Bindung von Adenosintriphosphat (ATP) an die Ca^{2+}-ATPase des Sarkoplasmatische Retikulums von Muskelzellen (Hasselbach et al., 1961; Hasselbach, 1974; Andersen, 1989; Lee et al., 2001), die daran anschließende Phosphorylierung und die Umwandlungsreaktionen des Phosphoenzyms sind untersucht worden. Das Sarkoplasmatische Retikulum reguliert die Muskelaktivität bei der Freisetzung und Wiederaufnahme von Calciumionen (Hasselbach, 1979). Die Ca^{2+} Freisetzung aus dieser Organelle induziert die Muskelkontraktion, wohingegen die Ca^{2+} Wiederaufnahme aus dem Cytosol die Kontraktion abschaltet, was die Muskelentspannung zur Folge hat. Die Ca^{2+} Wiederaufnahme erfolgt durch die Ca^{2+}-ATPase des Sarkoplasmatischen Retikulums gegen einen Konzentrationsgradienten vom Cytoplasma der Muskelzellen in das SR, um die Kontraktion zu verhindern und den Muskel zu entspannen. Die Energie, die für diesen aktiven Transportprozess benötigt wird, wird durch die Hydrolyse des Substrates ATP bereitgestellt. Die Substratspezifizität der SR Ca^{2+}-ATPase ist nicht genau genug, sodass nicht nur ATP, sondern auch einige andere Nucleotide und nicht-Nucleotid-Substrate die Ca^{2+} Aufnahme anschalten (Hasselbach, 1979, 1981; Inesi et al., 1985; Lacapere et al., 1990; Wakabayashi et al., 1990; McIntosh, 1998). In dieser Arbeit wurden ATP und mehrere ATP Analogons untersucht.

Ziel der Arbeit war, funktionelle Gruppen in einer Modellstudie zu identifizieren, die das pharmazeutische Potenzial der Infrarotspektroskopie demonstriert, den Einfluß funktioneller

Gruppen von ATP auf Konformationsänderungen eines Enzymzustandes zu einem anderen zu untersuchen, Kinetiken der Reaktionsschritte des Nucleotidbindens, der Enzymphosphorylierung und der Phosphoenzymumwandlung mit ATP und ATP-Analogons zu studieren und zu vergleichen: ADP, AMPPNP, 2'-deoxyATP, 3'-deoxyATP und ITP, AMP, Pyrophosphate, Ribosetriphosphate und TNP-AMP. Diese Analogons waren an spezifischen funktionellen Gruppen des Substrats ATP modifiziert.

Die Ergebnisse dieser Arbeit zeigen, dass IR-Spektroskopie in der Lage ist, Liganden-Protein Wechselwirkungen abzubilden und kann somit zu einer wichtigen Untersuchungsmethode für die Erforschung von Medikamenten- und Herbizidoptimierung werden kann.

In dem speziellen Fall der ATP Bindung an die SR Ca^{2+}-ATPase reduzieren Modifikationen an der ATP β- und γ-Phosphatgruppe, 2'-OH, 3'-OH und des Adenins die charakteristische Bewegung der Ca^{2+}-ATPase mit dem 6-fach besetzten Ring des Adenins, des 3'-OH der Ribose und Phosphatgruppen, die Schlüsselwechselwirkungen ausüben.

Nucleotidbinden scheint ein flexibler und interaktiver Prozess zu sein: die Konformation des Komplexes ist charakteristisch für das gebundene Nucleotid und die Wechselwirkungen zwischen einer gegebenen Ligandengruppe von ATP und der ATPase hängen von den Wechselwirkungen zwischen anderen Ligandengruppen von ATP und der ATPase ab. Dieser Befund wirft möglicherweise Licht auf die anhaltende Kontroverse bezüglich der Anzahl von Nukleotidbindestellen werfen. Viele dieser Studien wurden mit ATP Analogons durchgeführt. Wenn Binden eines ATP Analogons eine Konformation induziert, die nur für dieses Analogon charakteristisch ist, sind Ergebnisse mit verschiedenen Analogons nicht notwendigerweise vergleichbar und reflektieren nicht unbedingt die Effekte des ATP Bindens. Daher wird vorgeschlagen, dass widersprüchliche Ergebnisse durch verschiedene Konformationen erklärt werden können, die von Komplexen mit unterschiedlichen Analogons erhalten wurden.

Veränderungen von 2'-OH, 3'-OH und Adenin beeinflussen die Phosphorylierung der Ca^{2+}-ATPase, wobei 3'-OH der Ribose eine entscheidende Rolle spielt. Die Konformation des ADP-sensitiven Phosphoenzyms Ca_2E1P ist auch charakteristisch für das gebundene Nucleotid mit kleineren Konformationsänderungen bei der Phosphoenzymbildung, die für ATP Analogons beobachtet wurden. Mit ITP und 2'-deoxy ATP wird das volle Ausmaß an Phosphoenzym Ca_2E1P Akkumulierung erreicht, obwohl kleinere Konformationsänderungen beobachtet

wurden.

Veränderungen von 2'-OH und Adenin des ATP resultiert in einer beschleunigten Hydrolyse der ATP Analogons, die möglicherweise durch eine Verzweigungsreaktion hervorgerufen werden kann, welche die Nukleotid Hydrolyse und den Ca^{2+} Transfer entkoppelt. Mit 3'-deoxyATP wurde jedoch keine deutliche Phosphorylierung beobachtet, was die Schlüsselrolle von 3'-OH des Riboserings beim γ-Phosphat Transfer zum phosphorylierten Residuum Asp-351 der ATPase zeigt. Die Zeitkonstante der ATPase Phosphorylierung wird auch durch Veränderungen dieser Gruppen beeinflußt und die Phosphorylierung ist langsamer.

Veränderungen des 6-fach besetzten Ringes des ATP Adenins beeinflusst die Bildung des ADP-unempfindlichen Phosphoenzyms E2P, aber die Effekte sind schwächer als die, die in der Bindungs- und Phosphorylierungsreaktion beobachtet wurden. Konformationsänderungen der E2P Bildung sind größer als die aufgrund der Bildung des Nucleotid-ATPase Komplexes und Ca_2E1P.

Die Bindung der ATP Phosphatgruppen wurde mit Hilfe von [β,βγ-$^{18}O_3$]ATP und [γ-$^{18}O_3$]ATP untersucht. Beim Vergleich der Bandenverschiebungen in den Bindungsspektren mit den Phosphorylierungsspektren, die mit ATP und ATP Isotopomeren erhalten wurden, konnten drei neue Bandenzuordnungen erzielt werden: die Banden bei 1241 cm^{-1}, 1205 cm^{-1} und 1147 cm^{-1} werden der jeweiligen α-, β- und γ-Phosphatgruppe von gebundenem ATP zugeordnet.

Vier Konformationszuständer der ATPase wurden beobachtet, Ca_2E1N, Ca_2E1P, E2P und E2TG. Signifikante Unterschiede wurden zwischen dem Ca_2E1 Zustand und den Ca_2E1N, Ca_2E1P, E2P bzw. E2TG Zuständen beobachtet. Die IR-Differenzspektren zeigen, dass die Konformationsänderungen zwischen Ca_2E1 und Ca_2E1N, Ca_2E1P bzw. E2P immer größer werden.

Um ein Differenzspektrum zu erhalten, das nur die TNP-AMP Bindung an die Ca^{2+}-ATPase reflektiert, wurde die konkurrierende Bindung von TNP-AMP in einem zusätzlichen Experiment beobachtet. Für TNP-AMP, das als ATP Analogon in der Krisallstruktur der SR Ca^{2+}-ATPase verwendet wurde (Toyoshima et. al., 2000, *Nature*, **405**:647-655), konnte durch IR-Spektroskopie herausgefunden werden, dass es Konformationsänderungen bei Bindung an die ATPase induziert. Die Bindungweise ist unterschiedlich zu der von ATP, AMPPNP und anderen Tri- und Diphosphat Nucleotiden. Die TNP-AMP Bindung verursacht teilweise gegenläufige und

kleinere Konformationsänderungen verglichen mit ATP oder AMPPNP. Die Konformation des TNP-AMP-ATPase Komplex ist ähnlicher der Konformation des Ca_2E1 Zustandes als der des Ca_2E1ATP Zustandes. In Bezug auf den Einsatz der Infrarotspektroskopie als eine Technik für Liganden-Bindungsstudien zeigen die Resulate, dass Infrarotspektroskopie in der Lage ist, verschiedene Bindungweisen zu unterscheiden.

Vom methodologischen Standpunkt aus konnte hier gezeigt werden, dass konkurrierende Bindungsexperimente (TNP-AMP → AMPPNP, Pyrophosphat → ATP, and Ribosetriphosphat → AMPPNP) mit Hilfe der Infrarotspektroskopie durchgeführt werden können, von denen relative Dissoziationskonstanten ohne die Entwicklung von Bindungsassays erhalten werden können. Es wurde bestätigt, dass verschiedene Bindungsweisen von Liganden detektiert werden können wie sie bereits gezeigt worden waren (White et al., 1990; Murray et al., 1994; Ryan et al., 1999). Anwendungen wie diese werden bald Bedeutung in Grundlagen- und angewandter Forschung gewinnen, wenn Mischungseinheiten kommerziell verfügbar werden, die diese Experimente im infraroten Spektralbereich genauso leicht durchführbar machen wie im sichtbaren Spektralbereich. Der Vorteil der Infrarotspektroskopie als markierungsfreie Technik, die Protein und Ligand direkt beobachtet, kann dann voll ausgeschöpft werden.

5. Appendix

5.1 Abbreviations

Abbreviations	Full Name
ATP	Adenosine 5'-triphosphate
ADP	Adenosine 5'-diphosphate
AMP	Adenosine 5'-monophosphate
AMPPNP	(β,γ-imido)adenosine 5'-triphosphate
AMPPCP	(β,γ-methylene)adenosine 5'-triphosphate
2'-deoxyATP	2'-deoxyadenosine 5'-triphosphate
3'-deoxyATP	3'-deoxyadenosine 5'-triphosphate
A23187	Ca^{2+} ionophore
ADK	Adenylate kinase
Caged compound	P^3-1-(2-nitrophenyl)ethyl compound
Ca_2E1	the nucleotide-free and calcium-bound ATPase
Ca_2E1NTP	the calcium-nucleotide-ATPase complex
Ca_2E1P	ADP-sensitive phosphoenzyme
COBSI index	the change of backbone structure and interaction index
E2P	ADP-insensitive phosphoenzyme
E2TG	the TG-bound E2 state of the ATPase
DTT	dithiothreitol
DTGS	deuterated triglycine sulfate
EGTA	Ethylene glycol-bis(2-aminoethylether)-N,N,N',N'-tetraacetic acid
FITC	fluorescein isothiocyanate
FTIR	Fourier transform infrared
IR	infrared
ITP	inosine 5'-triphosphate
IMPPNP	(β,γ-imino)inosine 5'-triphosphate
A domain	actuator domain
N domain	nucleotide binding domain
P domain	phosphorylation domain
MSA	maximum signal amplitude
NTP	Nucleoside triphosphate
NDP	Nucleoside diphosphate
SR	sarcoplasmic reticulum
TNP-AMP	2',3'-*O*-(2,4,6-trinitrophenyl) adenosine 5'-monophosphate
TG	thapsigargin
ν_{as}	The antisymmetric stretching vibration
ν_s	The symmetric stretching vibration

Abbreviations of amino acid residues:

Arg	Arginine	Gln	Glutamine	Ser	Serine
Asn	Asparagine	His	Histidine	Thr	Threonine
Asp	Aspartic acid	Lys	Lysine	Trp	Tryptophan
Cys	Cystine	Phe	Phenylalanine	Tyr	Tyrosine
Glu	Glutamic acid	Pro	Proline		

5.2 Chemicals are purchased:

from *Sigma-Aldrich,* ATP, ADP, AMP, ITP, 2'-deoxyATP, 3'-deoxyATP, Ca^{2+} ionophore (A23187), adenylate kinase, DTT, 4-methylimidazole, KOH

from *Molecular Probes,* TNP-AMP

from *Merck,* $MgCl_2$, KH_2PO_4, K_2HPO_4

from *Fluka,* imidazole

from *Biomol,* MOPS

from *Serva,* $CaCl_2$

from *Roth,* KCl.

6. References

Abu-Abed, M., T.-K. Mal, M. Kainosho, D.-H. Maclennan, and M. Ikura. 2002. Characterization of the ATP-binding domain of the sarco(endo)plasmic reticulum Ca^{2+}-ATPase: probing nucleotide binding by multidimensional NMR. *Biochemistry* **41**:1156-1164.

Alberts, A., D. Bray, J. Lewis, M. Raff, K. Roberts, and J. D. Watson. 1989. Molecular biology of the cell. 2nd ed., Garland Publishing, Inc, New York & London.

Allin, C., and K. Gerwert. 2001. Ras catalyzes GTP hydrolysis by shifting negative charges from γ- to α-phosphate as revealed by time-resolved FTIR difference spectroscopy. *Biochemistry* **40**:3037-3046.

Amzel, L. M., and Pedersen, P. L. 1983. Proton ATPases: Structure and mechanism. *Annu. Rev. Biochem.* **52**:801-824.

Andersen, J. P. 1989. Monomer-oligomer equilibrium of sarcoplasmic reticulum Ca^{2+}-ATPase and the role of subunit interaction in the Ca^{2+} pump mechanism. *Biochim. Biophys. Acta* **988**:47-72.

Andersen, J. P. 1995. Dissection of the functional domains of the sarcoplasmic reticulum Ca^{2+}-ATPase by site-directed mutagenesis. *Biosci. Rep*. **15**:243-261.

Aravind, L., M. Y. Galperin, and E. V. Koonin. 1998. The catalytic domain of the P-type ATPase has the haloacid dehalogenase fold. *Trends Biochem Sci*. **23** (4):127-129.

Arrondo, J. L. R., F. M. Goñi, and J. M. Macarulla. 1984. Infrared spectroscopy of phosphatidylcholines in aqueous suspension. A study of the phosphate group vibrations. *Biochim. Biophys. Acta* **794**:165-168.

Arrondo, J. L. R., H. H. Mantsch, N. Mullner, S. Pikula, and A. Martonosi. 1987. Infrared spectroscopic characterization of the structural changes connected with the E1-E2 transition in the Ca^{2+}-ATPase of SR. *J. Biol. Chem*. **262**:9037-9043.

Baenziger, J. E., K. W. Miller, and K. J. Rothschild. 1993. Fourier transform infrared difference spectroscopy of the nicotinic acetylcholine receptor: evidence for specific protein structural changes upon desensitization. *Biochemistry* **32**:5448-5454.

Barth, A., W. Mäntele, and W. Kreutz. 1990. Molecular changes in the sarcoplasmic reticulum Ca^{2+}-ATPase during catalytic activity. A Fourier transform infrared (FTIR) study using photolysis of caged ATP to trigger the reaction cycle. *FEBS Lett*. **277**:147-150.

Barth, A., W. Mäntele, and W. Kreutz. 1991. Infrared spectroscopic signals arising from ligand binding and conformational changes in the catalytic cycle of sarcoplasmic reticulum Ca^{2+}-ATPase. *Biochim. Biophys. Acta* **1057**:115-123.

Barth, A., W. Kreutz, and W. Mäntele. 1994. Changes of protein structure, nucleotide microenvironment, and Ca^{2+} binding states in the catalytic cycle of sarcoplasmic reticulum Ca^{2+}-

ATPase: investigation of nucleotide binding, phosphorylation and phosphoenzyme conversion by FTIR difference spectroscopy. *Biochim. Biophys. Acta* **1194**:75-91.

Barth, A., K. Hauser, W. Mäntele, J. E. T. Corrie, and D. R. Trentham. 1995. Photochemical release of ATP from 'caged ATP' studied by time-resolved infrared spectroscopy. *J. Am. Chem. Soc*. **117**:10311-10316.

Barth, A., F. von Germar, W. Kreutz, and W. Mäntele. 1996. Time-resolved infrared spectroscopy of the Ca^{2+}-ATPase. The enzyme at work. *J. Biol. Chem.* **271**:30637-30646.

Barth, A., J. E. T. Corrie, M. J. Gradwell, Y. Maeda, W. Mäntele, T. Meier, and D. R. Trentham. 1997a. Time-resolved infrared spectroscopy of intermediates and products from photolysis of 1-(2-nitrophenyl)ethyl phosphates: reaction of the 2-nitrosoacetophenone byproduct with thiols. *J. Am. Chem. Soc.* **119**:4149-4159.

Barth, A., W. Mäntele, and W. Kreutz. 1997b. Ca^{2+} release from the phosphorylated and the unphosphorylated sarcoplasmic reticulum Ca^{2+}-ATPase results in parallel structural changes. An infrared spectroscopic study. *J. Biol. Chem*. **272**:25507-25510.

Barth, A., and W. Mäntele. 1998. ATP-induced phosphorylation of the sarcoplasmic reticulum Ca^{2+}-ATPase - molecular interpretation of infrared difference spectra. *Biophys. J*. **75**:538-544.

Barth, A. 1999. Phosphoenzyme conversion of the sarcoplasmic reticulum Ca^{2+}-ATPase. Molecular interpretation of infrared difference spectra. *J. Biol. Chem*. **274**:22170-22175.

Barth, A., and C. Zscherp. 2000. Substrate binding and enzyme function investigated by infrared spectroscopy. *FEBS Lett*. **477**:151-156.

Barth, A., and C. Zscherp. 2002. What vibrations tell us about proteins. *Quarterly Reviews of Biophysics* **35**(4):369-430.

Belasco, J. G., and J. R. Knowles. 1980. Direct observation of substrate distortion by triosephosphate isomerase using Fourier transform infrared spectroscopy. *Biochemistry* **19**:472-477.

Berman, M. C. 1986. Absorbance and fluorescence properties of 2'(3')-*O*-(2,4,6-trinitrophenyl)adenosine 5'-triphosphate bound to coupled and uncoupled Ca^{2+}-ATPase of skeletal muscle sarcoplasmic reticulum. *J. Biol. Chem*. **261**:16494-16501.

Bigelow, D. J., and G. Inesi. 1992. Contributions of chemical derivatization and spectroscopic studies to the characterization of the Ca^{2+} transport ATPase of sarcoplasmic reticulum. *Biochim. Biophys. Acta* **1113**:323-338.

Bio-Rad Laboratories. 1977. Technical Bulletin No 1051. Bio-Rad Laboratories, Richmond, CA.

Bishop, J. E., M. K. Al-Shawi, and G. Inesi. 1987. Relationship of the regulatory nucleotide site to the catalytic site of the sarcoplasmic reticulum Ca^{2+}-ATPase. *J. Biol. Chem*. **262**:4658-4663.

Bodley, A. L., and W. P. Jencks. 1987. Acetyl phosphate as a substrate for the calcium ATPase of sarcoplasmic reticulum. *J. Biol. Chem.* **262**:13997-14004.

Braiman, M. S., and K. J. Rothschild. 1988. Fourier transform infrared techniques for probing membrane protein structure. *Annu. Rev. Biophys. Biophys. Chem.* **17**:541-570.

Cantor, C. R., and P. R. Schimmel. 1980. Biophysical chemistry. Part II: Techniques for the study of biological structure and function. W. H. Freeman and Company, New York.

Carey, P. R., and P. J. Tonge. 1995. Unlocking the secrets of enzyme power using Raman spectroscopy. *Acc. Chem. Res.* **28**:8-13.

Cepus, V., A. J. Scheidig, R. S. Goody, and K. Gerwert. 1998. Time-resolved FTIR studies of the GTPase reaction of H-ras p21 reveal a key role for the α-phosphate. *Biochemistry* **37**:10263-10271.

Champeil, P., S. Riollet, S. Orlowski, F. Guillain, C. J. Seebregts, and D. B. McIntosh. 1988. ATP regulation of SR Ca^{2+}-ATPase. *J. Biol. Chem.* **263**:12288-12294.

Champeil, P., T. Menguy, S. Soulie, B. Juul, A. G. De Gracia, F. Rusconi, P. Falson, et al. 1998. Characterization of a protease-resistant domain of the cytosolic portion of sarcoplasmic reticulum Ca^{2+}-ATPase. *J. Biol. Chem.* **273**:6619-6631.

Chirgadze, Y. N., O. V. Fedorov, and N. P. Trushina. 1975. Estimation of amino acid residue side chain absorption in the infrared spectra of protein solutions in heavy water. *Biopolymers* **14**:679-694.

Clausen, J. D., D. B. McIntosh, D. G. Wooley, and J. P. Andersen. 2001. Importance of Thr-353 of the conserved phosphorylation loop of the sarcoplasmic reticulum Ca^{2+}-ATPase in MgATP binding and catalytic activity. *J. Biol. Chem.* **276**:35741-35750.

Clore, G. M., A. M. Gronenborn, C. Mitchinson, and N. M. Green. 1982. ^{1}H-NMR studies on nucleotide binding to the sarcoplasmic reticulum Ca^{2+}-ATPase. *Eur. J. Biochem.* **128**:113-117.

Coan, C., J. A. Amaral, and S. Verjovski-Almeida. 1993. Elimination of the hydroxyl groups in the ribose ring of ATP reduces its ability to phosphorylate the sarcoplasmic reticulum Ca^{2+}-ATPase. *J. Biol. Chem.* **268**:6917-6924.

Colthup, N. B., L. H. Daly, and S. E. Wiberley. 1990. Introduction to infrared and Raman spectroscopy. 3rd ed., Academic press,Inc., Boston,San Diego, New York, London, Sydney, Tokyo, Toronto.

Csermely, P., C. Katopis, B. A. Wallace, and A. Martonosi. 1987. The E1-E2 transition of calcium transporting ATPase in sarcoplasmic reticulum occurs without major changes in secondary structure. *Biochem. J.* **241**:663-669.

Danko, S., T. Daiho, Y. Yamasaki, M. Kamidochi, H. Suzuki, and C. Toyoshima. 2001a. ADP-insensitive phosphoenzyme intermediate of sarcoplasmic reticulum Ca^{2+}-ATPase has a compact conformation resistant to proteinase K, V8 protease and trypsin. *FEBS Lett.* **489**:277-282.

Danko, S., K. Yamasaki, T. Daiho, H. Suzuki, and C. Toyoshima. 2001b. Organization of cytoplasmic domains of sarcoplasmic reticulum Ca^{2+}-ATPase in E1P and E1ATP states: a limited proteolysis study. *FEBS Lett*. **505**:129-135.

Darnell, J., H. Lodish, and D. Baltimore. 1990. Molecular cell biology. 2nd ed., Scientific American Books, New York.

Davies, D. B., and S. S. Danyluk. 1974. Nuclear magnetic resonance studies of 5'-ribo- and deoxyribonucleotide structures in solution. *Biochemistry* **13**:4417-4434.

Davis, A. M., and S. J. Teague. 1999. Hydrogen bonding, hydrophobic interactions, and failure of the rigid receptor hypothesis. Angew. Chem. Int. Ed. **38**:736-749.

De Meis, L., and W. Hasselbach. 1971. Acetyl phosphate as substrate for calcium uptake in skeletal muscle microsomes. *J. Biol. Chem*. **246**:4759-4763.

De Meis, L., and M.-C.-F. de Mello. 1973. substrate regulation of membrane phosphorylation and of Ca^{2+} transport in the sarcoplasmic reticulum. *J. Biol. Chem*. **248**:3691-3701.

De Meis, L., and H. Masuda. 1974. Phosphorylation of the sarcoplasmic reticulum membrane by orthophosphate through two different reactions. *Biochemistry* **13**:2059-2062.

De Meis, L., and A. Vianna. 1979. Energy interconversion by the Ca^{2+}-dependent ATPase of the sarcoplasmic reticulum. *Annu. Rev. Biochem*. **48**:275-292.

De Meis, L. 1981. The Sarcoplasmic Reticulum. Wiley, New York.

De Meis, L., H. Wolosker, and S. Engelender. 1996. Regulation of the channel function of Ca^{2+}-ATPase. *Biochim. Biophys. Acta* **1275**:105-110.

Deng, H., J. Wang, R. Callender, and W. J. Ray. 1998. Relationship between bond stretching frequencies and internal bonding for [$^{16}O_4$]- and [$^{18}O_4$]phosphates in aqueous solution. *J. Phys. Chem. B* **1022**:3617-3623.

Deng, H., and R. Callender. 1999. Raman spectroscopic studies of the structures, energetics, and bond distortions of substrates bound to enzymes. *Methods Enzymol*. **308**:176-201.

Doyle, B. B., W. Traub, G. P. Lorenzi, and E. R. Blout. 1971. Conformational investigations on the polypeptide and oligopeptides with the repeating sequence L-alanyl-L-prolylglycine. *Biochemistry* **10**:3052-3061.

Du, X., H. Frei, and S.-H. Kim. 2000. The mechanism of GTP hydrolysis by Ras probed by Fourier transform infrared spectroscopy. *J. Biol. Chem*. **275**:8492-8500.

Dupont, Y. 1982. Low-temperature studies of the sarcoplasmic reticulum calcium pump mechanism of calcium binding. *Biochim. Biophys. Acta* **688**:75-87.

Dupont, Y., Y. Chapron, and R. Pougeois. 1982. Titration of the nucleotide binding sites of sarcoplasmic reticulum Ca^{2+}-ATPase with 2',3'-*O*-(2,4,6-trinitrophenyl) adenosine 5'-

triphosphate and 5'-diphosphate. *Biochem. Biophys. Res. Commun*. **106**:1272-1279.

Dupont, Y., and R. Pougeois. 1983. Evaluation of H_2O activity in the free or phosphorylated catalytic site of Ca^{2+}-ATPase. *FEBS Lett*. **156**:93-98.

Dux, L., and A. Martonosi. 1983. Two-dimensional arrays of proteins in sarcoplasmic reticulum and purified Ca^{2+}-ATPase vesicles treated with vanadate. *J. Biol. Chem*. **258**:2599-2603.

Ebashi, S. 1991. Excitation-contraction coupling and the mechanism of muscle contraction. *Annu. Rev. Physiol.* **53**:1-16.

Ellis, R. J. 2001. Macromolecular crowding: an important but neglected aspect of the intracellular environment. *Curr. Op. Struct. Biol.* **11**:114-119.

Ettrich, R., Melichercik.M, J. Teisinger, O. Ettrichova, R. Krumscheid, K. Hofbauerova, P. Kvasnicka, W. Schoner, and E. Amler. 2001. Three-dimensional structure of the large cytoplasmic H4-H5 loop of Na^+, K^+-ATPase deduced by restraint-based comparative modeling shows only one ATP binding site. *J.Mol.Model* **7**:184-192.

Fagan, M. J., and M. H. Saier. 1994. P-type ATPases of eukaryotes and bacteria - sequence analyses and construction of phylogenetic trees. *J. Mol. Evol*. **38**:57-99.

Faller, L. D. 1989. Competitive binding of ATP and the fluorescent substrate analogue 2',3'-*O*-(2,4,6-trinitrophenyl-cyclohexadienylidine)adenosine 5'-triphosphate to the gastric H^+,K^+-ATPase: Evidence for two classes of nucleotide sites. *Biochemistry* **28**:6771-6778.

Faller, L. D. 1990. Binding of the fluorescent substrate analogue 2',3'-*O*-(2,4,6-trinitrophenyl-cyclohexadienylidene)adenosine 5'-triphosphate to the gastric H^+,K^+-ATPase: evidence for cofactor-induced conformational changes in the enzyme. *Biochemistry* **29**:3179-3186.

Ferreira, S. T., and S. Verjovski-Almeida. 1988. Stoichiometry and mapping of the nucleotide sites in sarcoplasmic reticulum ATPase with the use of UTP. *J. Biol. Chem*. **263**:9973-9980.

Fortea, M. I., F. Soler, and F. Fernandez-Belda. 2000. Insight into the uncoupling mechanism of sarcoplasmic reticulum ATPase using the phosphorylating substrate UTP. *J. Biol. Chem.* **275**:12521-12529.

Fortea, M. I., F. Soler, and F. Fernandez-Belda. 2001. Unravelling the interaction of thapsigargin with the conformational states of Ca^{2+}-ATPase from skeletal sarcoplasmic reticulum. *J. Biol. Chem.* **276**:37266-37272.

Gafni, A., and P. D. Boyer. 1985. Modulation of stoichiometry of the sarcoplasmic reticulum calcium pump may enhance thermodynamic efficiency. *Proc. Natl. Acad. Sci. USA* **82**:98-101.

Georg, H., A. Barth, W. Kreutz, F. Siebert, and W. Mäntele. 1994. Structural changes of sarcoplasmic reticulum Ca^{2+}-ATPase upon Ca^{2+} binding studied by simultaneous measurement of infrared absorbance changes and changes of intrinsic protein fluorescence. *Biochim. Biophys. Acta* **1188**:139-150.

Goormaghtigh, E., V. Cabiaux, and J.-M. Ruysschaert. 1994a. Determination of soluble and membrane protein structure by Fourier transform infrared spectroscopy. I. Assignments and model compounds. *Subcell. Biochem.* **23**:329-362.

Goormaghtigh, E., V. Cabiaux, and J.-M. Ruysschaert. 1994b. Determination of soluble and membrane protein structure by Fourier transform infrared spectroscopy. III. Secondary structures. *Subcell. Biochem.* **23**:405-450.

Griffiths, P. R., and J. A. de Haseth. 1986. Fourier transform infrared spectrometry. John Wiley & Sons, New York, Chichester, Brisbane, Toronto, Singapore.

Hasselbach, W., and M. Makinose. 1961. Die Calciumpumpe der "Erschlaffungsgrana" des Muskels und ihre Abhängigkeit von der ATP-Spaltung. *Biochem. Z.* **333**:518-528.

Hasselbach, W. 1974. Sarcoplasmic Reticulum ATPases. In the Enzymes, 3rd ed. P. D. Boyer, editor. Academic Press, New York, London. 431-467.

Hasselbach, W., and R. The. 1975. The action of chaotropic anions on the sarcoplasmic calcium pump. *Eur. J. Biochem.* **53**:105-113.

Hasselbach, W. 1979. The sarcoplasmic calcium pump. *Top. Curr. Chem.* **78**:1-56.

Hasselbach, W. 1981. Calcium-activated ATPase of the sarcoplasmic reticulum membranes. In Membrane Transport. S. L. Bonting and J. J. H. H. M. De Pont, editors. Elsevier, Amsterdam. 183-208.

Hatefi, Y. 1985. The mitochondrial electron transport and oxidative phosphorylation system. *Annu. Rev. Biochem.* **54**:1015-1069.

Hebert, H., E. Skriver, M. Söderholm, and A. B. Maunsbach. 1988. Three-dimensional structure of renal Na,K-ATPase determined from two-dimensional membrane crystals of the p1 form. J. Ultrastruct. *Mol. Struct. Res.* **100**:86-93.

Henao, F., and C. Gutierrez-Merino. 1989. Inhibition of the sarcoplasmic reticulum (Ca^{2+}+Mg^{2+})-ATPase by Zn (II). *Biochim. Biophys. Acta* **984**:135-142.

Hienerwadel, R., A. Boussac, J. Breton, B. Diner, and C. Berthomieu. 1997. Fourier transform infrared difference spectroscopy of photosystem II tyrosine D using site-directed mutagenesis and specific isotope labeling. *Biochemistry* **36**:14712-14723.

Highsmith, S. 1984. Evidence that the ATP binding site of SR Ca^{2+}-ATPase has a Mg^{2+} ion binding subsite. *Biochem. Biophys. Res. Commun.* **124**:183-189.

Hobbs, A. S., R. W. Albers, J. P. Froehlich, and P. F. Heller. 1985. ADP stimulates hydrolysis of the "ADP-insensitive" phosphoenzyme in Na^+,K^+-ATPase and Ca^{2+}-ATPase. *J. Biol. Chem.* **260**:2035-2057.

Hua, S., G. Inesi, H. Nomura, and C. Toyoshima. 2002. Fe^{2+}-catalyzed oxidation and cleavage of sarcoplasmic reticulum ATPase reveals Mg^{2+} and Mg^{2+}-ATP sites. *Biochemistry* **41**:11405-

11410.

Huang, S., and T. C. Squier. 1998. Enhanced rotational dynamics of the phosphorylation domain of the Ca^{2+}-ATPase upon calcium activation. *Biochemistry* **37**:18064-18073.

Inesi, G. 1971. *p*-nitrophenyl phosphate hydrolysis and calcium ion transport in fragmented sarcoplasmic reticulum. *Science* **171**:901-903.

Inesi, G., M. Kurzmack, R. Nakamoto, L. de Meis, and S. A. Bernhard. 1980. Uncoupling of calcium control and phosphohydrolase activity in sarcoplasmic reticulum vesicles. *J. Biol. Chem*. **255**:6040-6043.

Inesi, G., and L. De Meis. 1985. Kinetic regulation of catalytic and transport activities in sarcoplasmic reticulum ATPase. In The Enzymes of Biological Membranes, 2nd ed. A. Martonosi, editor. Plenum Press, New York, London. 157-191.

Jackson, M., and H. H. Mantsch. 1995. The use and misuse of FTIR spectroscopy in the determination of protein structure. *Crit. Rev. Biochem. Mol. Biol*. **30**:95-120.

Jona, I., J. Matko, and A. Martonosi. 1990. Structural dynamics of the Ca^{2+}-ATPase of sarcoplasmic reticulum: Temperature profiles of fluorescence polarization and intramolecular energy transfer. *Biochim. Biophys. Acta* **1028**:183-199.

Kanazawa, T., H. Suzuki, T. Daiho, and K. Yamasaki. 1995. Fluorometric study on conformational changes in the catalytic cycle of sarcoplasmic reticulum Ca^{2+}-ATPase. *Biosci. Rep.* **15**:317-326.

Kaplan, J. H., B. Forbush, and J. F. Hoffman. 1978. Rapid photolytic release of ATP from a protected analogue: utilization by the Na:K pump of human red blood cell ghosts. *Biochemistry* **17**:1929-1935.

Kendrew, J., and E. Lawrence. 1994. editors. The encyclopedia of molecular biology. 1st ed., Blackwell Science, .

Kielley, W. W., and O. Meyerhof. 1948. Studies on adenosinetriphosphatase of muscle. II. A new magnesium-activated adenosinetriphosphatase . *J. Biol. Chem*. **176**:591-601.

Kijima, Y., E. Ogunbunmi, and S. Fleischer. 1991. Drug action of thapsigargin on the Ca^{2+} pump protein of sarcoplasmic reticulum. *J. Biol. Chem*. **266**:22912-22918.

Kubo, K., H. Suzuki, and T. Kanazawa. 1990. Characterization of the substrate-induced conformational change of *N*-iodoacetyl-*N'*-(5-sulfo-1-naphthyl)ethylenediamine-labeled sarcoplasmic reticulum Ca^{2+}-ATPase by using different kinds of substrate. *Biochim. Biophys. Acta* **1040**:251-259.

Lacapere, J.-J., N. Bennett, Y. Dupont, and F. Guillain. 1990. pH and Magnesium dependence of ATP binding to SR ATPase. *J. Biol. Chem*. **265**:348-353.

Lee, A. G. 2002a. Ca^{2+}-ATPase structure in the E1 and E2 conformations: mechanism, helix-

helix and helix-lipid interactions. *Biochim. Biophys. Acta* **1565**:246-266.

Lee, A. G. 2002b. A calcium pump made visible. *Curr. Op. Struct. Biol*. **12**:547-554.

Lee, A. G., K. A. Dalton, R. C. Duggleby, J. Malcolm East, and A. P. Starling. 1995. Lipid structure and Ca^{2+}-ATPase function. *Biosci. Rep*. **15**:289-298.

Lee, A., and J. East. 2001. What the structure of a calcium pump tells us about its mechanism. *Biochem. J*. **356**:665-683.

MacLennan, D. H., W. J. Rice, and N. M. Green. 1997. The mechanism of Ca^{2+} transport by sarco(endo)plasmic reticulum Ca^{2+}-ATPase. *J. Biol. Chem*. **272**:28815-28818.

MacLennan, D. H., and N. M. Green. 2000. Pumping Ions. *Nature* **405**:633-634.

Makinose, M., and R. The. 1965. Calcium accumulation and cleavage of nucleotide triphosphate cleavage by vesicles of sarcoplasmic reticulum. *Biochem. Z.* **343**:383-393.

Maruyama, K., D. M. Clarke, J. Fujii, G. Inesi, T. W. Loo, and D. H. MacLennan. 1989. Functional consequences of alterations to amino acids located in the catalytic center (isoleucine 348 to threonine 357) and nucleotide-binding domain of the Ca^{2+}-ATPase of sarcoplasmic reticulum. *J. Biol. Chem*. **264**:13038-13042.

Mata, A. M., H. I. Stefanova, M. G. Gore, Y. M. Khan, J. M. East, and A. G. Lee. 1993. Localization of Cys-344 on the (Ca^{2+}-Mg^{2+})-ATPase of sarcoplasmic reticulum using resonance energy transfer. *Biochim. Biophys. Acta* **1147**:6-12.

McIntosh, D. B. 1992. Glutaraldehyde cross-links Lys-492 and Arg-678 at the active site of sarcoplasmic reticulum Ca^{2+}-ATPase. *J. Biol. Chem*. **267**:22328-22335.

McIntosh, D. B., D. G. Woolley, B. Vilsen, and J. P. Andersen. 1996. Mutagenesis of segment ^{487}Phe-Ser-Arg-Asp-Arg-Lys^{492} of sarcoplasmic reticulum Ca^{2+}-ATPase produces pumps defective in ATP binding. *J. Biol. Chem*. **271**:25778-25789.

McIntosh, D. B. 1998. The ATP binding sites of P-type ion transport ATPase: properties, structure, conformations, and mechanism of energy coupling. *Advances in Molecular and Cell Biology* **23A**:33-99.

McIntosh, D.-B., D.-G. Woolley, D.-H. MacLenna, B. Vilsen, and J.-P. Andersen. 1999. Interaction of nucleotides with Asp^{351} and the conserved phosphorylation loop of sarcoplasmic reticulum Ca^{2+}-ATPase. *J. Biol. Chem*. **274**:25227-25236.

McIntosh, D. B. 2000. Portrait of a P-type pump. *Nature Struct. Biol*. **7**:532-535.

Mintz, E., A. M. Mata, V. Forge, M. Passafiume, and F. Guillain. 1995. The modulation of Ca^{2+} binding to sarcoplasmic reticulum ATPase by ATP analogues is pH-dependent. *J. Biol. Chem.* **270**:27160-27164.

Mintz, E., and F. Guillain. 1997. Ca^{2+} transport by the sarcoplasmic reticulum ATPase. *Biochim.*

Biophys. Acta **1318**:52-70.

Moczydlowski, E. G., and P. A. G. Fortes. 1981a. Characterization of 2',3'-*O*-(2,4,6-trinitrocyclohexadienylidine)adenosine 5'-triphosphate as a fluorescent probe of the ATP site of sodium and potassium transport adenosinetriphosphatase. *J. Biol. Chem*. **256**:2346-2356.

Moczydlowski, E. G., and P. A. G. Fortes. 1981b. Inhibition of sodium and potassium adenosine triphosphatase by 2',3'-*O*-(2,4,6-trinitrocyclohexadienylidene) adenine nucleotides. *J. Biol. Chem*. **256**:2357-2366.

Moller, J. V., B. Juul, and M. le Maire. 1996. Structural organization, ion transport, and energy transduction of P-type ATPases. *Biochim. Biophys. Acta* **1286**:1-51.

Moutin, M. J., M. Cuillel, C. Rapin, R. Miras, M. Anger, A. M. Lompre, and Dupont.Y. 1994. Measurements of ATP binding on the large cytoplasmic loop of the sarcoplasmic reticulum Ca^{2+}-ATPase overexpressed in *Escherichia coli*. *J. Biol. Chem.* **269**:11147-11154.

Mukohata, Y., M. Isoyama, and A. Fuke. 1986. ATP synthesis in cell envelop vesicles of *Halobacterium halobium* driven by membrane potential and/or base-acid transition. *J. Biochem*. **99**:1-8.

Murray, I. A., J. P. Derrick, A. J. White, K. Drabble, C. W. Wharton, and W. V. Shaw. 1994. Analysis of hydrogen bonding in enzyme-substrate complexes of chloramphenicol acetyltransferase by infrared spectroscopy and site-directed mutagenesis. *Biochemistry* **33**:9826-9830.

Nakamoto, R. K., and G. Inesi. 1984. Studies of the interactions of 2',3'-*O*-(2,4,6-trinitrocyclohexyldienylidine)adenosine nucleotides with the SR (Ca^{2+} + Mg^{2+})-ATPase active site. *J. Biol. Chem*. **259**:2961-2970.

Nakamura, Y., and Y. Tonomura. 1978. Reaction mechanism of *p*-nitrophenylphosphatase of sarcoplasmic reticulum. *J. Biochem*. **83**:571-583.

Ouali, M., R. Letellier, J. S. Sun, A. Akhebat, F. Adnet, J. Liquier, and E. Taillandier. 1993. Determination of G*G.C triple-helix structure by molecular modeling and vibrational spectroscopy. *J. Am. Chem. Soc*. **115**:4264-4270.

Pedersen, P. L., and E. Carafoli. 1987. Ion motive ATPases. I: Ubiquity, properties, and significance to cell function. *TIBS* **12**:146-150.

Petithory, J. R., and W. P. Jencks. 1986. Phosphorylation of the calcium ATPase of SR: rate-limiting conformational change followed by rapid phosphoryl transfer. *Biochemistry* **25**:4493-4497.

Petretski, J. H., H. Wolosker, and L. De Meis. 1989. Activation of Ca^{2+} uptake and inhibition of reversal of the sarcoplasmic reticulum Ca^{2+} pump by aromatic compounds. *J. Biol. Chem*. **264**:20339-20343.

Pick, U., and S. Bassilian. 1981. Modification of the ATP binding site of the Ca^{2+}-ATPase from

sarcoplasmic reticulum by fluorescein isothiocyanate. *FEBS Lett*. **123**:127-130.

Pickart, C. M., and W. P. Jencks. 1984. Energetics of the calcium-transporting ATPase. *J. Biol. Chem*. **259**:1629-1643.

Raimbault, C., R. Buchet, and C. Vial. 1996. Changes of creatine kinase secondary structure induced by the release of nucleotides from caged compounds - An infrared difference-spectroscopy study. *Eur. J. Biochem*. **240**:134-142.

Resnick, S. M., and A. J. B. Zehnder. 2000. In vitro ATP regeneration from polyphosphate and AMP by polyphosphate: AMP phosphotransferase and adenylate kinase from *Acinetobacter johnsonii* 210A. *Applied and Environmental Microbiology* **66**(5):2045-2051.

Rossi, B., F. de Assis Leone, C. Gache, and M. Lazdunski. 1979. Pseudosubstrates of the sarcoplasmic Ca^{2+}-ATPase as tools to study the coupling between substrate hydrolysis and Ca^{2+} transport. *J. Biol. Chem*. **254**:2302-2307.

Rubtsov, A. M., P. J. Quinn, and A. A. Boldyrev. 1988. Pathways of calcium release from heavy sarcoplasmic reticulum vesicles isolated from rabbit skeletal muscle. *FEBS Lett*. **238**:240-244.

Ryan, S. E., and J. E. Baenziger. 1999. A structure-based approach to nicotinic receptor pharmacology. *Mol. Pharmacol*. **55**:348-355.

Saenger, W. 1984. Structures and Conformational Properties of Bases, Furanose Sugars, and Phosphate Groups. In Principles of Nucleic Acid Structure. C. R. Cantor, editor. Springer Verlag, New York, Berlin, Heidelberg, Tokyo. 50-104.

Sagara, Y., and G. Inesi. 1991. Inhibition of the sarcoplasmic reticulum Ca^{2+} transport ATPase by thapsigargin at subnanomolar concentrations. *J. Biol. Chem*. **266**:13503-13506.

Sagara, Y., F. Fernandez-Belda, L. De Meis, and G. Inesi. 1992. Characterization of the inhibition of intracellular Ca^{2+} transport ATPases by thapsigargin. *J. Biol. Chem*. **267**:12606-12613.

Schleich, T., B. J. Blackburn, R. D. Lapper, and I. C. P. Smith. 1972. A nuclear magnetic resonance study of the influence of aqueous sodium perchlorate and temperature on the solution conformations of uracil nucleosides and nucleotides. *Biochemistry* **11**:137-145.

Scofano, H. M., A. Vieyra, and L. De Meis. 1979. Substrate regulation of the sarcoplasmic reticulum ATPase. *J. Biol. Chem*. **254**:10227-10231.

Senior, A. E., and J. G. Wise. 1983. The proton-ATPase of bacteria and mitochondria. *J. Membr. Biol*. **73**(2):105-124.

Shigekawa, M., S. Wakabayashi, and H. Nakamura. 1983. Effect of divalent cation bound to the ATPase of SR. *J. Biol. Chem*. **258**:14157-14161.

Siebert, F. 1995. Infrared spectroscopy applied to biochemical and biological problems. *Methods Enzymol*. **246**:501-526.

Skriver, E., A. B. Maunsbach, and P. L. Jorgensen. 1981. Formation of two-dimensional crystals in pure membrane-bound Na^+, K^+-ATPase. *FEBS Lett*. **131**:219-222.

Stahl, N., and W. P. Jencks. 1987. Reactions of the SR Calcium ATPase with ATP and Ca^{2+} that are not satisfactorily Described by an E1-E2 Model. *Biochemistry* **26**:7654-7667.

Stefanova, H. I., A. M. Mata, M. G. Gore, J. M. East, and A. G. Lee. 1993. Labeling the (Ca^{2+}-Mg^{2+})-ATPase of sarcoplasmic reticulum at Glu-439 with 5-(bromomethyl)fluorescein. *Biochemistry* **32**:6095-6103.

Stokes, D. L., and N. M. Green. 2000a. Modeling a dehalogenase fold into the 8-Å Density map for Ca^{2+}-ATPase defines a new domain structure. *Biophys. J*. **78**:1765-1776.

Stokes, D. L., and T. Wagenknecht. 2000b. Calcium transport across the sarcoplasmic reticulum. *Eur. J. Biochem*. **267**:5274-5279.

Suzuki, H., M. Obara, H. Kuwayama, and T. Kanazawa. 1987. A conformational change of *N*-iodoacetyl-*N*'-(5-sulfo-1-naphthyl)ethylenediamine-labeled SR Ca^{2+}-ATPase upon ATP binding to the catalytic site. *J. Biol. Chem*. **262**:15448-15456.

Suzuki, H., T. Kubota, K. Kubo, and T. Kanazawa. 1990. Existence of a low-affinity ATP-binding site in the unphosphorylated Ca^{2+}-ATPase of sarcoplasmic reticulum vesicles: evidence from binding of 2',3'-*O*-(2,4,6-trinitrocyclohexadienylidene)-[^{3}H]AMP and -[^{3}H]ATP. *Biochemistry* **29**:7040-7045.

Taillandier, E., J. P. Ridoux, J. Liquier, W. Leupin, W. A. Denny, Y. Wang, G. A. Thomas, and W. L. Peticolas. 1987. Infrared and Raman studies shows that poly(dA)poly(dT) and d(AAAAATTTTT)2 exhibit a heteronomous conformation in films at 75% relative humidity and a B-type conformation at high humidities and in solution. *Biochemistry* **26**:3361-3368.

Takeuchi, H., and I. Harada. 1986. Normal coordinate analysis of the indole ring. *Spectrochim. Acta A* **42**:1069-1078.

Takeuchi, H., H. Murata, and I. Harada. 1988. Interaction of adenosine 5'-triphosphate with Mg^{2+}: vibrational study of coordination sites by use of ^{18}O-labeled triphosphates. *J. Am. Chem. Soc*. **110**:392-397.

Teruel, J. A., M. Kurzmack, and G. Inesi. 1987. Kinetic and thermodynamic control of ATP syntheses by SR ATPase. *J. Biol. Chem*. **262**:13055-13060.

Toyoshima, C., M. Nakasako, H. Nomura, and H. Ogawa. 2000. Crystal structure of the calcium pump of sarcoplasmic reticulum at 2.6 Å resolution. *Nature* **405**:647-655.

Toyoshima, C., and H. Nomura. 2002. Structural changes in the calcium pump accompanying the dissociation of calcium. *Nature* **418**:605-611.

Venyaminov, S. Y., and N. N. Kalnin. 1990. Quantitative IR spectrophotometry of peptide compounds in water (H_2O) solutions. I. Spectral parameters of amino acid residue absorption bands. *Biopolymers* **30**:1243-1257.

Von Germar, F., A. Barth, and W. Mäntele. 2000. Structural changes of the sarcoplasmic reticulum Ca^{2+}-ATPase upon nucleotide binding studied by Fourier transform infrared spectroscopy. *Biophys. J.* **78**:1531-1540.

Wakabayashi, S., and M. Shigekawa. 1990. Mechanism for activation of the NBD labeled SR ATPase by Ca^{2+} and its modulation by nucleotides. *Biochemistry* **29**:7309-7318.

Walker, J. W., G. P. Reid, J. A. McCray, and D. R. Trentham. 1988. Photolabile 1-(2-nitrophenyl)ethyl phosphate esters of adenine nucleotide analogues. Synthesis and mechanism of photolysis. *J. Am. Chem. Soc*. **110**:7170-7177.

Wartell, R. M., and J. T. Harrell. 1986. Characteristics and variations of B-type DNA conformations in solution: a quantitative analysis of Raman band intensities of eight DNAs. *Biochemistry* **25**:2664-2671.

Watanabe, T., and G. Inesi. 1982. The use of 2',3'-*O*-(2,4,6-trinitrophenyl)adenosine 5'-triphosphate for studies of nucleotide interaction with sarcoplasmic reticulum vesicles. *J. Biol. Chem*. **257**:11510-11516.

Wharton, C. W. 2000. Infrared spectroscopy of enzyme reaction intermediates. *Nat. Prod. Rep*. **17**:447-453.

White, T. E., and T. G. Dewey. 1987. A fluorescence investigation of the nucleotide binding sites of the Ca^{2+}-ATPase. *Membrane Biochemistry* **7**:67-72.

White, A. J., and C. W. Wharton. 1990. Hydrogen-bonding in enzyme catalysis. Fourier-transform infrared detection of ground-state electronic strain in acyl-chymotrypsins and analysis of the kinetic consequences. *Biochem. J*. **270**:627-637.

Wolosker, H., and L. de Meis. 1995. Ligand-gated channel of the sarcoplasmic reticulum Ca^{2+} transport ATPase. *Biosci. Rep*. **15**:365-376.

Xu, C., W. J. Rice, W. He, and D. L. Stokes. 2002. A structural model for the catalytic cycle of Ca^{2+}-ATPase. *J. Mol. Biol*. **316**:201-211.

Yamada, S., and N. Ikemoto. 1980. Reaction mechanism of Ca^{2+}-ATPase of SR Substrates for phosphorylation reaction and back reaction, and further resolution of phosphorylated intermediates. *J. Biol. Chem*. **255**:3108-3119.

Yeagle, P. L. 1993. The Membranes of Cells. 2nd ed., Academic press INC., San Diego, New York, Boston, London, Sydney, Tokyo, Toronto.

Acknowledgments

I would like to express my deepest and sincere appreciation for the following who have helped me so much in my Ph.D studying:

Mr. PD. Dr. Andreas Barth for his invaluable supervise, support and suggestions of this Ph.D work, and for my learning the most important part of research philosophies from him.

Mr. Prof. Dr. Werner Mäntele for his precious support and suggestions of this Ph.D work.

Mr. Prof. Dr. Wilhelm Hasselbach for the generous gift of the *sarcoplasmic reticulum* Ca^{2+}-ATPase.

Mr. Dr. John E. T. Corrie and Mr. Dr. Frithjof von Germar for helping preparation of caged nucleotides.

Ms. Dr. Karin Hauser for the help of translating "Kurzfassung" and "Zusammenfassung".

All the colleagues in the Institute of Biophysics for the kind help, discussion, and advice over the three years.

Deutsche Forschungsgemeinschaft for the financial support.

My parents and my sister for their constant support and encouragement.

RESUME

Name**:**	Liu, Man
Birth:	March 11,1976, Heilongjiang / P.R.China
Nationality:	China
E-mail:	liuman100@hotmail.com

EDUCATION

Sep.1981 - Jul.1987:	primary school, in Jiamusi City, Heilongjiang Province, China
Sep.1987 - Jul.1990:	middle school, in Jiamusi City, Heilongjiang Province, China
Sep.1990 - Jul.1993:	high middle school in Jiamusi City, Heilongjiang Province, China
Sep.1993 - Jul.1997:	Bachelor of Science, Dept. of Physics, Nankai University, Tianjin, China
Sep.1997 - Jul. 2000:	Master' degree, Dept. of Biophysical Science and Technology, Nankai University, Tianjin, China
Nov.2000 - Nov.2003 :	Ph.D studying in Institut für Biophysik, Dept. of Physics, Johann Wolfgang Goethe-Universität, Frankfurt am Main, Germany

RESEARCH & PROJECTS

Sep.1996 - Dec.1998 :	"Effects of extremely low frequency weak electromagnetic fields on cell metabolism", Dept. of Biophysical Science and Technology, Nankai University
Oct.1998 - Jul. 2000 :	"Signal transduction of endotoxin and Chinese medicine's effects on immunocytes in pathogenesis and treatment of MODS (Multiple Organ Dysfunction Syndrome)",Dept. of Biophysical Science and Technology, Nankai University
Nov. 2000 - Nov. 2003 :	"Characteristics of the molecular binding pocket of protein studied by Infrared spectroscopy" (DFG project BA1887/2-1), Institut für Biophysik, Dept. of Physics, Johann Wolfgang Goethe-Universität

PUBLICATIONS IN THE PH.D STUDY

1) Mapping interaction between the Ca^{2+}-ATPase and its substrate ATP with infrared spectroscopy, *J. Biol. Chem.*, **278**: 10112-10118, 2003.
2) TNP-AMP binding to the sarcoplasmic reticulum Ca^{2+}-ATPase studied by infrared spectroscopy, *Biophys. J.*, accepted, **85**(5), 2003.
3) Mapping nucleotide binding site of calcium ATPase with IR spectroscopy: Effects of ATP γ-phosphate binding, *Biospectroscopy*, **67**(4-5): 267-270, 2002.